12-2011

Spectral Engineering of Optical Fiber Through Active Nanoparticle Doping

Tiffany Lindstrom-james
Clemson University, tljspritz@gmail.com

SPECTRAL ENGINEERING OF OPTICAL FIBER THROUGH ACTIVE NANOPARTICLE DOPING

A Dissertation
Presented to
The Graduate School of
Clemson University

In Partial Fulfillment
of the Requirements for the Degree
Doctor of Philosophy
Materials Science and Engineering

---

by
Tiffany Lindstrom-James
December 2011

Accepted by:
John Ballato, Committee Chair
Philip Brown
Stephen Foulger
Eric Skaar

ABSTRACT

The spectral engineering of optical fiber is a method of intentional doping of the core region in order to absorb/emit specific wavelengths of light therby providing enhanced performance over current fibers. Efforts here focused on developing an understanding of optically active nanoparticles based on alkaline earth fluorides that could be easily and homogeneously incorporated into the core of a silica based optical fiber preform and result in efficient and tailorable spectral emissions.

Doped and undoped calcium, strontium and barium fluoride nanoparticles were successfully synthesized and characterized for their physical, chemical, and optical behavior. Distinct spectroscopic differences as a result of different host materials, varying rare earth doping levels and processing conditions, indicated the ability to influence the spectral behavior of the doped nanoparticle. By using photoluminescence to predict diffusion behavior, the application of a simple one dimensional model for diffusion provided a method for predicting the diffusion coefficient of europium ions in alkaline earth fluorides with order of magnitude accuracy.

Modified chemical vapor deposition derived silica preforms were individually solution doped with europium doped alkaline earth fluoride nanoparticles. By using the rare earth doped alkaline earth fluoride nanoparticles as the dopant materials in the core of optical fiber preforms, the resultant optical

properties of the glass were significantly influenced by their presence in the core. The incorporation of these rare earth doped alkaline earth fluoride nanoparticles was found to significantly influence the local chemical and structural environment about the rare earth ion, demonstrated homogeneity and uniform distribution of the rare earth dopant and resulted in specifically unique spectral behavior when compared to conventional doping methods. A more detailed structural model of the doped core glass region has been developed based on the spectral behavior of these active fiber preforms.

It has been shown that rare earth doping of alkaline earth fluoride nanoparticles provides a material which can be ‘tuned’ to specific applications through the use of different host materials, processing conditions and doping levels of the rare earth and when used as dopant materials for active optical fibers, provides a means to tailor the optical behavior.

DEDICATION

To my beautiful, amazing, tenacious, witty, bright blue-eyed babies, Kirin and Cooper…. I started this quest with the intent to better our lives as a family and I end it hoping I have shown you to persevere, endure and remain strong no matter what the universe throws in your way. The road to success is not always the shortest distance between two points, but if you lead with your heart, you can never go wrong. I couldn't have done this without you, I am so very proud to be your mom, and I love you to infinity and back…

To my sweet, angel baby Griffin…..I know you have been with me every step of the way. Thanks for being my inspiration in times of desperation and the sunshine when things have seemed the darkest. You were one tough little guy, and you have taught me so much about life, inner strength and unconditional love. Oh and thanks for being my guardian angel; It's a tough job, but I think you are handling it beautifully.

ACKNOWLEDGEMENTS

Many thanks, first and foremost, to my advisor and friend, John Ballato. I realize this took a bit longer than you had anticipated but your patience and understanding during the many trials and tribulations of my life made this endeavor much ‘easier’ and definitely have not gone unnoticed. My kids gained the most as a result and I will be forever indebted to you for it.

Thanks to my committee members, Phil Brown, Eric Skaar and Steve Foulger. You all have managed to push me along in subtle ways through the course of my academic career and I leave here with much appreciation for your wisdom and thoughtfulness.

To my AMRL-Clemson Family and the entire staff at Clemson Elementary School; your tremendous support over the course of the last two years whether in the lab or in my home is a gift I will forever treasure. Each of you have helped me get to this point in some way, whether it was providing a much needed laugh, venting session, hug, adult beverage, lab work, yard work or sitting services. Thank you.

Much gratitude is owed to my dear friend and true colleague, Kate Stevens. Thanks for treating me like an equal when I felt like a peon, finding a way to help me breathe when the academic part of my world had me by the throat, reminding me I was, in fact, worthy of this and most of all, being my friend

when life would have me think I had none. You are an amazing woman and I am so honored to call you my friend. Thank you.

And that leaves MaryAlice Lohmeier, my soul sister. The reason I finally get Oprah and Gayle. There are no words that can convey what it has meant to me to have you in my life. At times when I thought there was no way I was going to survive, you were always there to tell me I absolutely would. I could not have done this part without you. Period. Thank you, love you and now, I'm done, so we can go play!

This five year journey has been long and arduous, with many personal tragedies along the way. The people I have been blessed with in my life, who have supported me through all the ups and downs, have provided me an opportunity to enhance the lives of my children and given me the courage to carry on when most would have packed their toys and gone home. They say friends are the family you choose so…. to my family of choice as well as the family I was lucky to be born into….I am humbled by your love and unending support and I thank you all from the bottom of my heart.

TABLE OF CONTENTS

Page

Table of Contents (Continued)

Page

LIST OF TABLES

Table Page

LIST OF FIGURES

Figure Page

List of Figures (Continued)

Figure Page

List of Figures (Continued)

Figure Page

List of Figures (Continued)

Figure Page

List of Figures (Continued)

Figure Page

CHAPTER I

OVERVIEW

The spectral engineering of optical fiber is a method of intentional doping of the core region in order to absorb/emit specific wavelengths of light thereby providing enhanced performance over current fibers. The development of optically active fibers has been driven by the continuing demand for more efficient, cost effective and easily produced fiber amplifiers which operate in the telecommunications transmission window of 1550 nm[1.1,1,2]. These fibers are produced by doping the core region of an optical fiber, commonly silica glass, with optically active rare earth ions.

The most commonly known amplifier is the erbium doped fiber amplifier (EDFA) which provides amplification in the 1550 nm regime. Other rare earth doped glasses such as fluorides, tellurides and chalcogenides are of interest for amplification of the 1300 nm region due to their low phonon energy and increased solubility of rare earth ions, however, their mechanical and chemical properties, in addition to their inability to be spliced efficiently to commercial silica optical fiber, limit their use. Fluoride fibers, in particular melt at temperatures considerably lower than silica making fusing of the two fibers difficult[1.3-1.5].

Rare earth ion emissions in silica fiber are limited by the phonon energy of the glass matrix and the solubility of the ions into the matrix. This makes control

of the distribution and concentration of the dopant ions of primary interest for improving overall active fiber spectroscopic characteristics.[1.4,1.6].

Given this desire for improved performance, efforts here focused on providing a material that could be easily and homogeneously incorporated (i.e., is soluble) into the core of a silica-based optical fiber preform and result in efficient, and potentially tailorable spectral emissions. Therefore, this dissertation advances the fundamental understanding of the behavior of optically active nanoparticles, based on alkaline-earth fluorides, through the synthesis, characterization (physical, chemical and optical) and ultimately, use as primary core dopants in optical fiber. This initial overview serves to provide a general background, definitions and foundation for the study of these optically active materials.

Optically Active Materials:

Rare Earth Elements and Spectroscopy

The f-block elements of the periodic table are comprised of two groups, 14 elements each, the lanthanides and actinides. Lanthanides are referred to as the 'rare earths'. The term rare earth has its origins in the early discovery of these elements and refers to the fact they were originally found in scarce minerals and the difficulty in obtaining them in a pure state by chemical extraction[1.7]. The

lanthanide elements are generally defined as those which the 4f orbitals are progressively filled. This includes cerium (z=58) to lutetium (z=71)[1.8]. The actinides include thorium (z=90) to lawrencium (z=103) and involve the filling of 5f shell electrons. The first commercial application of these materials was a gas mantle consisting of 99% ThO_2 and 1% CeO_2 in 1891 which enabled widespread use of incandescent gas lamps[1.8]. Current notable commercial use of lanthanum is in the batteries of hybrid vehicles, cerium (the most abundant of the rare earth elements) is most notably known for its use in catalytic converters, europium (as well as terbium) is widely used as a phosphor in color television tubes and has more recently been used as an anti-counterfeiting phosphor in the European Union's paper currency[1.9].

The electronic configuration of the lanthanide series is found to be that of the Xenon structure plus the corresponding number of 4f electrons, $[Xe]f^n$, where n=1-14. Ionization preferentially removes any 6s and 5d electrons which results in the 3+ oxidation state as generally the most stable state for these elements[1.10-1.12]. The radii of both the atomic and ionic species are found to decrease with increasing atomic number and is referred to as the lanthanide contraction. Due to limited screening by the 4f electrons, there is an increase in effective nuclear charge and the 4f electrons become more tightly bound with increasing atomic number[1.11]. The 4f electrons are 'inside' the 5s, 5p and 6s orbitals, (Figure 1.1), which results in a shielding affect from bonding with neighboring atoms, making their electronic and magnetic spectra virtually

independent of environment[1.13], and results in well defined, sharp bands in the absorption spectra of the corresponding ionic species[1.12].

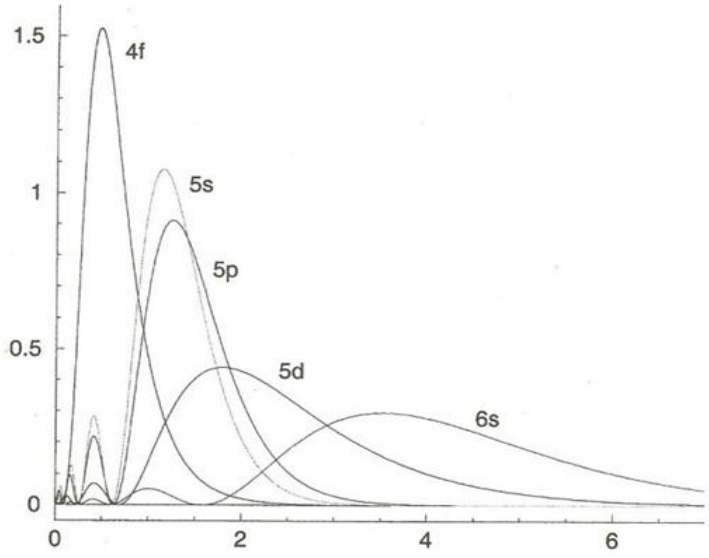

Figure 1.1. Electronic Wavefunctions of a Gd^{3+} ion[1.8].

The observed infrared and visible optical spectra of trivalent rare earth ions are a consequence of transitions of electrons between 4f energy levels, or the ground state and excited states of the ions. Energy levels are represented in figure 1.2 as reported by Dieke and White in 1963[1.14]. The lowest energy level is referred to as the ground state, with higher energy levels referred to as excited states. Each level is designated using the Russell-Saunders or spin-coupling scheme which takes into account the spin (s) and momentum (orbital (L) and

angular (J)) of the electrons in the atom or ion and is given in the general form[1.11-1.13].

$$^{(2s+1)}L_J$$

An influx of energy, or absorption, can lead to two different effects in rare earth ions: fluorescence and up-conversion. The probability the electron will move between states is dictated by guidelines known as the selection rules[1.10-1.13]. The likelihood an electron will choose one energy level over another depends upon the amount of change (with regard to spin, momentum) required between the states, i.e. the electron will decay 'along the path of least resistance' when given the proper amount of energy to do so. For example, the ground state of Er^{3+} is $^4I_{15/2}$ and the first excited state is $^4I_{13/2}$. There is a small difference between angular momentum values, making the probability of this transition high, whereas a transition to one a higher energy state, $^2D_{5/2}$, requires a change to all three quantum states, making the probability of transition low.

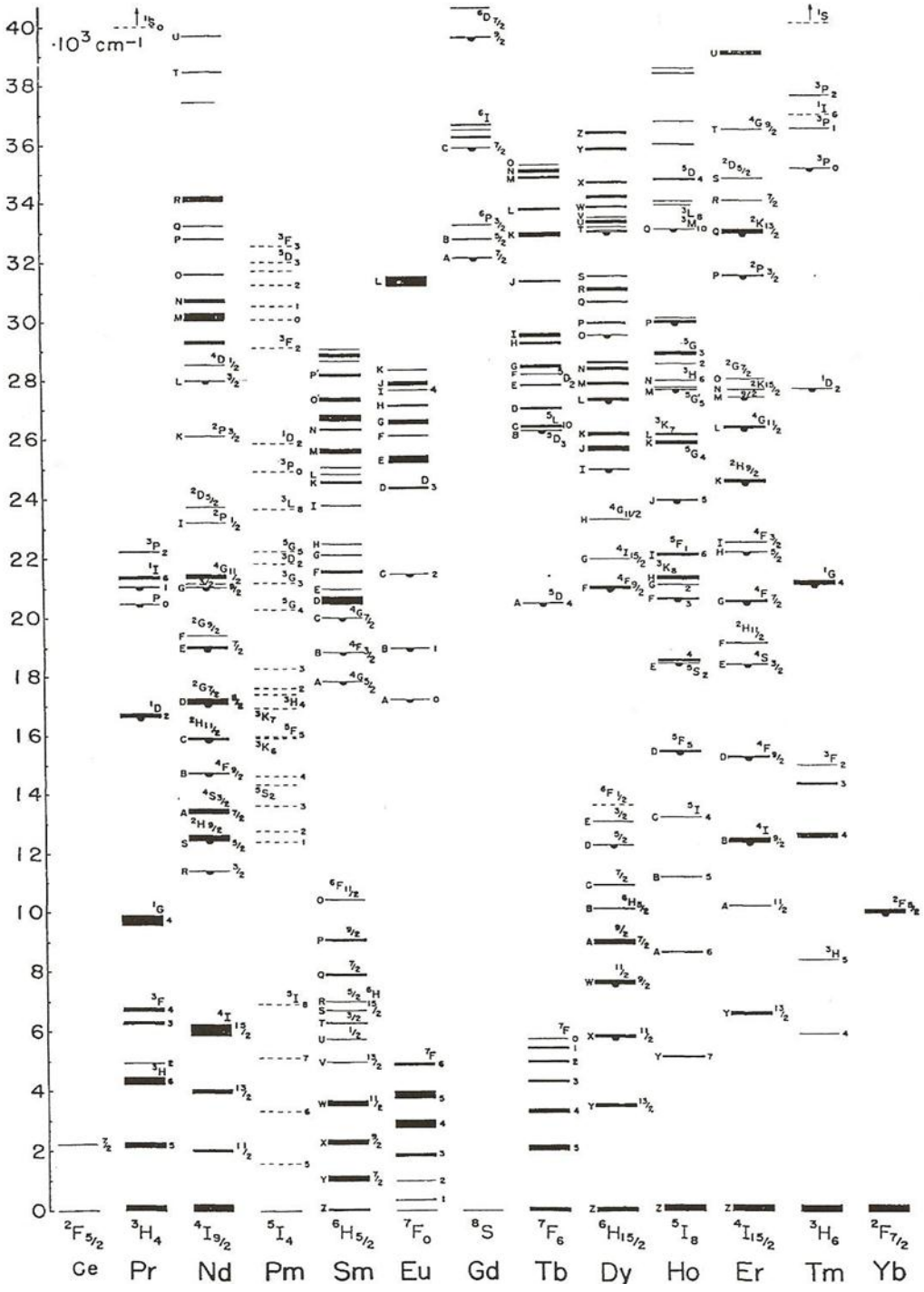

Figure 1.2.. Energy level diagram of the trivalent lanthanide ions[1.14]

Fluorescence, depicted in figure 1.3a, occurs as electrons are excited into higher energy levels by the absorption of photons. The electrons then relax to a lower energy state. The resultant energy emitted by the photon is less than that of the incident photon.

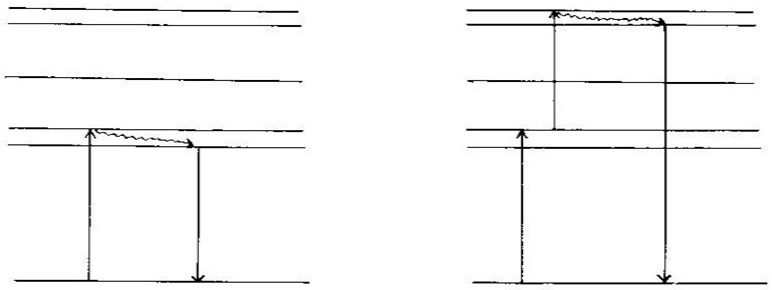

Figure 1.3. a) General fluorescence mechanism, b) general up- conversion mechanism[1.10]

Up-conversion, figure 1.3b, results when excited electrons absorb another photon and are excited to even higher energy levels. The electron eventually decays back to a lower energy state and in doing so, results in an emission of a photon whose energy is greater than the initial incident photon. This phenomenon does not necessarily produce photons of higher energy if the electron only relaxes to an energy level above the incident photon but below the

excited state. Generally, up-conversion describes a process by which an excited electron absorbs one or more 'extra' photons and moves to a higher energy level, regardless of emission wavelength[1.8,1.10]. Up-conversion is a fairly unusual process which tends to require a high flux of incident light or a long radiative lifetime such that it can occur prior to fluorescence.

In systems where co-doping is employed (two different rare earth ions present), energy transfer or sharing of energy between ions can occur. By partnering specific rare earth ions to allow their intrinsic states to communicate with each other, scientists can create innovative solutions that take advantage of energy transfer mechanisms which could otherwise be deemed detrimental, as was demonstrated by the use of Yb^{3+} energy transfer to Er^{3+} to improve pumping efficiency of solid state lasers. However, same species energy transfer can also occur, which is detrimental to the overall rare earth behavior and result in reduced efficiency and lower emissions[1.10].

Energy out of a system generally is classified as either radiative (light, photons) or non-radiative (heat, phonons). The quantum efficiency of the system is therefore affected by the concentrations of single rare earth ions or co-doping, as well as the host material containing the emitting ions. In order to quantify the quantum efficiency of a given rare earth system, excited state lifetime measurements are used. The theoretical radiative lifetime, τ, is the time for natural (spontaneous) emission to occur after exciting the ion to a specific

wavelength. These values are found by monitoring emission as a function of time while exciting a sample with a pulse or modulated excitation[1.15]. Quantum efficiency is used to account for the difference between theoretical and measured lifetime values and reveals non-radiative losses due to heat and/or host material. The total lifetime is the sum of the measured lifetime and the contribution from the host material, or the non-radiative lifetime[1.4,1.15].

Optically Active Materials:

Alkaline Earth Fluorides as Hosts

Rare earths are used as dopants in various materials, as defined by the application. Rare earth doped glasses allow for broader emission and absorption spectral properties (with respect to crystalline hosts), making them ideal for many optical fiber devices. Other applications require crystalline hosts for their inherently superior thermal properties and narrower linewidths[1.15]. Regardless of type of use, the final characteristics of luminescent devices are dependent upon the optical properties resulting from the ion-host interactions. In order to increase the efficiency of a given device, the excitation efficiency needs to be increased. The quantum efficiency of a material system is give as a ratio of the emitted to absorbed photons and varies between 0 to 1. A quantum efficiency of less than one implies a portion of the absorbed energy has been lost to non-radiative processes, i.e., heat, phonons[1.16]. The lower the vibrational

energy of the host material, the less the non-radiative contribution to electron decay, which ultimately increases the quantum efficiency. Therefore, choosing a host material is a crucial step in the design of optical devices.

The vibrational energy of a host material is a result of the inherent oscillations between ions in solids about an equilibrium position. If the difference in energy levels is comparable to that of the lattice vibrations, any emission becomes more difficult, as the relaxation path is more likely to generate phonons (heat), rather than photons (light), or it takes more energy/phonons to stimulate the decay[1.16].

When looking at conventional luminescent materials, fluorides emerge as advantageous host materials due to their low intrinsic vibrational energies which extend transmission to the far ultra-violet and infrared spectral regimes, minimally quench the excited state of rare earth ions, have high transparency over a wide wavelength range, high iconicity and fundamentally reduce absorption when compared to oxide based materials[1.17,1.18].

In choosing what specific fluorides to use, looking at the interaction between rare earth (RE) ions and host is useful, as well as the luminescent efficiency of the materials. Lanthanum trifluoride, LaF_3, is a very suitable host because the RE^{3+} can easily substitute for the La^{3+} of the same valency[1.19]. The vibrational or phonon energy of LaF_3 is reported to be ~350 cm^{-1}, has a high RE solubility and has significant environmental and thermal stability[1.20].

Alkaline earth (calcium, strontium and barium) fluorides possess similar characteristics and have been studied in limited areas. Their cubic lattice structure enables transmission for a wide range of wavelengths as well as indicates independence of absorption from induced polarization. They have similarly matched refractive index values that can be exactly matched to a glass or polymer for use in composite materials.[1.21-1.23]. The cubic fluoride structure also allows for the aggregation and clusters of RE^{3+} ions, making the distance between the active ions short and interactions strong[1.24], implying a propensity for ease of energy transfer when the materials are co-doped with differing RE^{3+} ions.

More specifically, CaF_2 is reported to exhibit transparency over a wide range of wavelengths, can easily be doped with trivalent rare earth ions and with the incorporation of rare earths, an increase of refractive index results, making it a desirable material for active waveguides[1.21,1.23,1.25]. Moreover, the substitution of RE^{3+} ions for Ca^{2+} ions results in broad absorption and emission bands, due to the necessary charge compensation, which is important in optical device development[1.23]. Barium fluoride, BaF_2, is found to have transparency in the visible and near-IR region[1.26]. In addition, BaF_2 has slight solubility in water and is non- hygroscopic, and due to its cubic structure, has one refractive index and can be exactly matched to a glass or polymer matrix material to avoid significant light scattering, making it desirable for use of composites [1.22,1.26,1.27].

In the realm of glass making, alkaline earth elements are known to serve as glass modifiers. These elements are added to assist in the formation of a glass; they form highly ionic bonds with oxygen which can serve to modify the local network structure within a glass[1.28]. The addition of an alkaline earth perturbs the short range order of the silica glass matrix by affecting the inter-atom connectivity and the silica bond angles[1.29]. Commercially, bulk laser glasses typically require the presence of glass modifier ions such as Ca^{2+} to 'open' up the silicate structure to aid in RE solubility[1.10].

Application of Optically Active Materials:

Rare Earth Doped Nanoparticles

Particles with diameters ranging from a few to 100 nanometers with chemical and physical properties that can differ from those of the analogous bulk material are termed nanoparticles[1.30,1.31]. In recent years, this nanotechnology has been used in a variety of applications from drug carriers to pigments, catalysts to sensors and magnetic to optical materials[1.32]. The unique size and shape tuning abilities of these materials are of particular interest in the optical community because they provide a wide range of physical properties not found in their bulk counterparts and have a higher chemical reactivity which allows the creation of ceramic and transparent ceramic materials at lower temperatures[1.22,1.25,1.33]. Several methods are employed to synthesize

nanoparticles such as gas and laser evaporation, sol-gel reaction, microemulsion and hydrothermal treatment[1.22,1.30,1.33].

Of interest here is the development of nanoparticles which efficiently up and down convert light which can easily be incorporated into bulk polymeric or glass matrices. This requires active rare earth dopants in low vibrational energy hosts, dispersion of the nanoparticles in organic solvents, as well as a refractive index that can be matched to a polymer or glass composite host for designing practical optical devices. Materials made of alkaline earth fluorides are a means of satisfying the host and refractive index requirements and synthesis of the nanoparticles with different surfactants/ligands (the attachment of long chain hydrocarbons to the surface) is a key component in facilitating their dispersibility in organic solvents . Previous studies[1.34-1.36] to produce nanoparticles involving $LaPO_4$ and LaF_3 as the host for rare earth ions are the foundation for experimentation in this work.

In 2002, Stouwdam and van Veggel reported their ability to produce rare earth doped lanthanum fluoride particles that disperse well in organic solvents[1.34, 1.35]. Upon verification of rare earth incorporation via emission spectra and lifetime measurements, they determined that as dopant level increased, luminescent lifetime increased. This implied a relationship between surface ions and quenching effects and suggested a layer of undoped host material around the particles could improve the overall luminescence[1.35]. Rare earth doped

inorganic core-shell nanoparticles produced by Hasse, et. al, yielded a $LaPO_4$ shell around a $CePO_4$: Tb core[1.36] and rare earth doped $LaPO_4$ with undoped $LaPO_4$ shells[1.37] which improved quantum yield. However, these particles were made with a high-temperature procedure which eliminates any organic groups on their surface, making it extremely difficult to disperse in organic solvents.

By modifying a solution-precipitation method initially developed by Dang, et. al,[1.38] for LaF_3 nanoparticles, van Veggel, et. al, produced surface-coated nanoparticles of LaF_3 and $LaPO_4$ doped with a variety of rare-earth ions[1.39] and further improved their luminescent properties by utilizing organic materials or ligands[1.40]. These core-shell nanoparticles were developed based on the following premises: 1. The core is doped with luminescent ions and the shell is not. 2. The use of a ligand will improve the solubility of the particles in an organic solvent, control particle growth, prevent clustering and improve luminescence. 3. LaF_3 is presumed to provide low enough vibrational energy to allow emission of lanthanide ions in the visible and near infrared[1.39,1.40].

Core-shell nanoparticles were taken further by DiMaio, et. al,[1.41, 1.42] with the development of complex architectures which utilize the shells as luminescent layers allowing for energy transfer between rare earth ions. Using LaF_3 as a host, these particles provide the ability to tailor emissions as well as provide a system to study the 'basic science' of rare earth ions. By enhancing van

Veggel's solution precipitation approach, these complex core-shell nanoparticles are easily produced and dispersible in organic solvents.

Alkaline earth (calcium, strontium and barium) fluoride (AEF_2) nanoparticles possess similar characteristics to RE doped LaF_3 nanoparticles and have been studied in limited areas. Bender et. al,[1.27] produced neodymium doped BaF_2 particles, on the order of 100 nm, Lian, et. al,[1.26] synthesized erbium doped BaF_2 particles using a reverse microemulsion technique for use in composite polymer matrices and Hua et. al,[1.22] produced 50-150 nm BaF_2:Ce^{3+} particles using a 2-octanol/water microemulsion reaction. Previous studies by Wang, et. al,[1.21] reported synthesis of 15-20 nm Eu^{3+}:CaF_2 particles via a low temperature solution precipitation process, Labeguerie et. al,[1.25], produced Eu^{3+}:CaF_2 nanoparticles on the order of 15 nm utilizing a non-aqueous process to limit introduction of hydroxide groups and Sun & Li[1.33] synthesized single crystal CaF_2 350 nm nanocubes using a hydrothermal procedure. CaF_2, SrF_2 and BaF_2 particles of sizes ranging from 20 to greater than 100 nm made by flame synthesis are also reported by Grass and Stark[1.43] These processes prove the ability to make alkaline earth nanoparticles by various means, however, none of these methods provide a way in which organic constituents can be incorporated, making them interesting but not practical for application.

Application of Optically Active Materials:

Fundamentals of Optical Fiber

In general terms, an optical fiber is a thin, cylindrical piece of glass about the diameter of a human hair (~125 μm) through which light can travel. This light can be turned on and off and gradually changed in amplitude, phase or frequency dependent upon the information being transmitted by that light. When compared to other communication technology such as copper cable, radio or microwave transmission, optical fiber has distinct advantages as it is less affected by noise, does not conduct electricity and can carry data over long distances at extremely high rates. Optical fibers were first contemplated in the early 1960s, with Kao and Hockham first suggesting that low loss optical fiber could be a viable and competitive means for telecommunications and Corning Glass Works producing optical fiber with losses of less than 10 dB/km in 1970. Since that time, the commercial and scientific applications of optical fiber has been vast and varied due to the realization that very small changes in material properties result in big gains in transmission distances and uses[1.44-1.46].

The basic structure of an optical fiber is pictured in Figure 1.4a. A core (where the light travels) of refractive index n_0 is surrounded by a cladding layer of lower refractive index n_1. The difference in refractive index is required to 'trap' any light within the waveguide core. In order to achieve this total internal reflectance, the light inside the fiber must be incident at an angle greater than the

critical angle, Θ_c, at the interface (illustrated in Figure 1.4b) and is given by[1.45,1.46]:

$$\Theta_c = \sin^{-1}\left(\frac{n_1}{n_0}\right)$$

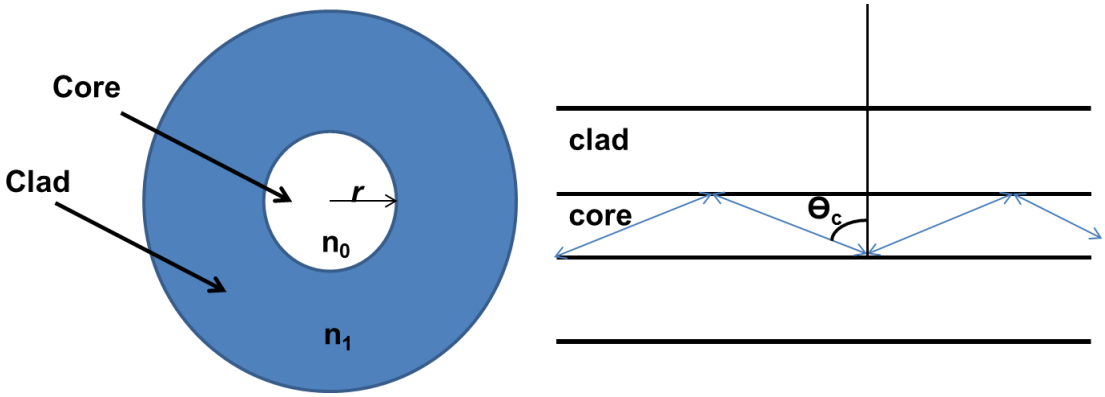

Figure 1.4. *Left*: Generic optical fiber cross-section of core radius r.

Right: demonstration of light propagation path at critical angle, Θ_c

In order to achieve the mandatory difference in refractive index, the core and clad are comprised of two different materials which are transparent to light in the transmission space. To avoid losses due to scattering and defects, the materials of choice are generally limited to either glasses or certain polymers. Commercial optical fiber is typically comprised of silica (SiO_2) and germania (GeO_2) in the core region and pure SiO_2 in the cladding, however, for specialty applications manipulation of core glass composition with the addition of dopant materials, such as rare earth elements, is employed[1.46].

Conventional fabrication of optical fibers requires the production of a preform with the desired refractive index profile in macroscopic dimensions. To make the preform, chemical vapor deposition (CVD) techniques are used in one of two processes to produce high purity and precise index profiles. Modified Chemical Vapor Deposition (MCVD) and Plasma-Assisted Chemical Vapor Deposition (PCVD) are considered 'inside' processes, whereby submicron particles (soot) of the desired compositional constituents are deposited layer by layer inside a rotating silica substrate tube, which is then sintered. Outside Chemical Vapor Deposition (OCVD) and Vapor Axial Deposition (VAD) are methods by which the soot is deposited layer by layer on the outside of a thin, rotating, cylindrical target or bait rod, which must be removed before sintering[1.45].

Beyond telecommunications, optical fibers are of interest in the areas of amplification and lasing[1.4,1.45-1.47]. By incorporating rare earth ions into the core

of an optical fiber, the glass has the ability to absorb light at one wavelength and emit at another[1.47], which results in desired amplification or gain of the optical signals over wide spectral bandwidths[1.46]. Pure silica glass is not readily doped with RE^{3+} due to the absence of network modifiers, making the local structure very rigid and virtually eliminating non-bridging Si-O groups. This influences the coordination of the RE^{3+}, limits solubility and leads to clustering of the ions within the glass. Clustering has detrimental effects on the luminescence qualities of the RE^{3+} by inducing loss of ion excitations, resulting in decreasing luminescence lifetime with increasing RE^{3+} concentration[1.47,1.48]. To increase the solubility of RE^{3+}, decrease the effects of clustering and somewhat control RE^{3+} absorption and fluorescence spectra co-doping with materials that alter these spectroscopic properties is employed. Aluminum is commonly incorporated and typically works as a network modifier by sharing non-bridging oxygen ions with RE^{3+} and reducing clustering, as well as aiding in solubility[1.47]. Alkali and alkaline earth metals may also be included as co-dopants to alter the host glass composition for better RE^{3+} incorporation[1.47,1.48]. Ultimately, the addition of co-dopants is to tailor the absorption and emission spectra and improve the glass-forming ability of the host glass for the desired application[1.47].

The conventional method developed in the late 1980s for incorporating rare earth ions into optical fiber preforms is referred to as solution doping[1.49], where an aqueous solution of rare earths and aluminum, usually as chloride salts, is used in an additional step during the MCVD process. Recently,

materials on the nanoscale have been receiving interest as an alternate method of delivering the same dopants to the core of an optical fiber preform. Liekki Corporation[1.50] has developed a method using OVD technology referred to as "Direct Nanoparticle Deposition" where Er and Al rich 'crystallites' are created through evaporation/condensation of atomized liquid raw materials.

Blanc et al.[1.6] and Dussidier[1.51] report using commercially available nanopowders of rare earth and calcium chloride and Pordasky et al.[1.4] used alumina and erbium oxide nanopowders suspended in the soaking solution of the traditional solution doping method and 100-250 nm particles are reported to form during the subsequent MCVD processing. Both groups report this results in localized areas of Er/Al that influence the overall fiber performance. However, this method is only a small variation of conventional solution doping and the isolated areas referred to as nanoparticles are too large to allow acceptable transmission as a result of scattering.

Work by Draka Communications (France)[1.52] and Alcatel Research and Innovations (France)[1.2] ,where erbium doped nanoparticles are synthesized and then used in the solution doping step, results in fiber with improved performance when compared to conventional Er/Al solution doped fiber. This method demonstrates the ability to use rare earth doped nanoparticles for dopant delivery to the core of an optical fiber, however, these nanoparticles are comprised of the traditional co-dopant Er and Al ions.

Purpose Statement

This study aimed to advance the spectral engineering of optical fiber by providing a unique method to control local area chemistry within the core of an optical fiber through the fundamental understanding and utilization of optically active alkaline earth fluoride nanoparticles.

References

1.1 Bjarklev, A., Optical Fiber Amplifiers: Design and System Applications, Artech House, Boston, 1993.

1.2 Le Sauze, A., Simonneau, C., Pastouret, A., Gicquel, D., Bigot, L., Choblet, S., Jurdyc, A.M., Jacquier, B., Bayart, D. and Gasca, L., "Nanoparticle Doping Process: towards a better control of erbium incorporation in MCVD fibers for optical amplifiers," in Optical Amplifiers and Their Applications, OSA Technical Digest Series, (Optical Society of America, 2003), paper WC5.

1.3 Tanabe, S., "Optical properties and local structure of rare-earth-doped amplifier for broadband telecommunication," Journal of Alloys and Compounds, 408-412 [2006] 675.

1.4 Podrazky, O., Kasik, I., Pospisilova, M. and Matejec, V., "Use of nanoparticles for preparation of rare-earth doped silica fibers," Physica Status Solidi C, 6 [2009] 2228.

1.5 Gupta, M.C. and Ballato, J., ed., Handbook of Photonics, CRC Press, Boca Raton, Florida, 2007

1.6 Blanc, W., Dussardier, B., Monnom, G., Peretti, R., Jurdyc, A., Jacquier, B., Foret, M. and Roberts, A., "Erbium emission properties in nanostructured fibers," Applied Optics, 48 [2009] G119.

1.7 Barrett, S.D. and Dehsi, S.S., The Structure of Rare-Earth Metal Surfaces, Imperial College Press, London, 2001.

1.8 Apsinall, H.C., Chemistry of f-Block Elements, Gordon & Breach Sci. Pub., Singapore, 2001.

1.9 www.cnbc.com/id/4000207130/How_Are_Rare_Earth_Elements_Used

1.10 Digonnet, M.J.F. ed., Rare-Earth-Doped Fiber Lasers and Amplifiers, Marcel Dekker, Inc., New York, New York, 2001.

1.11 Brown, D., Halides of the Lanthanides and Actinides, Wiley-Interscience, London, 1968**.**

1.12 Kaltsoyannis, N. and Scott, P., The f Elements, Oxford University Press, New York, 1999.

1.13 Cotton, S., Lanthanide and Actinide Chemistry, John Wiley & Sons Ltd., West Sussex, England, 2006**.**

1.14 Dieke, G.H. and Crosswhite, H.M., " The Spectra of the Doubly and Triply Ionized Rare Earths," Applied Optics, 2 [1963] 675.

1.15 Demas, J.N., Excited State Lifetime Measurements, Academic Press, New York, New York, 1983.

1.16 Garcia Sole, J., Bausa, L.E. and Jaque, D., An Introduction to the Optical Spectroscopy of Inorganic Solids, Wiley & Sons, West Sussex, England, 2005.

1.17 Joubert, M.F., Guyot, Y., Jacquier, B., Chaminade, J.P., and Garcia, A., "Fluoride Crystals and high lying excited states of rare earth ions," Journal of Fluorine Chemistry, 107 [2001] 235.

1.18 Wang, Z.L., Z.W. Quan, Jia, P.Y., Lin, C.K., Luo, Y., Chen, Y., Fang, J., Zhou, W., O'Connor, C.J. and Lin, J., "A Facile Synthesis and Photoluminescent Properties of Redispersible CeF_3, CeF_3:Tb^{3+}, and CeF_3:Tb^{3+}/LaF_3 (Core/Shell) Nanoparticles," Chemistry of Materials, 18 [2006] 2030.

1.19 Chen, D., Wang, Y., Yu, Y, and Huang, P., "Structure and Optical Spectroscopy of Eu-Doped Glass Ceramics Containing GdF_3 Nanocrystals," Journal of Physical Chemistry, 112 [2008] 18943.

1.20 Dejneka, M.J., "The luminescence and structure of novel transparent oxyfluoride glass-ceramics," Journal of Non-Crystalline Solids, 239 [1998] 149.

1.21 Wang, F. Fan, X. Pi, D. and Wang, M., "Synthesis and luminescence behavior of Eu^{3+}-doped CaF_2 nanoparticles," Solid State Communications, 133 [2005] 775.

1.22 Hua, R., Zang, C., Shao, C., Xie, D. and Shi, C., "Synthesis of barium fluoride nanoparticles from microemulsion," Nanotechnology, 14 [2003] 588.

1.23 Lucca, A., Jacquemet, M., Druon, F., Balembois, F., Georges, P., Camy, P., Doualan, J.L., and Moncorge, R., "High-power tunable diode-pumped Tb^{3+}:CaF_2 laser," Optics Letters, 29 [2004] 1879.

1.24 Petit, V., Camy, P., Doualana, J.L., and Moncorge, R., "cw and tunable laser operation of Yb^{3+} in Nd:Yb:CaF_2," Applied Physics Letters, 88 [2006] 051111.

1.25 Labeguerie, J., Gredin, P., Mortier, M., Patriarche, G., and de Kozak, A., "Syntheses of Fluoride Nanoparticles in Non-Aqueous Nanoreactors. Luminescence Study of Eu^{3+}:CaF_2," Zeitschrift fur anorganische und allgemeine Chemie, 632 [2006] 1538.

1.26 Lian, H., Liu, J., Ye, Z., and Shi, C., "Synthesis and photoluminescence properties of erbium-doped BaF_2 nanoparticles," Chemical Physics Letters, 386 [2004] 291.

1.27 Bender, C.M., Burlitch, J.M., Barber, D. and Pollock, C., "Synthesis and Fluorescence of Neodymium-Doped Barium Fluoride Nanoparticles," Chemistry of Materials, 12 [2000] 1969.

1.28 Shelby, J.E., Introduction to Glass Science and Technology, Royal Society of Chemistry, Cambridge, 1997.

1.29 Manolescu, G., Poumellec, B., Burov, E. and Gasca, L., "Raman extra wide band silica based glasses for amplification in telecommunications," Glass Technology: European Journal of Glass Science and Technology Part A, 50 [2009] 143.

1.30 Iskandar, F., "Nanoparticle processing for optical applications- A review," Advanced Powder Technology, 20 [2009] 283.

1.31 Auffan, M., Rose, J., Bottero, J.Y., Lowry, G.V., Jolivet, J.P. and Wiesner, M.R., "Towards a definition of inorganic nanoparticles from an environmental, health and safety perspective," Nature Nanotechnology, 4 [2009] 634.

1.32 Roco, M.C., "Nanotechnology: convergence with modern biology and medicine," Current Opinion in Biotechnology, 14 [2003] 337.

1.33 Sun, X. and Li, Y., "Size-controllable luminescent single crystal CaF_2 nanocubes," Chemical Communications, [2003] 1768.

1.34 Hebbink, G.A., Stouwdam, J.W., Reinhoudt, D.N. and van Veggel, F.C.J.M., "Lanthanide(III)-Doped nanoparticles that Emit in the Near-Infrared," Advanced Materials, 14 [2002] 1147.

1.35 Stouwdam, J.W. and van Veggel, F.C.J.M., "Near-infrared Emission of redispersible Er^{3+}, Nd^{3+} and Ho^{3+} Doped LaF_3 Nanoparticles," Nano Letters, 2 [2002] 733.

1.36 Kömpe, K., Borchert, H., Storz, J., Lobo, A., Adam, S., Moller, T. and Haase, M., "Green-emitting $CePO_4$:Tb/$LaPO_4$ core-shell Nanoparticles with 70% Photoluminescence Quantum Yield," Angewandte Chemie, 42 [2003] 5513.

1.37 Lehmann, O., Kömpe, K. and Haase, M., "Synthesis of Eu^{3+}-doped core and Core/shell nanoparticles and Direct spectroscopic Identification of Dopant sites at the Surface and in the Interior of the Particles," Journal of the American Chemical Society, 126 [2004] 14935.

1.38 Zhou, J., Wu, Z., Zhang, Z., Liu, W., and Dang, H., "Study on an antiwear and extreme pressure additive of surface coated LaF_3 nanoparticles in liquid paraffin," Wear, 249 [2001] 333.

1.39 Stouwdam, J.W., Hebbink, G.A., Huskens, J. and van Veggel, F.C.J.M., "Lanthanide –Doped Nanoparticles with Excellent Luminescent Properties in Organic Media," Chemistry of Materials, 15 [2003] 4604.

1.40 Stouwdam, J.W., and van Veggel, F.C.J.M., "Improvement in the Luminescence Properties and Processability of LaF_3/Ln and $LaPO_4$ Nanoparticles by Surface Modification," Langmuir, 20 [2004] 11763.

1.41 DiMaio, J.R., Kokuoz, B., James, T.L., and Ballato, J., "Structural Determination of Light-Emitting Inorganic Nanoparticles with Complex Core/Shell Architectures," Advanced Materials, 19 [2007] 3266.

1.42 DiMaio, J.R., Sabatier, C., Kokuoz, B., and Ballato, J., "Controlling Energy Transfer between Multiple Dopants in a Single Nanoparticle," Proceedings of the National Academy of Sciences, 105 [2008] 1809.

1.43 Grass, R.N. and Stark, W.J., "Flame synthesis of calcium-, strontium-, barium fluoride nanoparticles and sodium chloride," Chemical Communications, [2005] 1767.

1.44 Bailey, D. and Wright, E., Practical Fiber Optics, Elsevier, Oxford, 2003.

1.45 Bass, Michael and Van Stryland, E.W., eds., Fiber Optics Handbook, McGraw-Hill, New York, 2002.

1.46 Senior, J.M., Optical Fiber Communications, Prentice Hall, Hertfordshire, 1992.

1.47 Mendez, A. and Morse, T.F., Specialty Optical Fibers Handbook, Elsevier, Burlington, MA, 2007.

1.48 Ainslie, B.J., "A Review of the Fabrication and Properties of Erbium-Doped Fibers for Optical Amplifiers," Journal of Lightwave Technology, 9 [1991] 220.

1.49 Townsend, J.E., Poole, S.B., and Payne, D.N., "Solution-Doping Technique for Fabrication of Rare Earth Doped Optical Fibres," Electronics Letters, 23 [1987] 329.

1.50 Tammela, S., Soderlund, M., Koponen, J., Philippov, V. and Stenius, P., "The Potential of Direct Nanoparticle Deposition for the Next Generation of Optical Fibers," Proceedings of SPIE Photonics West, 6116-16 [2006].

1.51 Dussardier, B., Blanc, W., and Monnom, G., "Luminescent Ions in Silica-Based Optical Fibers," Fiber and Integrated Optics, 27 [2008] 484.

1.52 Boivin, D., Fohn, T., Burov, E., Pasouret, A., Gonnet, C, Cavani, O., Collet, C. and Lempereur, S., "Quenching investigation on New Erbium Doped Fibers using MCVD Nanoparticle Doping Process," Proceedings of SPIE, 7580 [2010] 75802B-1.

CHAPTER II

ACTIVE NANOPARTICLES:

CHARACTERIZATION OF ALKALINE EARTH FLUORIDE NANOPARTICLES

In order to determine a material that could be homogeneously and easily incorporated into the core of an optical fiber preform, an understanding of the fundamental structural and optical characteristics of lanthanide doped alkaline earth fluoride materials in nanoparticle form was obtained through a series of physical and spectroscopic measurements. Calcium, strontium and barium fluoride nanoparticles were synthesized with varying levels of rare earth dopant for determination of the basic morphology and luminescent behavior of these nano-systems, as well as the local area environment of the lanthanide ion and thermally induced changes to the behavior.

Introduction

Why nanoparticles?

There are consistently acknowledged limitations for rare earth doped silica fiber produced via the conventional solution doping MCVD method:

1. Rare earth solubility is low in silica[2.1,2.2]
2. Rare earth concentration must remain low to avert clustering and subsequently, quenching effects of the rare earth ion emissions[2.1,2.2,2.3]
3. Scattering due to inhomogeneities in the core region result in fiber with high attenuation when compared to communication fiber[2.3,2.4]

Traditional solution doping uses alumina and rare earth salts as co-dopant materials as a means to incorporate the rare earth ions into the glass matrix, however, these limitations remain. Therefore, a material which could sufficiently deliver lanthanide ions to the core region of these fibers, while alleviating these spectroscopic challenges would be ideal, and led to this investigation of rare earth doped alkaline earth fluoride nanoparticles.

In order to address the difficulties of scattering effects of active optical fibers, rare earth doped nanoparticles were chosen for investigation. Nanoparticles are defined to be on the order of 1-100 nm, provide a wide range

of physical properties not found in their bulk counterparts and are readily doped with rare earth ions[2.5-2.8]. Their size proves to be advantageous for this application, as any dopant used in conventional fiber lasers and amplifiers should be sufficiently small enough to keep scattering loss within acceptable limits[2.4].

Additionally, nanoparticles can be augmented with organic ligands during synthesis to improve the solubility of the particles in an organic solvent, control particle growth, prevent clustering and in some cases, improve luminescence. Capping ligands are most commonly used due to the chemical stability they provide at extreme values of pH[2.9]. By coating the nanoparticles with surfactants or 'stabilizing ligands', the dispersability of the nanoparticles is increased, which aids in homogeneous incorporation of the materials into composite matrices such as polymers and glass[2.10,2.11].

The ligands used are typically comprised of a polar inorganic 'head' which coordinates to the nanoparticle surface and a nonpolar alkyl hydrocarbon 'tail'. For simplicity, a previously successful ligand used in the production of LaF_3 nanoparticles was chosen[2.10-2.12], ammonium di-n-octadectyldithiophosphate (ADDP), $[NH_4]$-$[S_2P(OC_{18}H_{37})_2]$, for use in this study. Lo et al.,[2.10] characterized lanthanide doped LaF_3 nanoparticles which were capped with di-n-octadectyldithiophosphate ligands and suggest the schematic depicted in Figure 2.1 represents this type of 'coated' nanoparticle.

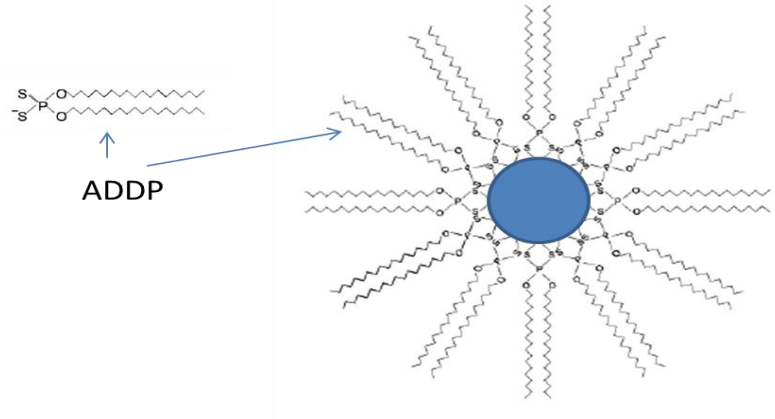

Figure 2.1. Schematic representation of ligand capped nanoparticle[2.10].

Why Alkaline Earth Fluorides?

The purpose for using alkaline earth fluorides (AEF_2) is two-fold: (1) the inherent optical characteristics of AEF_2 make them a preferred host for rare earth dopants and (2) known network modifier properties of AEs within glass matrices, make them a viable dopant material for active optical fiber.

A majority of the work on lanthanide/rare earth doped nanoparticles has focused on using $LaPO_4$[2.5,2.11], LaF_3[2.5,2.6,2.10-2.12], and a variety of yttrium based compounds[2.5] as the host material for the dopant ion. Fluorides are typically preferred as they are optically applicable because of their high transparency in wide wavelength ranges, low vibrational energies which minimizes the probability of non-radiative transitions and many fluorides have cubic structures, making them optically isotropic[2.6,2.13]. In particular, LaF_3 is often utilized because of the

additional advantage of ease of species exchange, i.e., a RE^{3+} ion readily substitutes for a La^{3+} ion in the host matrix. The vibrational energy of LaF_3 is lower than that of oxide counterparts (~350 cm^{-1} vs. ~1000 cm^{-1})[2.14,2.15] which additionally minimizes quenching of the excited state of the chosen rare earth ion.

Low vibrational energy is especially important for RE^{3+} ions emitting in the near infrared due to their propensity to quench via high energy vibrations[2.6]. Fluorides made with alkaline earth elements (Ca, Sr, Ba) exhibit comparable and in some cases, lower vibrational energy than LaF_3, making them viable and interesting candidates for optically active nanoparticle applications[2.7,2.16-2.18].

In order to address the difficulties associated with rare earth solubility and concentration effects, conventional solution doping involves the incorporation of aluminum to act as a network modifier in the glass network. Alkali and alkaline earth ions are incorporated into a glass network to act as modifiers as well. The alkaline earth ions occupy interstitial spaces within the glass structure and cause the creation of non-bridging oxygens (NBO), which results in a reduction in the overall connectivity of the glass network. This acts to improve the mass-transport- related properties of the glass and therefore, improve solubility of dopant ions[2.19,2.20].

Europium as a Spectral Probe

The trivalent europium ion, Eu^{3+}, is widely used as a probe to investigate the environment around lanthanide ions in different host materials due to its unique optical properties[2.21-2.23], in addition to being used practically as a red light emitter in various LED and phosphor applications[2.24].

The Eu^{3+} ion has a fluorescence spectrum which consists of transitions originating from the ^5D_J levels, in particular the $^5D_{0,}$ to the ^7F_J (J= 0-6) levels of the $4f^6$ configuration[2.21,2.25] (Figure 2.2). The $^7F_0$ ground state is considered non-degenerate as well as the emitting $^5D_0$ state, which results in a simple energy level structure (neither state is split by the crystal field) and straightforward information about the excited state[2.24]. Additionally, the emission and excitation transitions between the $^5D_0$ and ^7F_J (J >1) levels, can be used to identify any crystallographic or local area environment changes about the Eu^{3+} ion within a given host material. The splitting of the emission lines is dependent upon the symmetry of the ligand field about the Eu^{3+}, as it can remove the degeneracy of a given $^{2S+1}L_J$ term partially or completely. The Eu^{3+} ^7F_J levels are closely spaced, with energy level differences on the order of kT, so they are populated at room temperature unlike other lanthanides and well-defined spectral emissions exist when a sample is excited at 393 nm[2.26]. The intensity and splitting patterns of the resultant luminescent emission spectra are primarily indicative of the environment around the Eu^{3+} in the host, allowing for comparison of host material

to host material. The $^5D_0 \rightarrow {}^7F_J$ transitions are therefore considered a very suitable corollary to survey the transition probabilities of the rare earths in different host materials.

Transitions between levels of the $4f^n$ configuration technically are forbidden but this constraint is relaxed by perturbations by the host crystal (or glass) including local crystal symmetry and phonon spectrum[2.25]. Electric dipole transitions can be hypersensitive, that is their intensity is strongly dependent upon local structure (hence chemistry), when the $\Delta J = 0, \pm 2$ and such transitions are enhanced by crystal asymmetry. On the other hand, magnetic dipole transitions are insensitive to host crystal symmetry as there are no material-dependent factors in their linestrength. In the specific case of Eu^{3+}, the $^5D_0 \rightarrow {}^7F_2$ transition is electric dipole, with its intensity very sensitive to its surrounding. The hypersensitivity ratio, HR, is the relative emission spectral ratio of the electric dipole emission ($^5D_0 \rightarrow {}^7F_2$ for Eu^{3+}) to the magnetic dipole emission ($^5D_0 \rightarrow {}^7F_1$ for Eu^{3+}) and its value is a qualitative measure of the nature and symmetry of the rare earth ion within a lattice host. The hypersensitivity ratio will increase with increasing asymmetry within a crystal lattice. For Eu^{3+} emissions, the magnetic dipole transition, $^5D_0 \rightarrow {}^7F_1$, is used as the normalization peak for spectra comparison, due to this aforementioned lack of dependency on environment[2.26,2.27].

a.

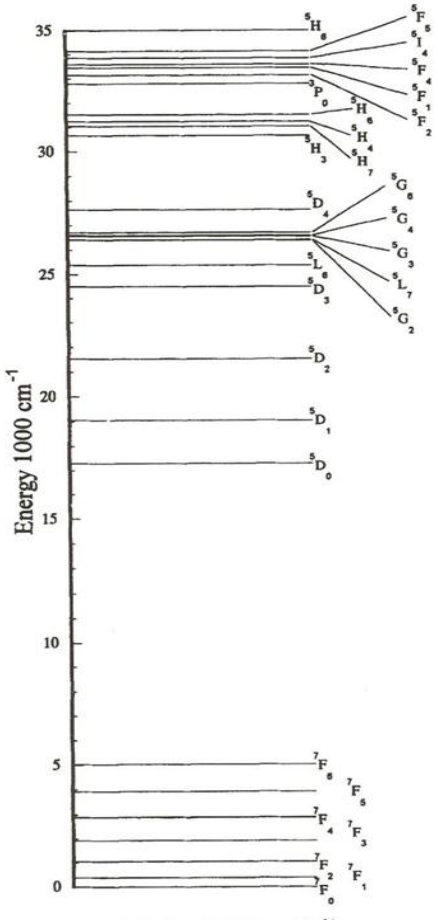

b.

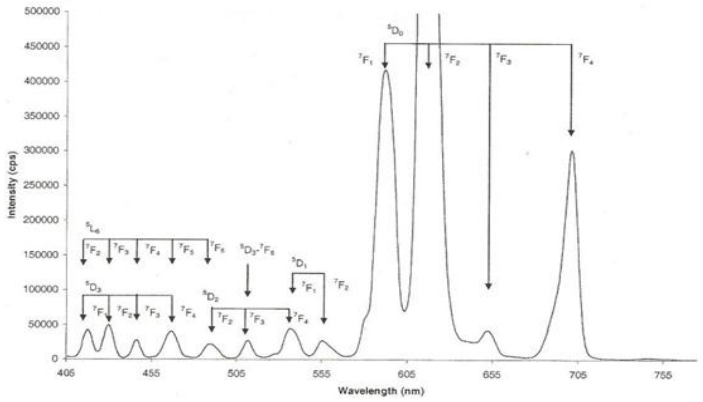

Figure 2.2. a) Trivalent europium (Eu^{3+}) Energy level diagram[2.26], **b)**Corresponding Eu^{3+} emission spectrum[2.28].

Lattice vibrations from the host crystal cause dopant ions to be displaced from their equilibrium positions and as a result, the electric field about the ion is altered. These vibrations are then coupled to the electronic levels of the system and are equivalent to an electron-phonon interaction, which can result in sidebands of the phonon frequency being induced on the electronic levels. In some instances, it is possible to identify these distinct sidebands in optical spectra which correlate directly to specific phonon frequencies associated with the host crystal[2.29].

By exciting a europium doped material at 613 nm (the $^5D_0 \rightarrow {}^7F_2$ electric dipole emission), a sideband feature/peak will appear on the higher energy side of the peak corresponding to the $^5D_0 \leftarrow {}^7F_0$ transition (~464 nm). The energetic difference between the two peaks is the vibrational or phonon energy of the host material[2.30] and is termed the phonon sideband (PSB)[2.26,2.30,2.31]. This provides an optical method to obtain the vibrational energies of the host materials to compare to Raman measurements. PSB gives specific information about the local influence of the host vibrations on the rare earth along with its environment[2.26].

Thermal Influence on Optical Properties of Nanoparticles

Beyond the scientific 'wow' factor of novel nanoscale materials, determining the practicality of these particles for use in various applications is necessary. Incorporating these materials into composites comprised of glass will require processing at elevated temperatures for extended periods of time. Therefore, the influence of thermal conditions on the internal structure and optical properties of the nanoparticles is of great interest. With structures on the order of a few nanometers, diffusion is expected to play a significant role in the resulting emission behavior of the nanoparticles.

DiMaio et al., determined that diffusion of a rare earth ion could be reasonably approximated using optical methods[2.32]. The photoluminescence emissions were used to approximate the severity of diffusion within structured LaF_3 nanoparticles. Europium doped LaF_3 core nanoparticles with varying shell thickness of undoped LaF_3 were used to study these effects. Core, one and two shell LaF_3 nanoparticles were heat treated at 650ºC in fifteen minute intervals and the emission spectra was monitored. At elevated temperatures it was found that the diffusion of the ions was significant enough to result in emission color changes from emissions of higher Eu^{3+} manifolds as a result of a reduction in concentration quenching of the Eu^{3+} ions and an approximated 1-dimensional diffusion coefficient on the same order of magnitude of their bulk counterparts was reported. This suggested the particles were stable for applications in

ambient conditions and the diffusion rate may be reduced with modifications to the core/shell structure. This study was used as a template for investigating the time at elevated temperature effects of the alkaline earth fluoride nanoparticles produced in this study.

Experimental Procedures

Nanoparticle Synthesis

Basic Core: Individual alkaline earth nitrates, $AE(NO_3)_2$, (Alfa Aesar), were dissolved in deionized water and added dropwise at a rate of ~0.5 ml/min, to a 250 rpm stirring, clear solution of 175 ml of 1:1 water:ethanol, 0.630 g ammonium fluoride, (NH_4F), and 3.07 g of ammonium di-n-octadecyldithiophosphate, (ADDP), $[NH_4]$-$[S_2P(OC_{18}H_{37})_2]$, maintained at 75ºC in a water bath. All batching proportions were calculated using an Excel™ spreadsheet equipped with the appropriate calculations to yield the correct molar ratios for synthesis (Appendix A). ADDP was produced in the lab, specifically for use in this synthesis process. The procedure and pertinent information about its production and behavior can be found in Appendix B.

It was observed that with each drop of $AE(NO_3)_2$ solution, an opaque 'spot' would appear and dissipate in the stirring solution, implying the formation of an insoluble product. Following the complete addition of the nitration solutions, the resulting mixture had a slightly opaque color and was allowed to stir in a water bath at 75ºC for 2 hours at 250 rpm. The solution was removed from the water bath, poured equally into 50ml centrifuge tubes (VWR International) and allowed to cool to room temperature. It was observed, upon cooling, solid white material precipitated out of solution and loosely settled to the bottom of the centrifuge tubes.

After cooling, cleaning of the solid material was completed using the following procedure. The solution/precipitant filled tubes were centrifuged (Damon/IEC Division CU-5000) at 3000 rpm for 15 minutes to separate solid product from solution. The excess, clear solution was discarded and an additional ~40 ml of equal parts water/ethanol was added to each centrifuge tube, sonicated (VWR Scientific Products Aquasonic Model 150HT) for ~20 minutes to re-suspend the solid material in solution and centrifuged for 15 minutes at 3000 rpm. The excess, clear solution was discarded and the solid, white precipitant was dried for ~24 hours over phosphorous pentoxide, P_2O_5, in a dessicator. The solid material was then dispersed by sonicating for 15 minutes following the addition of 5 ml of dichloromethane (Acros, anhydrous, AcroSeal, 99.9%), and precipitated with addition of 20 ml of ethanol (Acros, 200 proof). The solution was then centrifuged for 15 minutes at 3000 rpm, the excess, clear liquid was discarded and the resulting solid, white material was dried for 2 days over P_2O_5 in a desiccator.

Basic Core Doped: A combination of $AE(NO_3)_2$, (Alfa Aesar) and europium nitrate, $Eu(NO_3)_3 \bullet 6H_2O$, (Alfa Aesar, 99.9%) were dissolved in deionized water and added dropwise at a rate of ~0.5 ml/min, to a 250 rpm stirring, clear solution of 175 ml of 1:1 water:ethanol, 0.630 g ammonium fluoride, (NH_4F), and 3.07 g of ammonium di-n-octadecyldithiophosphate, (ADDP), $[NH_4]$-$[S_2P(OC_{18}H_{37})_2]$, maintained at 75ºC in a water bath. All batching proportions were calculated using an Excel™ spreadsheet equipped with the appropriate calculations to yield

the correct molar ratios for synthesis (Appendix A). ADDP was produced in the lab, specifically for use in this synthesis process. The procedure and pertinent information about its production and behavior can be found in Appendix B.

It was observed that with each drop of $AE(NO_3)_2$ solution, an opaque 'spot' would appear and dissipate in the stirring solution, implying the formation of an insoluble product. Following the complete addition of the nitration solutions, the resulting mixture had a slightly opaque color and was allowed to stir at 75ºC in a water bath for 2 hours at 250 rpm. The solution was removed from the water bath, poured equally into 50 ml centrifuge tubes (VWR International) and allowed to cool to room temperature. It was observed, upon cooling, solid white material precipitated out of solution and loosely settled to the bottom of the centrifuge tubes.

After cooling, cleaning of the solid material was completed using the following procedure. The solution/precipitant filled tubes were centrifuged (Damon/IEC Division CU-5000) at 3000 rpm for 15 minutes to separate solid product from solution. The excess, clear solution was discarded and an additional ~40 ml of equal parts water/ethanol was added to each centrifuge tube, sonicated (VWR Scientific Products Aquasonic Model 150HT) for ~20 minutes to re-suspend the solid material in solution and centrifuged for 15 minutes at 3000rpm. The excess, clear solution was discarded and the solid, white precipitant was dried for ~24 hours over phosphorous pentoxide, P_2O_5, in a

desiccator. The solid material was then dispersed by sonicating for 15 minutes following the addition of 5 ml of dichloromethane (Acros, anhydrous, AcroSeal, 99.9%), and precipitated with addition of 20 ml of ethanol (Acros, 200 proof). The solution was then centrifuged for 15 minutes at 3000rpm, the excess, clear liquid was discarded and the resulting solid, white material was dried for 2 days over P_2O_5 in a desiccator.

Europium Core Doped AEF_2 with Undoped AEF_2 Shells: : A combination of $AE(NO_3)_{2,}$ (Alfa Aesar) and europium nitrate, $Eu(NO_3)_3 \bullet 6H_2O$, (Alfa Aesar, 99.9%) were dissolved in deionized water and added dropwise at a rate of about 0.5 ml/min, to a 250 rpm stirring, clear solution of 175 ml of 1:1 water:ethanol, 0.630 g ammonium fluoride, (NH_4F), and 3.07 g of ammonium di-n-octadecyldithiophosphate, (ADDP), $[NH_4]$-$[S_2P(OC_{18}H_{37})_2]$, maintained at 75ºC in a water bath. All batching proportions were calculated using an Excel™ spreadsheet equipped with the appropriate calculations to yield the correct molar ratios for synthesis (Appendix A). Following the complete addition of the nitrate solutions, the resulting mixture had a slightly opaque color and was allowed to stir at 75ºC for 20 minutes at 250 rpm to form the core particles doped with 20 mole percent europium. A portion of the stirring solution was then removed by bulb syringe, was equally portioned into 50 ml centrifuge tubes (VWR International) and set aside to cool to room temperature. Next, an aqueous NH_4F solution and an $AE(NO_3)_2$ solution were added alternately to the still stirring core solution, to yield a layer of undoped AEF_2, referred to as a core/shell

nanoparticle. This process was repeated until a total of three shells were grown. It was observed, upon cooling, solid white material precipitated out of solution and loosely settled to the bottom of the centrifuge tubes with each step.

After cooling, cleaning of the solid material was completed using the following procedure. The solution/precipitant filled tubes were centrifuged (Damon/IEC Division CU-5000) at 3000 rpm for 15 minutes to separate solid product from solution. The excess, clear solution was discarded and an additional ~40 ml of equal parts water/ethanol was added to each centrifuge tube, sonicated (VWR Scientific Products Aquasonic Model 150HT) for ~20 minutes to re-suspend the solid material in solution and centrifuged for 15 minutes at 3000 rpm. The excess, clear solution was discarded and the solid, white precipitant was dried for ~24 hours over phosphorous pentoxide, P_2O_5, in a desiccator. The solid material was then dispersed by sonicating for 15 minutes following the addition of 5 ml of dichloromethane (Acros, anhydrous, AcroSeal, 99.9%), and precipitated with addition of 20 ml of ethanol (Acros, 200 proof). The solution was then centrifuged for 15 minutes at 3000 rpm, the excess, clear liquid was discarded and the resulting solid, white material was dried for 2 days over P_2O_5 in a desiccator.

X-Ray Diffraction (XRD)

In order to determine the crystallinity of the resultant basic core nanoparticles and verify phase purity, x-ray diffraction was performed on the

dried powders using a Scintag XDS 4000 using CuK_{α} radiation. Crystalline phases within a material can be identified by their unique diffraction pattern. Diffraction occurs from crystals oriented at the angle, Θ, that satisfies Bragg's law: $2d\sin\Theta = n\lambda$. In XRD, a powder sample is bombarded with a monochromatic beam at an appropriate wavelength, λ, and a diffracted beam results at the appropriate, Θ, to satisfy Bragg's equation. The final diffraction pattern corresponds to specific interplanar spacing and identifies the crystallinity and composition of the sample using JCPDS standards[2.32,2.33].

Transmission Electron Microscopy (TEM)

High resolution transmission electron microscopy (HRTEM) was performed on the nanoparticle powders to provide nanometer scale images which were used to visually determine particle size and shape. Less than 0.001 g of each powder type was suspended in ~10 ml of tetrahydrafuran (Acros, anhydrous, Acroseal, 99.9%), and a single drop of the solution was placed on a 200 mesh copper grid (Ted Pella, Inc., Support films, formvar/carbon), allowed to dry and used for analysis. HRTEM was performed on a Hitachi H9500 operating at an accelerating voltage of 300kV.

Raman Spectroscopy

Raman spectroscopy is a method to study vibrational modes of a given material. Here, it was used to determine the vibrational energy due to lattice vibrations of the alkaline earth fluorides in nanoparticle form.

A laser excites/interacts with phonons in the material, causing scattering (Raman shift, reported in cm^{-1}), which results in the incident laser photons being shifted with respect to their incident energy. The shift is a direct measure of the vibrational energy of the system[2.34,2.35]. Nanoparticles were measured with a Senterra 178 Raman Microscope (Bruker Optics) operating at a laser wavelength of 532 nm, laser power of 20 mW and integration time of 100 s.

Photoluminescence Measurements

Emission and excitation spectra were determined for all europium doped AEF_2 nanoparticle samples using a Jobin Yvon Fluorolog 3 specrofluorometer with a double grating configuration, an excitation bandpass of 2 nm and a scan rate of 0.1-1 nm/min. Emission scans were perfomed at an excitation wavelength of 393 nm. Phonon sideband (PSB) measurements were performed at an emission wavelength of 613 nm.

Results and Discussion

Physical Characterization: Morphology, Size and Vibrational Energy

Particles were synthesized using a modified version of solution/precipitation synthesis previously developed[2.36,2.37] for LaF_3 nanoparticles. Calcium, strontium and barium fluoride nanoparticles were produced and ADDP was used as the ligand. The ligand aids in controlling the growth of the particles by weakly coordinating to the host ions, but they coordinate strongly enough to deter aggregation[2.38]. The presence of the ligand also allows dispersability of the materials in organic solvents such as THF and dichloromethane (DCM).

Morphology and Particle Size Analysis

Figures 2.3-2.5 are representative TEM images of alkaline earth fluoride nanoparticles produced. The shape of the individual nanoparticles, particularly strontium fluoride hosted nanoparticles in figure 2.4, aid in demonstrating the cubic nature of the fluoride host. Particle size analysis was completed by measuring a broad sampling of identified particles ($n > 150$) via TEM imaging. The average particle size of the alkaline earth nanoparticles is shown to increase with increasing atomic radius of alkaline earth ion (Table 2.1). It should be noted that this method was not optimized kinetically for uniform particle growth, however, the aim here was to produce sufficiently small particles (<50 nm) for later use.

Verification of Crystallinity

Figure 2.6 shows the XRD patterns of the alkaline earth fluoride nanoparticles. The patterns exhibit prominent peaks in accordance with JCPDS standards (35-0816, 06-0262, 04-0452, and 41-1443) of the cubic CaF_2, SrF_2 and BaF_2 crystals, which verifies the successful synthesis of the individual AEF_2 nanoparticles.

Vibrational Energy of Alkaline Earth Fluorides

In order to further verify the successful synthesis of alkaline earth fluoride nanoparticles, Raman analysis was completed on the individual as-made, undoped nanopowders as well as heat treated samples of the undoped powders. The Raman spectra of each of the undoped alkaline earth fluoride nanoparticles are depicted in figures 2.7-2.9. A well-defined change in vibrational energy (VE) is demonstrated with mass for the fluoride systems ($VE_{Ba-F} < VE_{Sr-F} < VE_{Ca-F}$). Values correlate well with published values (table 2.2) and the trend is corroborated by different measurement techniques[2.42-2.44].

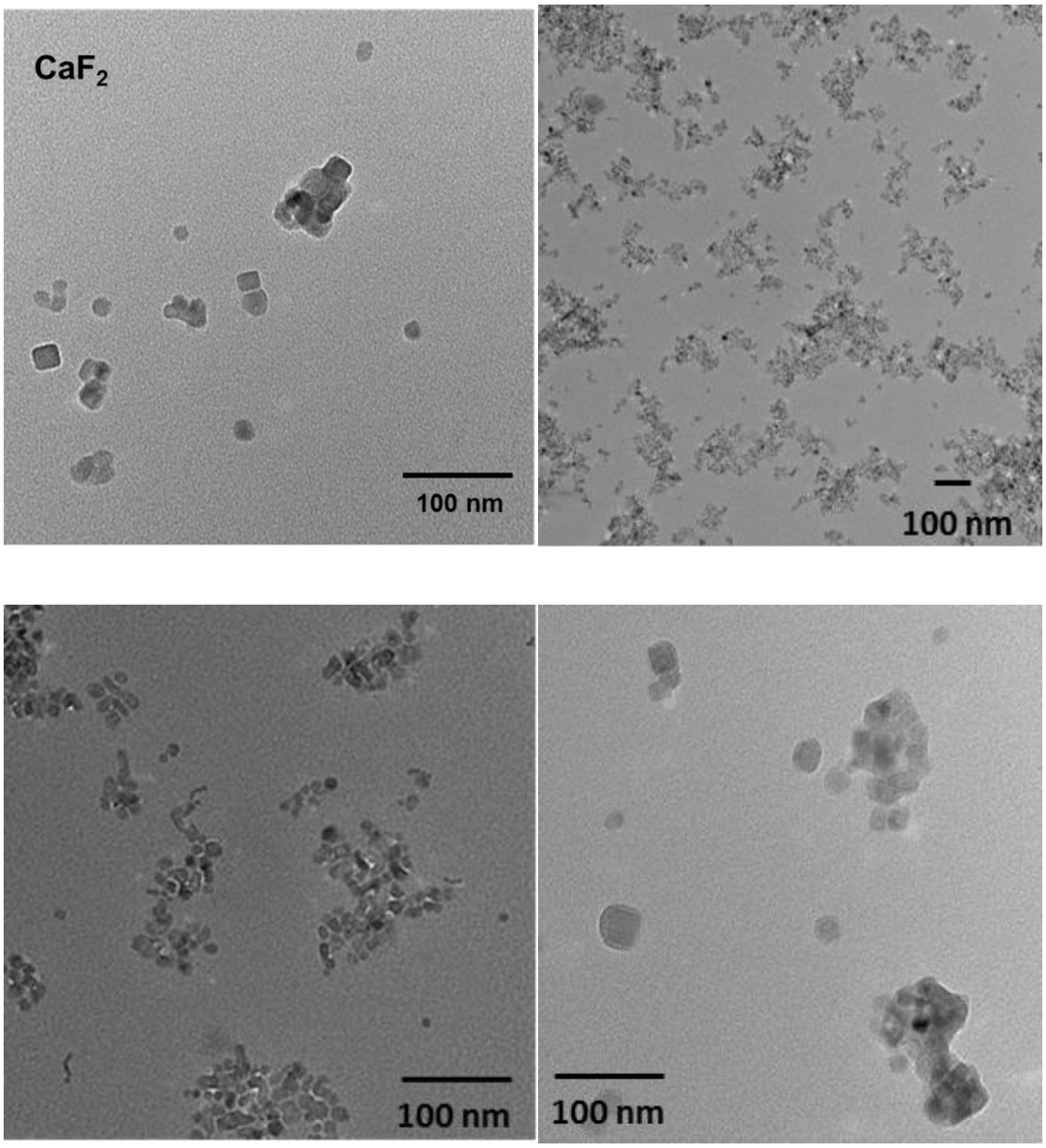

Figure 2.3. TEM images of as-made calcium fluoride, CaF_2, nanoparticles.

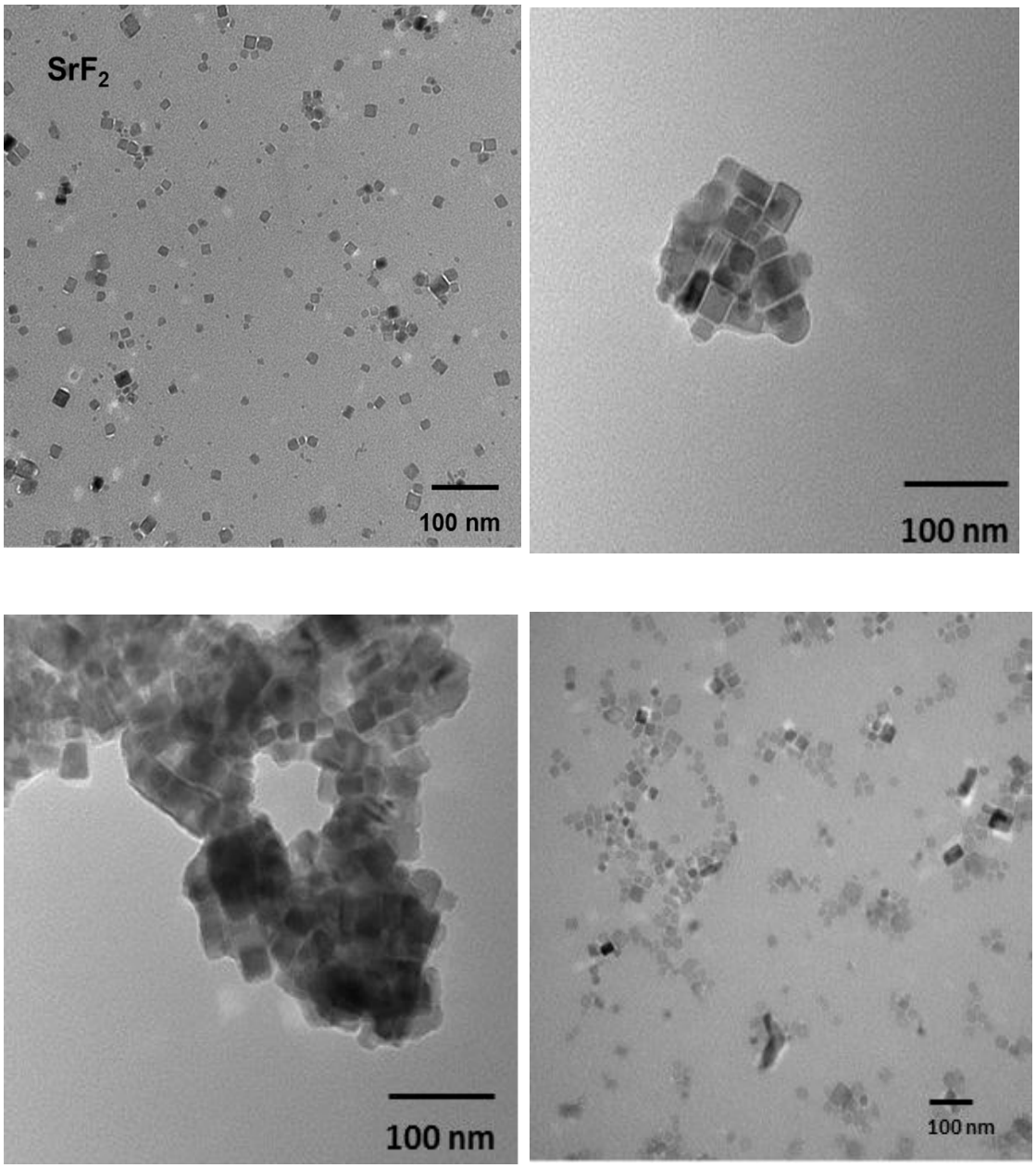

Figure 2.4. TEM images of as-made strontium fluoride, SrF_2, nanoparticles.

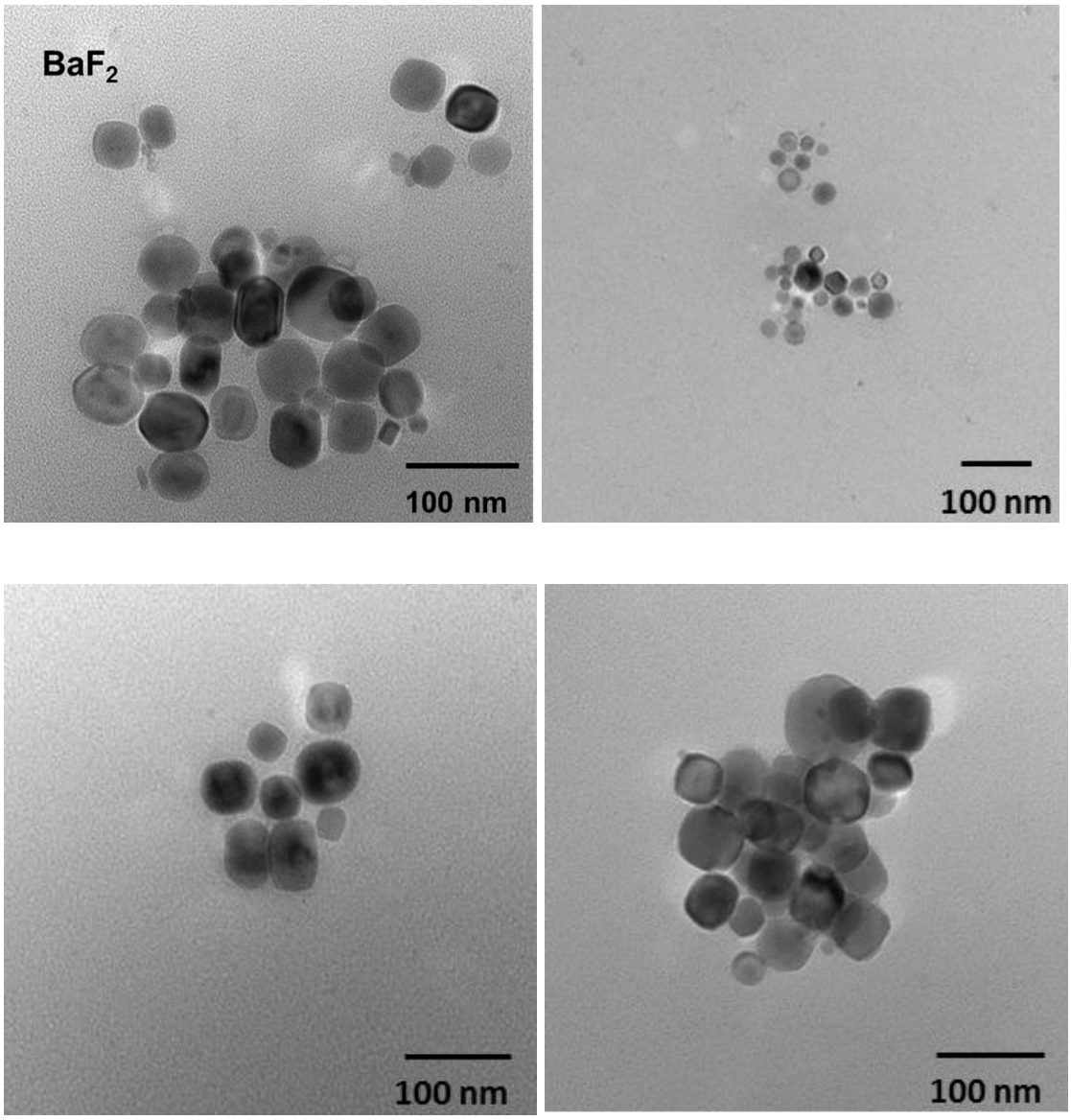

Figure 2.5. TEM images of as-made barium fluoride, BaF_2, nanoparticles.

Table 2.1

Alkaline Earth Fluoride Nanoparticle Size Analysis

	CaF_2	SrF_2	BaF_2
Average Size (nm)	**9.2**	**19.5**	**24.3**
Standard Deviation	**1.9**	**4.3**	**5.8**
Mode (nm)	**8.4**	**17.6**	**20.9**
Median (nm)	**8.4**	**18.5**	**23.3**

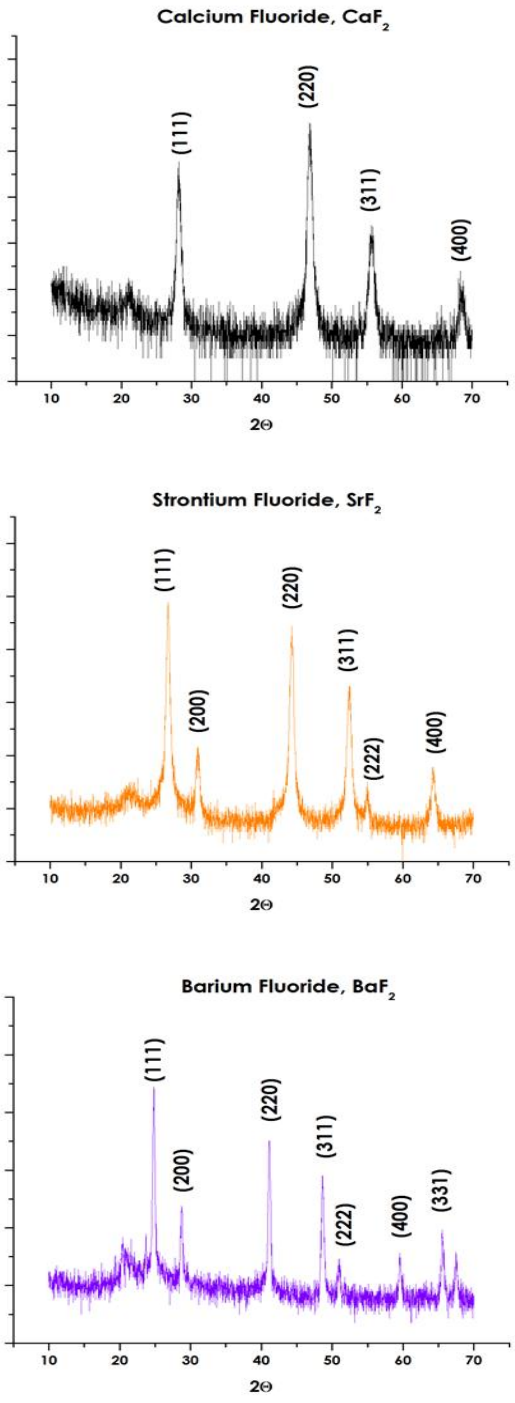

Figure 2.6. X-Ray diffraction patterns indicate a match with fluorite crystal structure of CaF_2, SrF_2, and BaF_2.

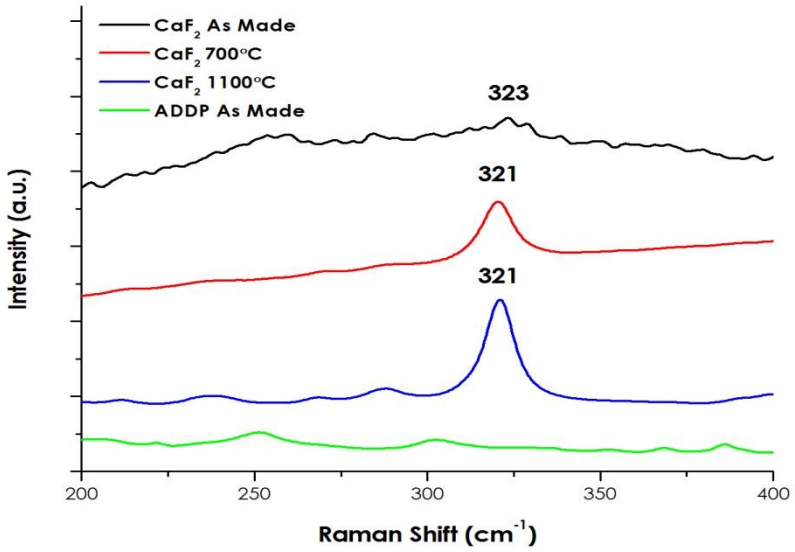

Figure 2.7. Raman spectra for undoped CaF_2 nanoparticles.

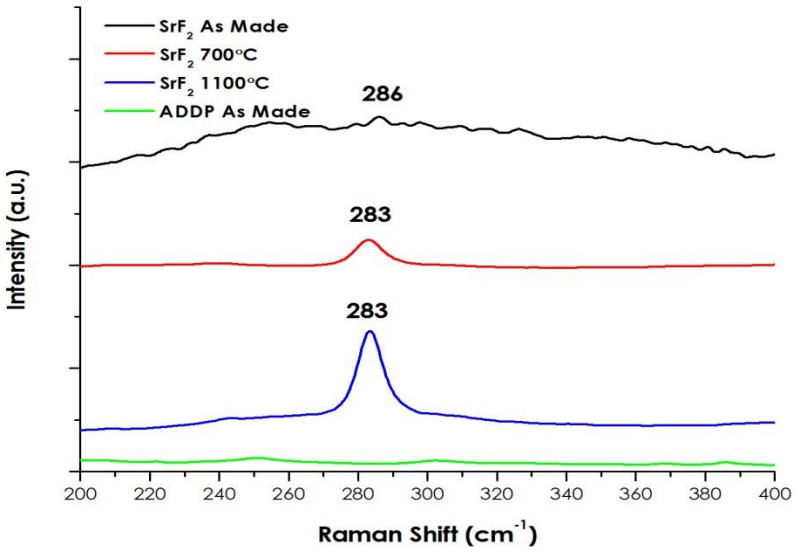

Figure 2.8. Raman spectra for undoped SrF_2 nanoparticles.

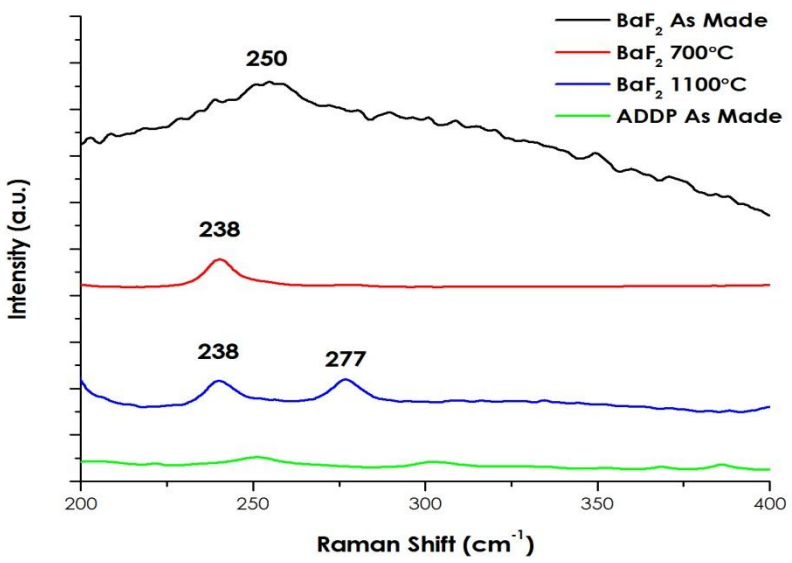

Figure 2.9. Raman spectra for undoped BaF_2 nanoparticles.

Table 2.2

Summary of Raman Vibrational Energies for Alkaline Earth Fluoride Nanoparticles

Host Material	As Measured (cm^{-1})	Reported Value (cm^{-1})	Reference
CaF_2	320	323	2.39
SrF_2	280	285	2.40
BaF_2	238	240	2.41

Emission Behavior

Calcium, Strontium and Barium fluoride nanoparticles were doped separately with 5, 15 and 25 mole percent europium and their photoluminescence was measured at an excitation wavelength of 393 nm. The resulting spectra (normalized to the 590 nm transition) are summarized in figure 2.10. The signature emissions of Eu^{3+} are clearly demonstrated with single peaks at 590 and 610 nm. In comparing the 5 mole percent Eu^{3+} doped samples (figure 2.10a), the CaF_2 nanoparticles show a similar site environment between the $^7F_1$ and $^7F_2$ levels, while the SrF_2 and BaF_2 exhibit a marked difference in these two emissions. The $^5D_0 \rightarrow {}^7F_4$ emission (~700nm) for each of the individual lattices best indicates the difference between the alkaline earth hosts, as the spectral linewidth narrows from host to host, and the extent of the resultant splitting of the emission inverts which implies a change in the ligand field about the Eu^{3+} ions within the host crystal. This difference in behavior correlates to the change in host ion size- as the radius of the ion increases, the 'area' influenced by the ligand field associated with the ion increases, and impacts the local environment of the Eu^{3+} ion in the lattice. In figures 2.10b and 2.10c, there are increasing electric dipole $^7F_2$ emissions for the SrF_2 and BaF_2 nanoparticles while the CaF_2 emissions remain relatively constant. The low intensity emissions from the $^5D_1$ manifold are seen in the inset portions of figure 2.10 at ~536nm ($^5D_1 \rightarrow {}^7F_1$) and ~554nm ($^5D_1 \rightarrow {}^7F_2$). These emissions appear to decrease with increasing europium content. Eu^{3+} transitions are sensitive to

quenching (reduction in emission and therefore, decrease in emission intensity) due to dipole-dipole interactions and the $^5D_1$, $^5D_2$ and $^5D_3$ manifolds have negligible visible emission when concentrations of Eu^{3+} are greater than about three percent[2.26,2.37].

In order to assess the differences in environment for the different alkaline earth fluorides, the hypersensitivity ratio (HR) for each of the nanoparticle types was calculated and plotted as a function of europium concentration (figure 2.11). The environment for the Eu^{3+} in the CaF_2 is markedly different from the SrF_2 and BaF_2 and the HR is seen to remain relatively constant (~1), indicating a consistent environment around the Eu^{3+} ion, despite the increase in europium content. There is a slight increase in HR with increasing europium content for the SrF_2 and BaF_2 nanoparticles, which indicates an increase in asymmetry as a result. The difference in behavior between the hosts may be explained by the differences in host ion size; the incorporation of larger amounts of Eu^{3+} within the smaller Ca^{2+} sites (r_{Ca} =0.112 nm) is more influenced by the electric field about the dopant ion as a result of the required charge compensation, therefore the electric charges about the Eu^{3+} ion are in closer proximity to one another and increasing the amount of Eu^{3+} does not change the electric dipole transition ($^5D_0 \rightarrow {}^7F_2$) significantly. Whereas, the larger diameter host ions of the Sr^{2+} (r_{Sr} =0.125 nm) and Ba^{2+} (r_{Ba} = 0.142 nm) are more influenced with the increase in required charge compensation as a result of the presence of more Eu^{3+} ions.

This difference in emission behavior between the host ions demonstrates the ability to control/engineer the spectral behavior of the rare earth ion by the choice of alkaline earth as well as the dopant level. This provides a potential tool for tailoring these nanoparticles for specific emissions when used within glass preforms.

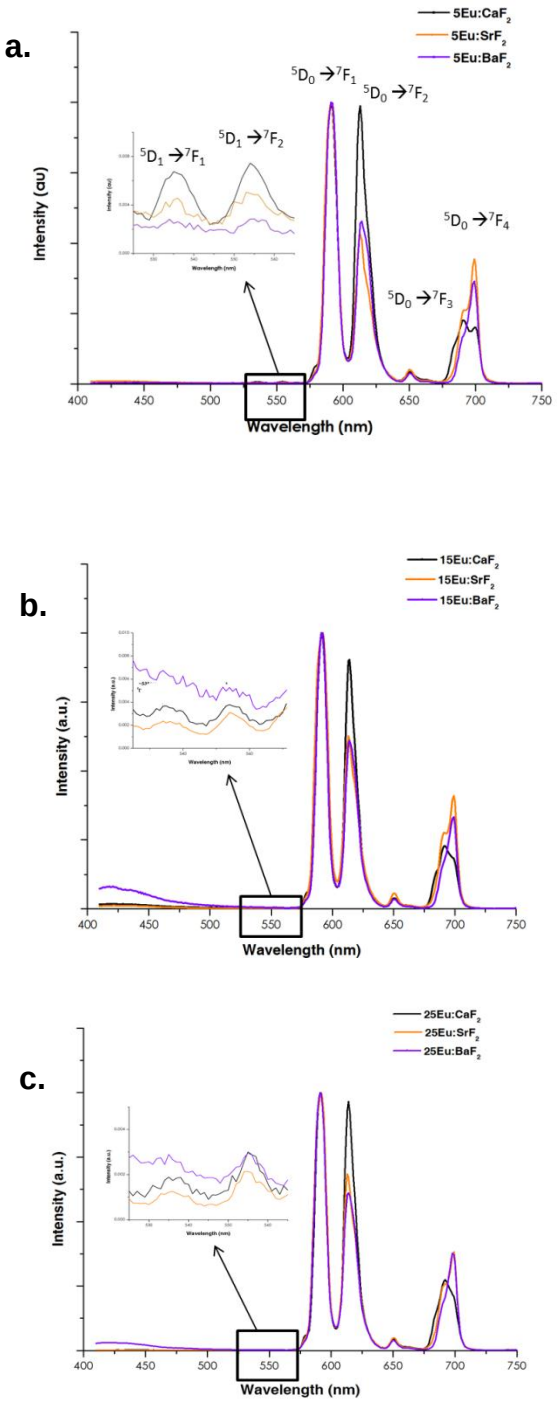

Figure 2.10. Emission spectra of AEF_2 nanoparticles doped with europium a) 5 mol% b) 15 mol% c) 25 mol%.

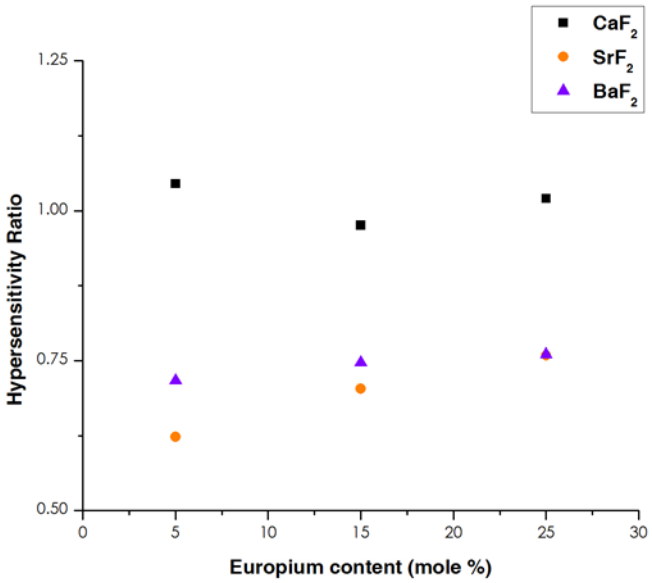

Figure 2.11. Effect of europium concentration on hypersensitivity ratio

Phonon Energy Assessment

The vibrational energy of the host lattice for the Eu^{3+} can be determined using the excitation of its hypersensitive peak, $^5D_0 \rightarrow {}^7F_2$ (λ_{em} = 613 nm). The resulting excitation spectra for a sample doped with europium at an emission wavelength of 613 nm will yield a peak at a wavelength of ~464 nm (21551 cm^{-1}) and the phonon sideband is defined as a shoulder/peak on the higher energy side of the hypersensitive peak. The energetic difference between these two peaks is then defined to be the vibrational or phonon energy of the host material[2.30].

The phonon sideband excitation spectra (λ_{em} = 613 nm) for various doping levels of Eu^{3+} in AEF_2 nanoparticles and the corresponding change in energy with respect to the 464 nm peak are shown in figures 2.12-2.14. The wavelength (x-axis) is reported in cm^{-1} to allow for calculation of the energy difference.

The sideband for CaF_2 becomes more distinct with increasing europium content, with an average phonon energy of 295 cm^{-1}. The SrF_2 is found to have an average value of 276 cm^{-1} and the BaF_2 has an average value of 255 cm^{-1}. The values calculated here vary by less than two percent of each other and indicate a well-defined trend with mass:

$$BaF_2 < SrF_2 < CaF_2$$

These values and this trend corroborates with previously published values[2.39-2.41] and match well with measured values found via Raman spectroscopy on undoped alkaline earth nanoparticle powders (Table 2.2).

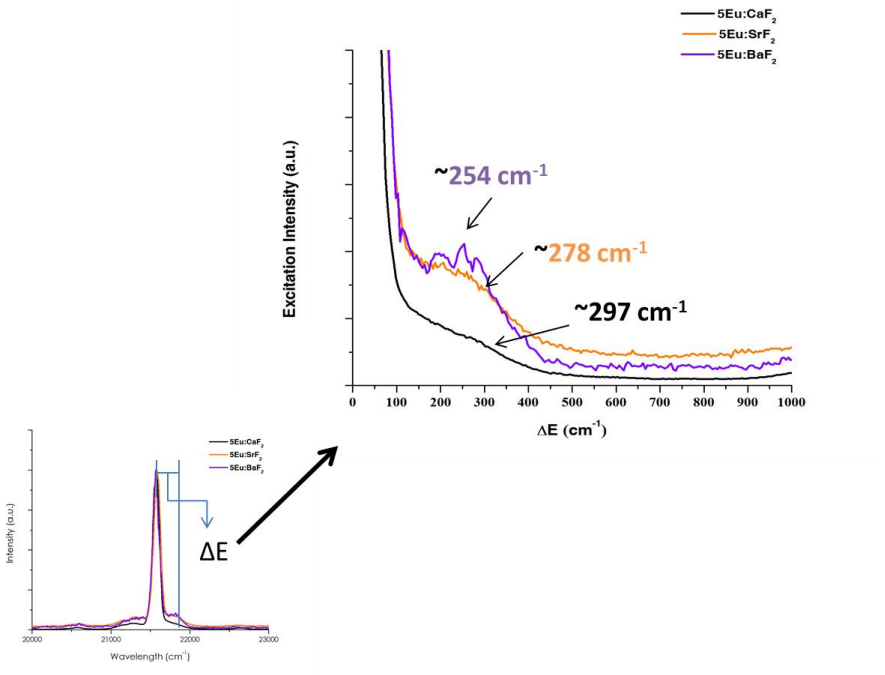

Figure 2.12. PSB excitation spectra and corresponding ΔE_{464} for 5Eu:AEF_2 nps

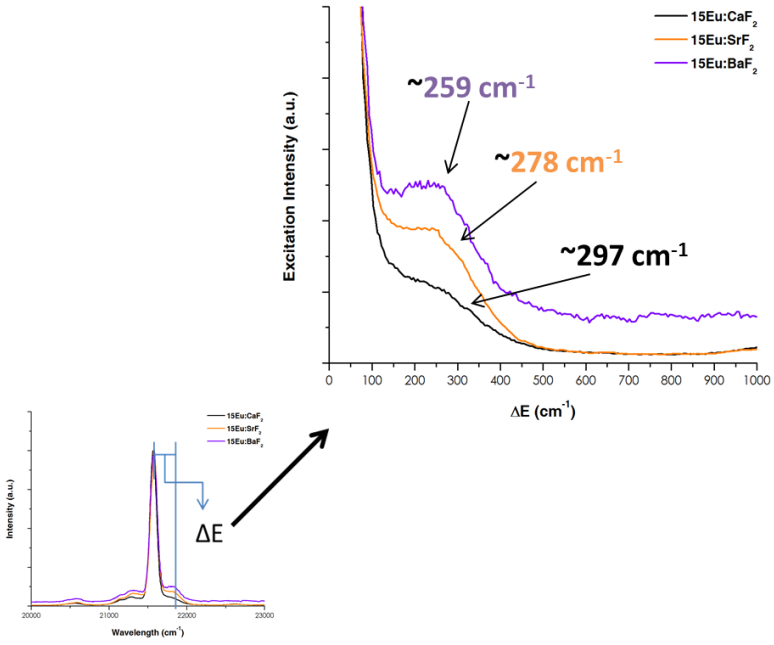

Figure 2.13 PSB excitation spectra and corresponding ΔE_{464} for 15Eu:AEF_2 nps

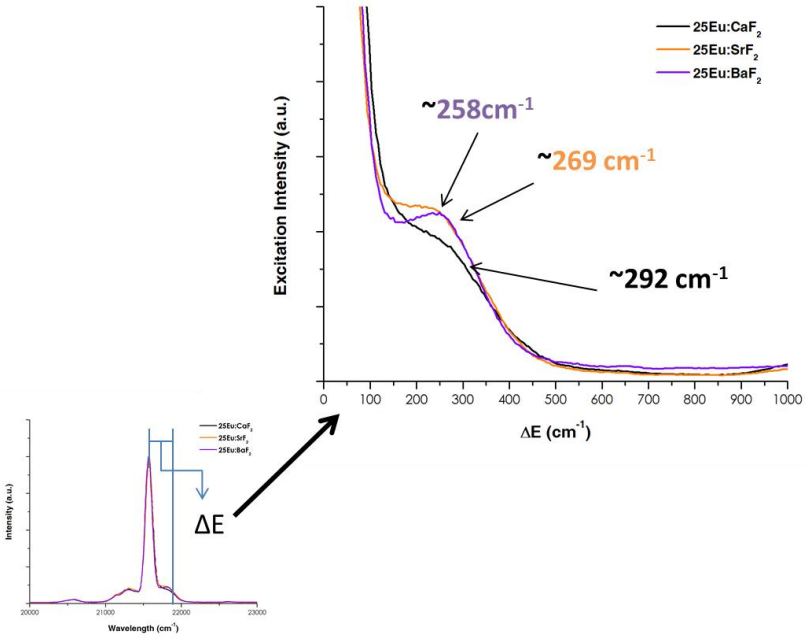

Figure 2.14. PSB excitation spectra and corresponding ΔE_{464} for 25Eu:AEF_2 nps

Thermal Effects on Optical Behavior of Eu:AEF_2 nanoparticles

Understanding the effects that elevated temperatures will have on the emission and structural characteristics of nanoparticles is necessary for further utilization of these materials in composite systems. In order to analyze these effects in Eu:AEF_2 nanoparticles a replicate experiment to the LaF_3 study detailed earlier by DiMaio et al.,[2.37] was completed for these nanoparticles.

Twenty mole percent europium doped AEF_2 nanoparticles were individually produced with three additional layers or shells of undoped AEF_2 added in stages. To eliminate batch to batch variation, each set of particles was produced from the same core batch, i.e. 20Eu:CaF_2 nanoparticles (core) were made and three additional layers of undoped CaF_2 were added in stages. Upon the completion of each stage, a portion of the particles was removed to isolate each type of particle: core (20Eu:CaF_2), one shell (core with one CaF_2 addition), two shell (core with two CaF_2 additions) and three shell (core with three CaF_2 additions). Samples were then heat treated at 650ºC in fifteen minute intervals, for a total of 75 minutes. Following each time interval, photoluminescence was measured.

Particle Size Analysis

Particle size analysis of the core and core/shell 20Eu:AEF_2 nanoparticles produced was completed by measuring a broad sampling of identified nanoparticles (n > 100) via TEM imaging. The average particles sizes for each type and host lattice are summarized in Table 2.3. They show the self-shelled particles have average diameters progressively increasing from the original core diameter and particle size distributions coincide with those reported by Jacobsohn et al.,[2.13,2.45] It should be noted that this synthesis method for core/shell AEF_2 nanoparticles was not optimized kinetically for uniform particle growth, however, the aim here was to produce europium core doped particles with increasing amounts of undoped host material. This was verified by the particle size analysis, therefore, the particles were used in this experiment to further understand the thermal influence on europium emission behavior when incorporated into alkaline earth nanoparticles.

TABLE 2.3

Average Size in nm of Core and Core/Shell

Alkaline Earth Fluoride Nanoparticles

	Core	1 Shell	2 Shells	3 Shells
Eu:CaF_2	8.3	10.7	13.9	35
Eu:SrF_2	10.2	11.4	12.2	24.2
Eu:BaF_2	20	35.8	68.2	105.3

In order to best analyze the diffusion behavior in these nanoparticles, the alkaline earth fluorides emission spectra as they are progressively heat treated and hypersensitivity ratios are assessed individually, then the behavior of each type of nanoparticle are compared to assess the differences (if any) in alkaline earth host material.

Calcium Fluoride, CaF_2

The emission spectra (λ_{ex} = 393 nm) and representative TEM images for the individual particle types of 20Eu:CaF_2 are seen in figures 2.15 and 2.16. The core particles are found to have an average particle size of ~8 ± 1 nm. There is a steady increase in particle size with the addition of undoped CaF_2, (Table 2.3), and the increase and distribution is similar to that reported by Jacobsohn et al.[2.13]

In all four emission spectra, the $^5D_0$ signature transitions are consistently present, with a general overall increase in intensity seen with increasing time at temperature. Upon looking at the overall emission behavior as a function of size, the 610 nm emission is noted to increase with the introduction of undoped shells of CaF_2. The hypersensitivity ratio is calculated and presented in figure 2.17. The difference in hypersensitivity ratios between particle type (core vs. 1 shell vs. 2 shell, vs. 3 shell) indicates that the environment about the Eu^{3+} ion is different for each particle type and is especially apparent in the 3 shell case. There is a distinct difference seen in the particles with largest volume of undoped CaF_2 available to the Eu^{3+}. The hypersensitivity here changes, indicating the environment about the rare earth is more asymmetric as more volume is available for the Eu^{3+} to diffuse into, as well as the more time the Eu^{3+} is given to diffuse from the core to the surface of the nanoparticle. This induced concentration gradient with the additional volume of undoped material allows for the relief of high concentration effects seen in the smaller particles and the

change in HR and emissions. This indicates a progressive movement/diffusion of the Eu^{3+} within the nanoparticle itself- increased intensity as a result of a decrease in concentration as the Eu^{3+} ions diffuse/ 'spread out' to alleviate Eu^{3+} ion-ion quenching effects which is evidenced by the increased intensity of the 610nm emission with increasing available undoped volume..

Upon further examination of the 2 shell and 3 shell emission spectra (figure 2.16), a broad transition peak is seen at approximately ~424 nm. This peak emission corresponds to the $4f^7 \rightarrow 4f^6 5d^1$ transition of the Eu^{2+} ion and is broad due to the influence of lattice vibrations of the local surroundings on the 5d wave function of the ion, which is not shielded from adjacent ligand fields by the 5s and 5p electrons[2.46]. This reduction of $Eu^{3+} \rightarrow Eu^{2+}$ ion in this host material is a well-documented phenomenon in bulk[2.47-2.49] CaF_2 and nanocrystal[2.47,2.50] CaF_2 form. The Eu^{2+} emissions in the 2 shell sample reach maximum intensity after 30 minutes at temperature, while the Eu^{2+} emissions decrease as the amount of heat treatment time increases. To further understand the interplay between the Eu^{3+} and Eu^{2+} within these samples, the ratio of their emissions is plotted in Figure 2.18. The Eu^{2+} emission is not seen in either as made sample(unfired), and both samples demonstrate a decrease in Eu^{2+} emissions as the emissions due to the hypersensitive Eu^{3+} transition increase. This implies a greater stability of Eu^{3+} in these materials as well as a conversion to behavior similar to that of the bulk. Hong and Kawano[2.48] Eu^{3+} doped thin films heated to 600ºC resulted in strong Eu^{2+} photoluminescence intensities at 425 nm and large concentration

quenching at Eu^{3+} doping levels greater than one mole percent. The rare earth doped compounds are not believed to be decomposed at the high temperature because the influence of crystal fields of the ligand ions about the RE^{3+} and due to the high dissociation energies between alkaline earth and fluorine ions. They attribute the strong Eu^{2+} photoluminescence as a result of the ease of substitution for Eu^{2+} (r_{Eu2+} = 0.125 nm) into a Ca^{2+} site (0.112 nm). Luminescence peaks associated with the $^5D_0$ manifold of Eu^{3+} were seen to increase with temperature as well.

Pandey et al.,[2.47] report a similar behavior in nano CaF_2:Eu phosphors. They found that during heating, in air, the conversion of $Eu^{3+} \rightarrow Eu^{2+}$ began at ~573K (500ºC) and reached a maximum at ~873K (600ºC). After prolonged heating at ~973K (700ºC), the europium containing nanocrystals are reported to agglomerate and the sample was converted to 'bulk', as the sample no longer contains Eu^{2+} emission and the Eu^{3+} emission spectra is similar to that of their bulk CaF_2 samples.

Luo et al.,[2.49] addressed the reduction of $Eu^{3+} \rightarrow Eu^{2+}$ in glass ceramics containing SrF_2 crystals. Eu^{2+} emissions are greatly influenced by composition and structure of the host material. When trivalent Eu ions are doped into bulk materials containing AE^{2+}, Eu^{3+} replaces the AE^{2+} ion. In order to keep charge balance, two Eu^{3+} ions substitute for three AE^{2+} ions to form an $Eu_{AE}^{\bullet}$ defect and one cation vacancy with two negative charges, $V_{AE}^{''}$ is created. The vacancy

acts as a donor electron while the $Eu_{AE}^{\bullet}$ defect becomes an acceptor of electrons. By thermal stimulation, the electrons in the vacancy defect, $V_{AE}^{''}$ were transferred to a $Eu_{AE}^{\bullet}$ site and Eu^{3+} ions reduce to Eu^{2+} ions. In Kroger-Vink notation, the reactions for the calcium fluoride nanoparticles are:

$$3Ca_{Ca} + 2Eu^{3+} = 3Ca^{2+} + 2\,Eu_{Ca}^{\bullet} + V_{Ca}^{''}$$

$$V_{Ca}^{''} = V_{Ca}^{x} + 2e^{-}$$

$$2\,Eu_{Ca}^{\bullet} + 2e^{-} = 2Eu_{Ca}^{x}$$

$$3Ca_{Ca} + 2Eu^{3+} = 3Ca^{2+} + 2Eu_{Ca}^{x} + V_{Ca}^{''}$$

Verification and quantification of the amount of Eu^{2+} by other measurement techniques was attempted (Appendix C), however, this was an anomalous case and was noted but was not pertinent for pursuit in this study.

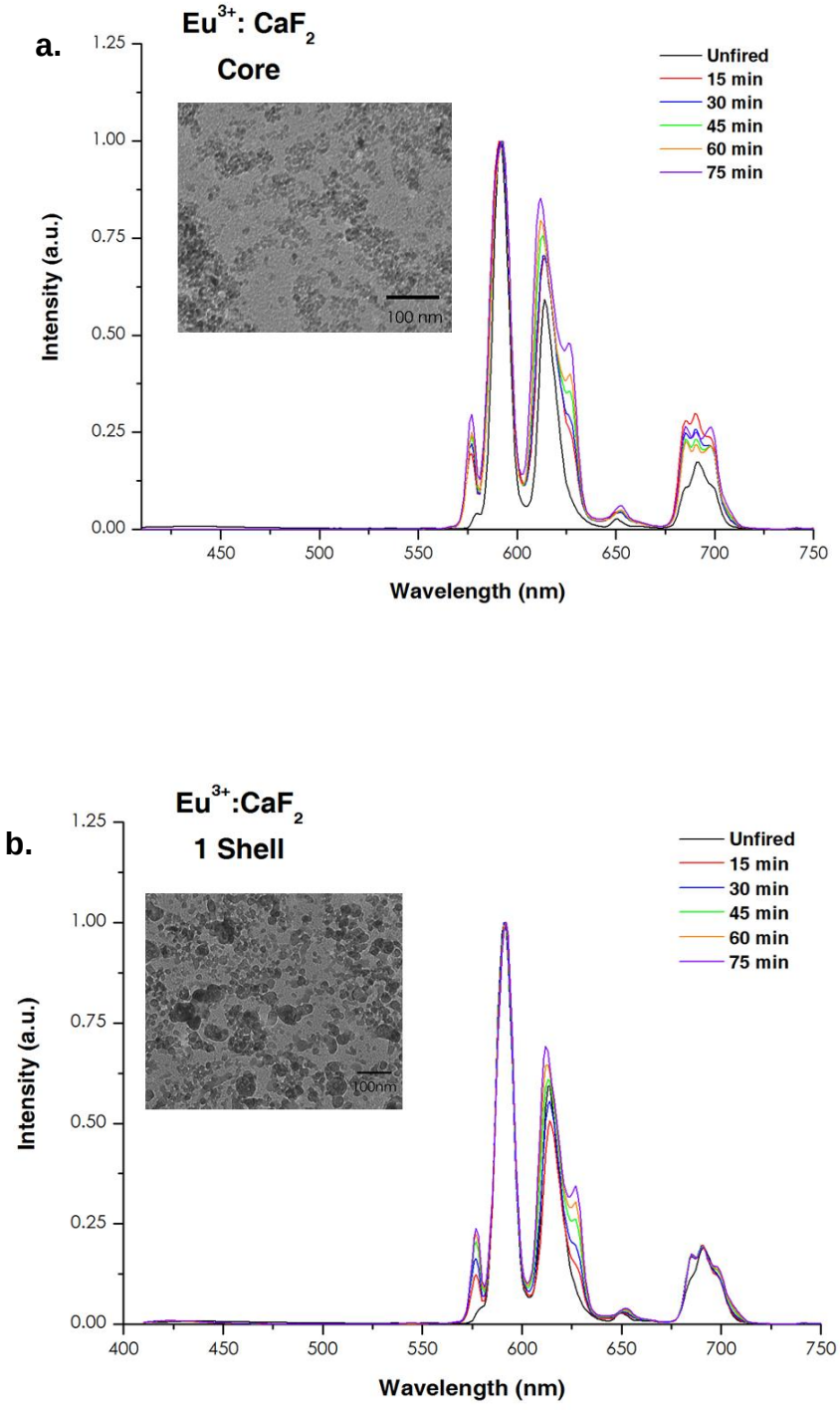

Figure 2.15. 20Eu:CaF_2 emission spectra as a function of time at 650ºC and corresponding TEM images for **a)** Core particles **b)** 1 CaF_2 shell particles

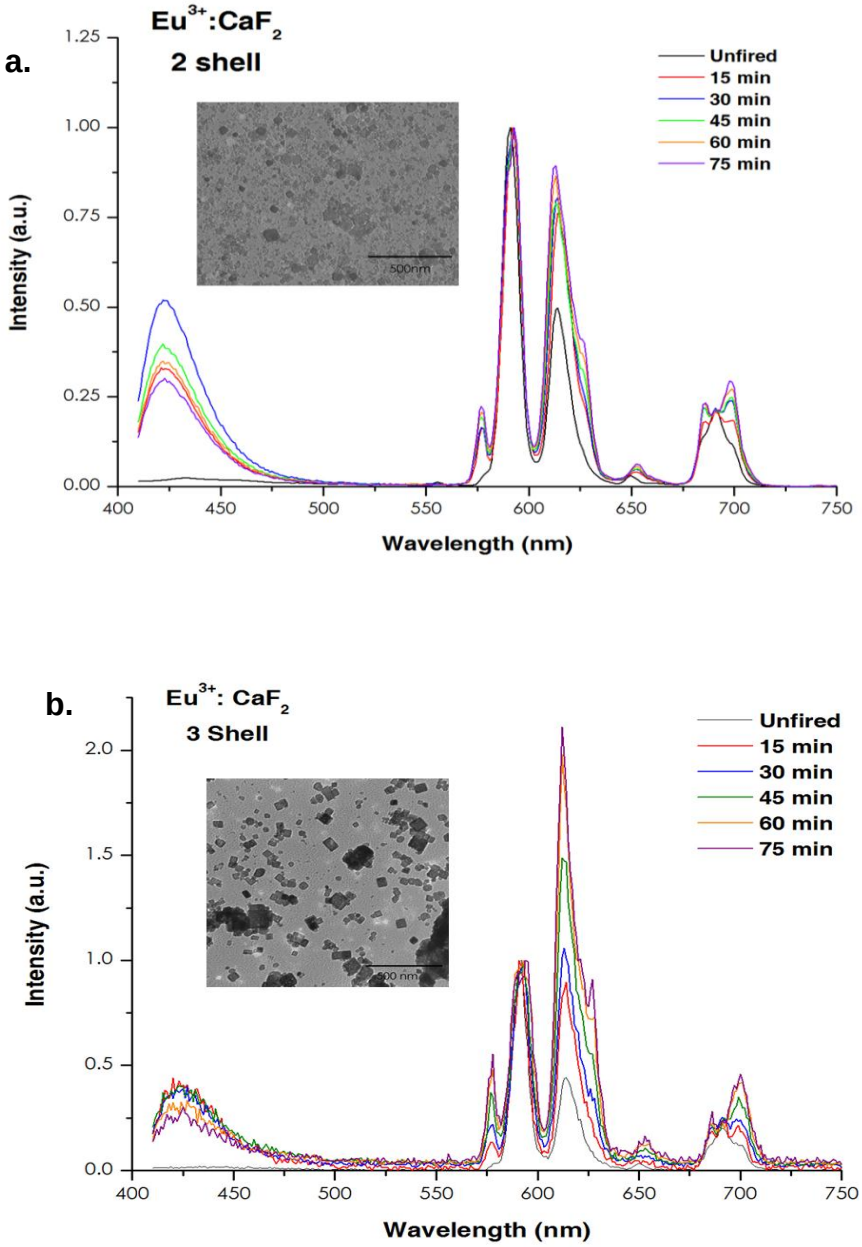

Figure 2.16. 20Eu:CaF_2 emission spectra as a function of time at 650ºC and corresponding TEM images for **a)** 2 CaF_2 shell particles **b)** 3 CaF_2 shell particles

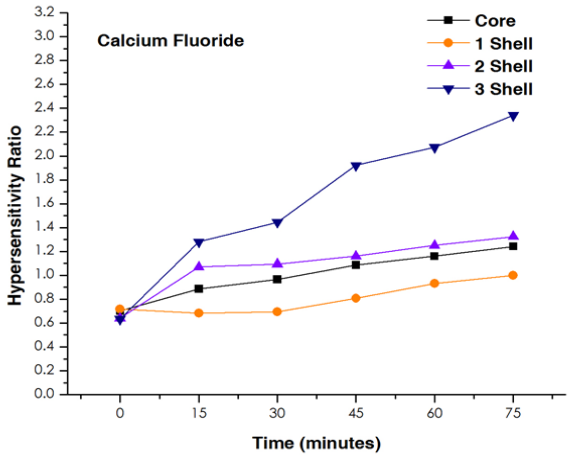

Figure 2.17. Comparison of individual 20Eu:CaF_2 nanoparticles hypersensitivity ratio as a function of time at 650ºC

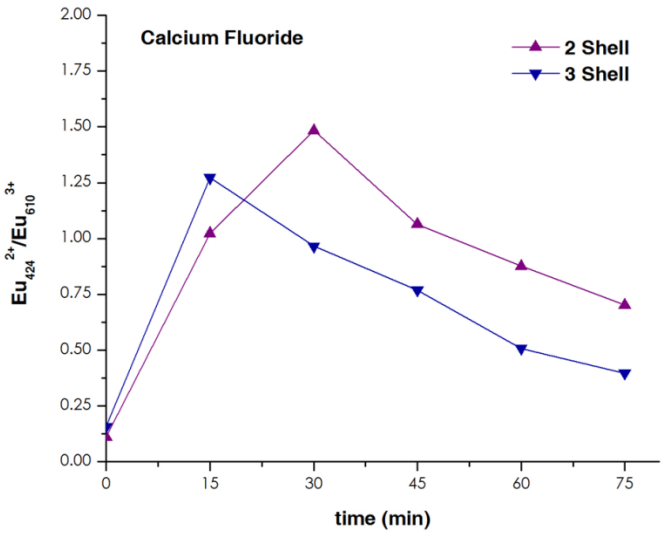

Figure 2.18. Ratio of Eu^{2+} to Eu^{3+} as a function of time at 650^0C in Eu:CaF_2 nanoparticle

Strontium Fluoride, SrF_2

The emission spectra (λ_{em} = 393 nm) and representative TEM images for the individual particle types of 20Eu:SrF_2 are seen in figures 2.19 and 2.20. The core particles are found to have an average particle size of ~10 ± 1.3 nm. There is a steady increase in particle size with the addition of undoped SrF_2, (Table 2.3). The increase in size per shell for the first two shells is very small, ~1 nm per addition, while the 3 shell is more than double that of the original core particle.

In all four emission spectra, the $^5D_0$ signature transitions are consistently present, with the linewidths narrowing and intensities decreasing following the first addition of excess undoped material. It appears that environment about the Eu^{3+} ions in SrF_2 remains relatively consistent in emission and is reflected in the hypersensitivity ratios (figure 2.21). The low value of HR also suggests a more symmetric environment exists about the Eu^{3+} ions within the SrF_2 host lattice, however, there is a slight increase for each particle type with increasing time at temperature. There appears to be a slight splitting of the $^5D_0 \rightarrow {}^7F_2$ emission that grows more pronounced with heat treatment and additional undoped SrF_2 layers. The induced concentration gradient with the additional volume of undoped material allows for the relief of high concentration effects seen in the emissions of core particles (figure 2.19a), which results in narrower emission linewidths and more distinct splitting patterns as is evidenced in the $^5D_0 \rightarrow {}^7F_4$ (~695 nm)

transition of the 1 shell (figure 2.19b), 2 shell (figure 2.20a) and 3 shell (figure 2.20b) particles. Therefore, it is concluded that the local environment about the Eu^{3+} ion in SrF_2 nanoparticles remains relatively consistent in elevated temperature conditions as well as with increased particle size, based on emission behavior. However, the extremely small increase in particle size from core to 1 and 2 shell particles suggest the HR values remain relatively consistent because the particles themselves are remaining relatively similar in size, making changes in the local environment about the Eu^{3+} ion less significant.

Barium Fluoride, BaF_2

The emission spectra (λ_{em} = 393 nm) and representative TEM images for the individual particle types of 20Eu:BaF_2 are seen in figures 2.22 and 2.23. The core particles are found to have an average particle size of ~20 ± 2.7 nm. There is a steady increase in particle size with the addition of undoped BaF_2, (Table 2.3), with average diameters of the shelled particles significantly larger than the original core particles, as also reported in [2.13].

The emissions of the $^5D_0$ manifold are distinct and become constant with increasing particle size and time at elevated temperature for the europium doped BaF_2 nanoparticles. The environment about the Eu^{3+} ion in this host lattice is constant with increasing time, and is demonstrated by the hypersensitivity ratio trend in figure 2.24. This indicates a stable environment for the Eu^{3+} ion,

suggesting similar diffusion behavior to that of LaF_3 (ref 2.37), and the large size of the particles from core to 3 shell nanoparticle provides sufficient relief of concentration quenching to provide a stable and consistent environment for the Eu^{3+} ions.

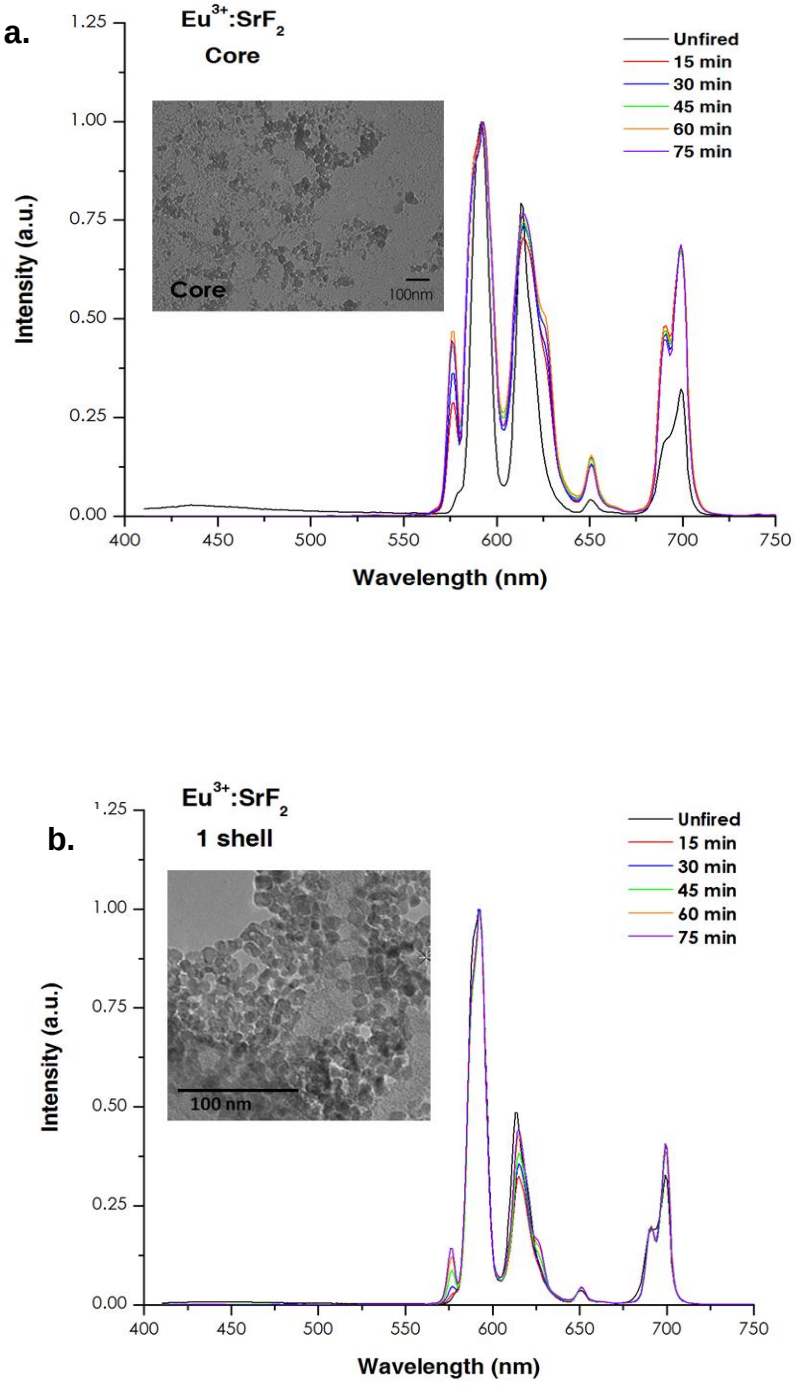

Figure 2.19. 20Eu:SrF_2 emission spectra as a function of time at 650ºC and corresponding TEM images for **a)** Core particles **b)** 1 SrF_2 shell particles

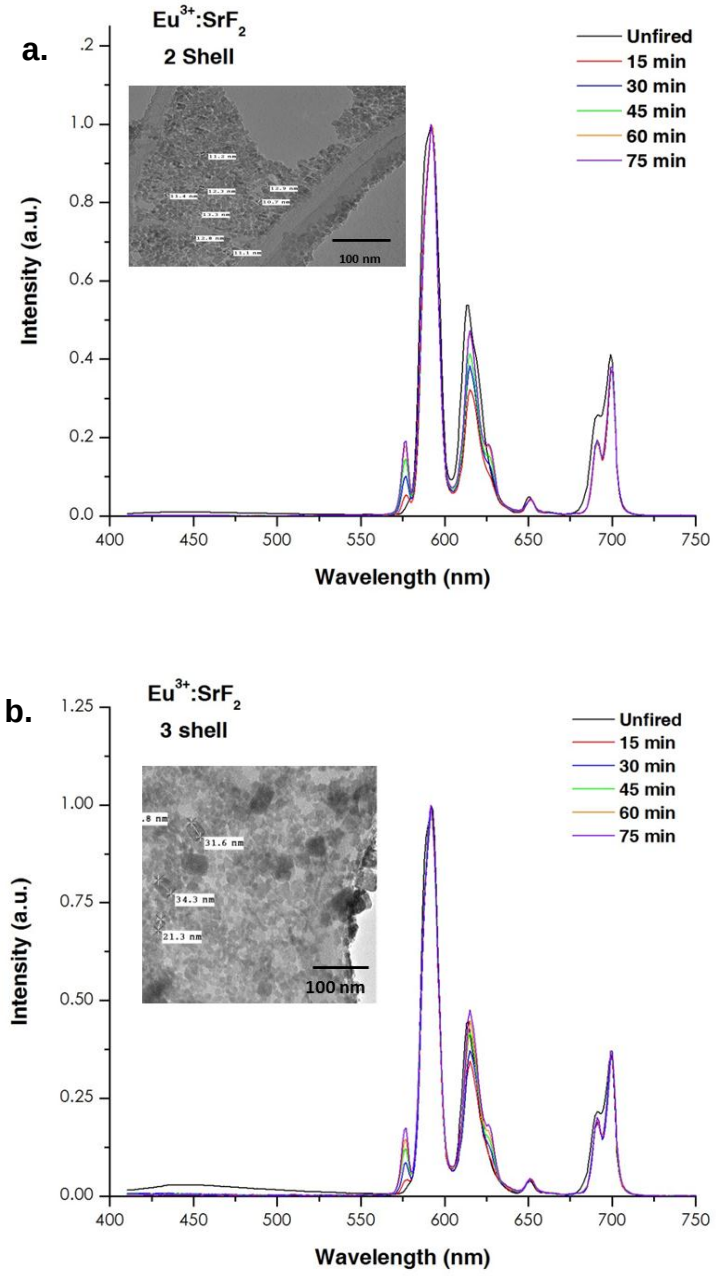

Figure 2.20. 20Eu:SrF_2 emission spectra as a function of time at 650ºC and corresponding TEM images for **a)** 2 SrF_2 shell particles **b)** 3 SrF_2 shell particles

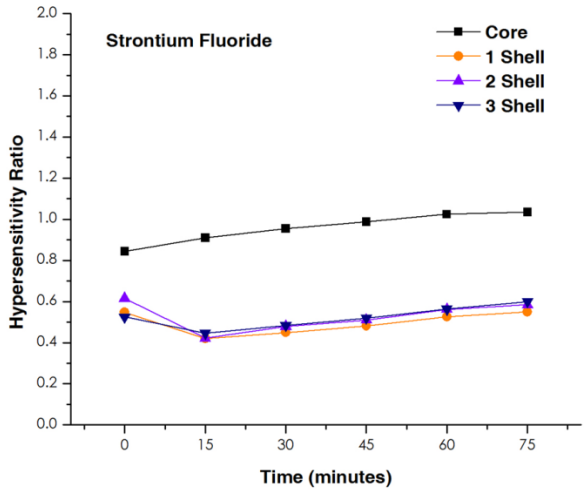

Figure 2.21. Comparison of individual 20Eu:SrF_2 nanoparticles hypersensitivity ratio as a function of time at 650ºC

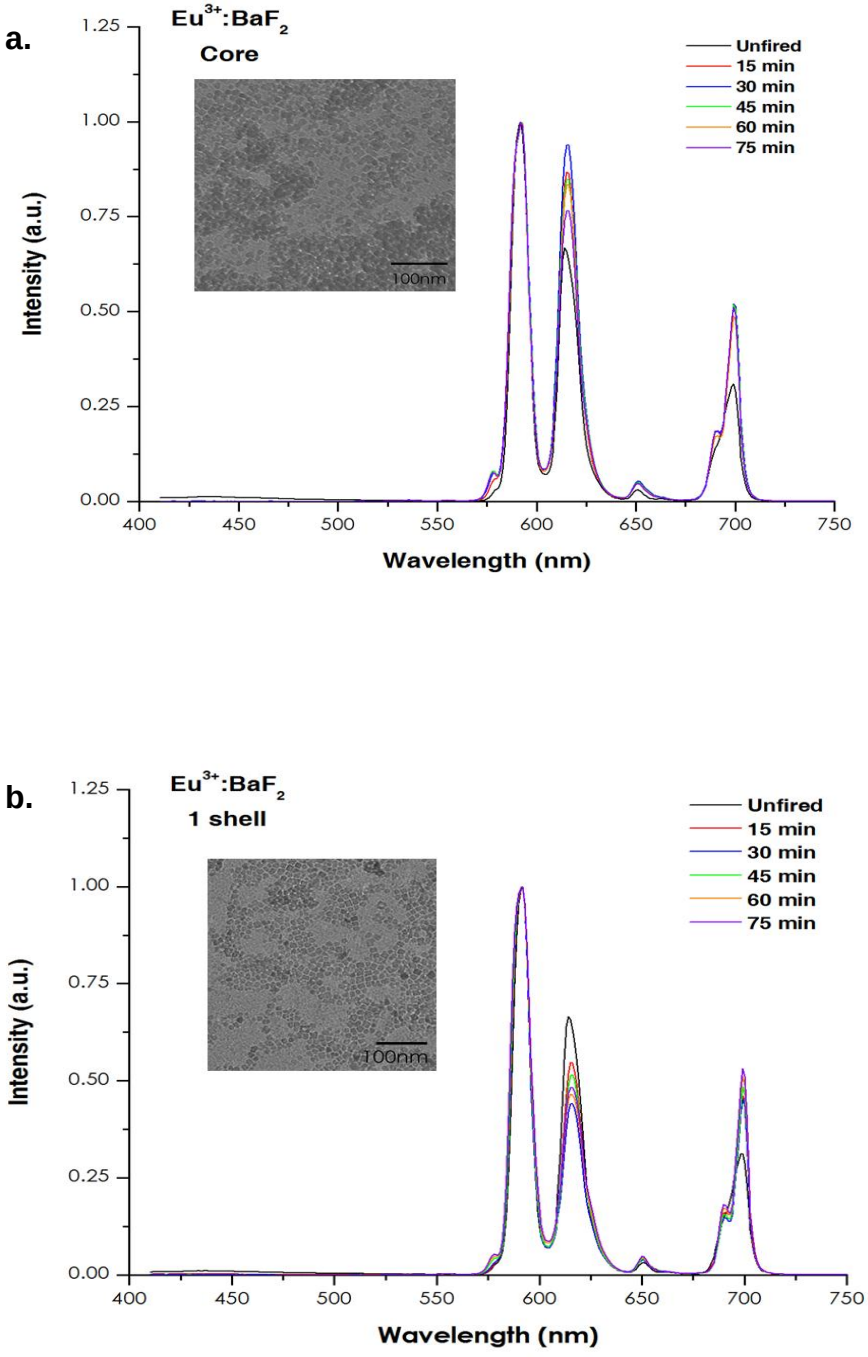

Figure 2.22. 20Eu:BaF_2 emission spectra as a function of time at 650ºC and corresponding TEM images for **a)** Core particles **b)** 1 BaF_2 shell particles

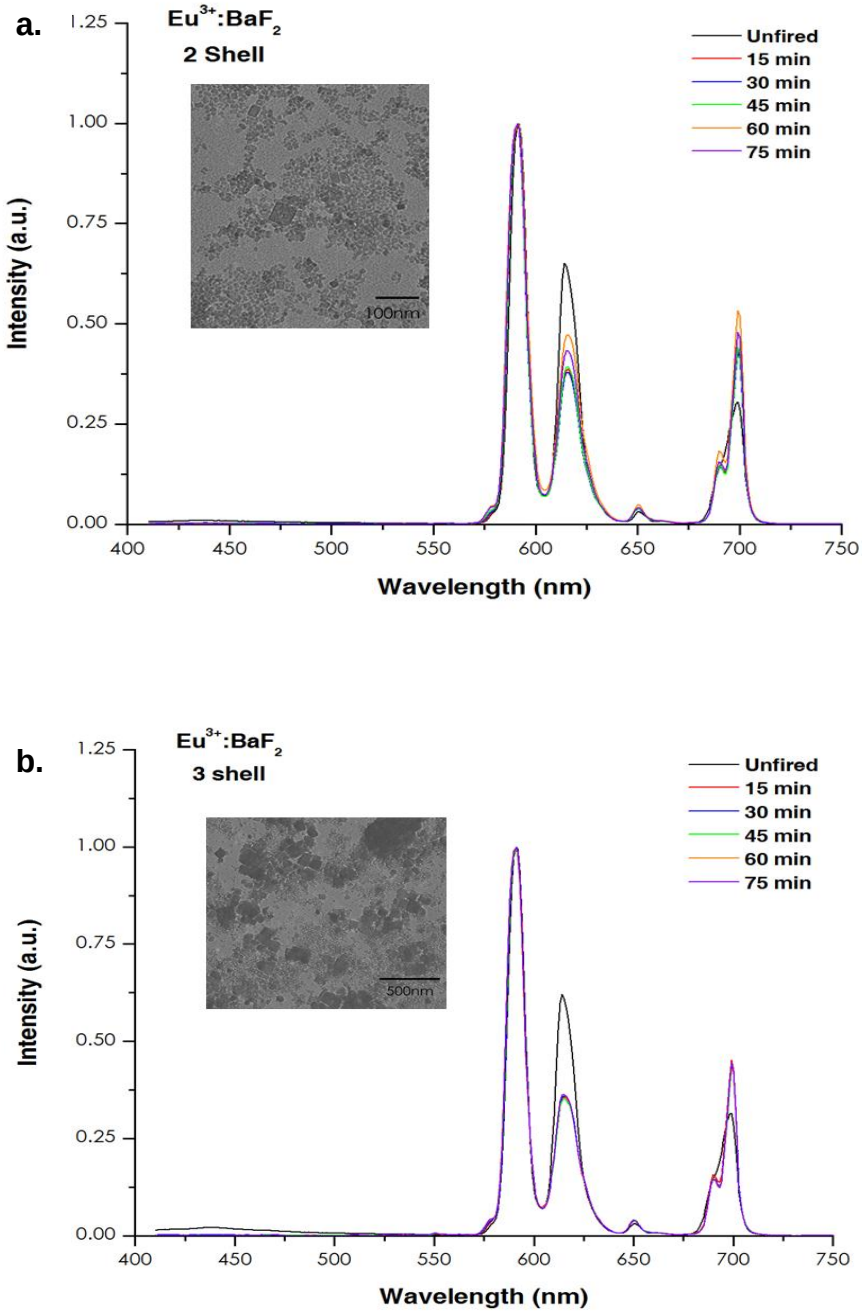

Figure 2.23. 20Eu:BaF_2 emission spectra as a function of time at 650ºC and corresponding TEM images for **a)** 2 BaF_2 shell particles **b)** 3 BaF_2 shell particles

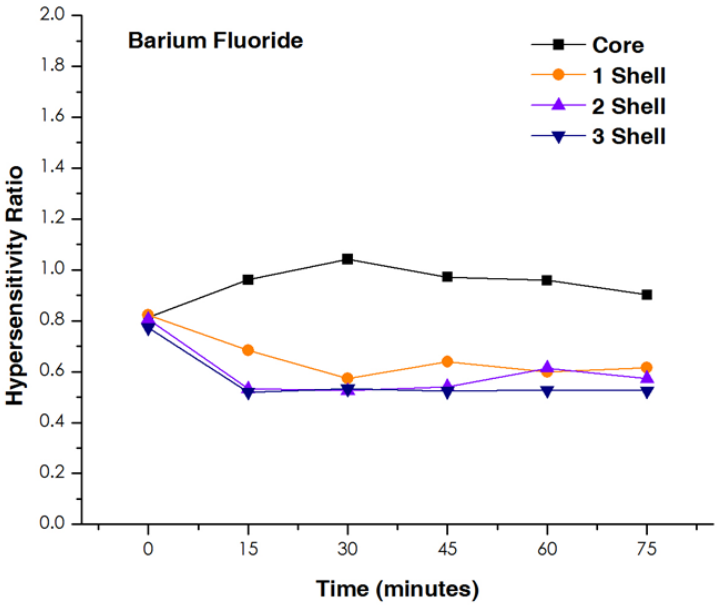

Figure 2.24. Comparison of individual 20Eu:BaF_2 nanoparticles hypersensitivity ratio as a function of time at 650ºC

Comparison of Alkaline Earth Fluoride Hosts

In order to determine differences between alkaline earth host species, the emission spectra for the individual particle types (figures 2.25-2.28) was compared and analysis of the corresponding hypersensitivity ratios (figure 2.29) was used. It should be noted that in all spectra there is a low intensity, broad emission at ~440 nm, which is due to the presence of ADDP in the unfired (as-made) samples (Appendix B).

Core

Within the core nanoparticles (figure 2.25), there are low intensity emissions from the $^5D_1$ and $^5D_2$ manifolds for all three alkaline earth species. CaF_2 and SrF_2 show a decrease in intensity for these emissions with processing time and temperature, while the $^5D_0 \rightarrow {}^7F_0$ emission (~577 nm) increases. This correlates with the increase in HR (figure 2.29a), suggesting a slight shift to a more asymmetric environment as a result of thermal stimulation. The BaF_2 nanoparticle emissions show no change in the higher manifold emissions with time, while the $^5D_0 \rightarrow {}^7F_0$ emission increases to its maximum at thirty minutes and remains constant. The low intensity of these emissions for all samples can be attributed to the quenching due to dipole-dipole interactions for the $^5D_2$ and $^5D_1$ manifolds as a result of the high concentration of Eu present within the core particle[2.26,2.37].

1 Shell

The difference in behavior begins to become more distinct with the addition of undoped host material . Here, the 1 shell CaF_2 sample (figure 2.26a) begins to have emissions due to Eu^{2+} (~424 nm) with little change in intensity with processing conditions, while the Eu^{3+} $^5D_1$ and $^5D_0$ manifold emissions begin to reduce, suggesting the Eu^{2+} emissions are dominant under these processing conditions as the concentration gradient is introduced for CaF_2. The interaction of the different ligand fields and the difference in charge compensation as a result of the conversion of a portion of the Eu^{3+} ions to Eu^{2+} ions will have an effect on the overall electric field of the ions in the lattice, as evidenced by an increase in the hypersensitivity ratio (figure 2.29b).

The 1 shell SrF_2 $^5D_1$ and $^5D_0$ emissions (figure 2.26b) decrease in intensity and broaden suggesting the movement within the host lattice to a less stable, more asymmetric environment, which is further substantiated by the slight increase in HR with processing time (figure 2.29b). The 1 shell BaF_2 (figure 2.26c) shows a slight increase in the higher manifold emissions and the $^5D_0 \rightarrow {}^7F_0$ emission increases with increasing processing time. The HR for BaF_2 decreases after thirty minutes and remains constant. This suggests the Eu^{3+} ions have diffused sufficiently within the excess volume provided by the first shell to reach a stable state.

2 Shell

In the 2 shell nanoparticle type, Eu^{2+} emissions (figure 2.27a) from the CaF_2 lattice overwhelm the higher manifold emissions of Eu^{3+}, while the $^5D_1$ and $^5D_2$ manifold emissions (figure 2.27b) increase in SrF_2 and in addition to the $^5D_1$ and $^5D_2$ manifold emissions, $^5D_3$ emissions (figure 2.27c) emerge in BaF_2. The increase in emissions from higher manifolds of the Eu^{3+} within the BaF_2 lattice with increasing processing time is indicative of the reduction of concentration quenching as a result of the Eu^{3+} diffusion. This coupled with the lower phonon energy of the BaF_2, enables the transitions in this region. There is a distinct difference in the HR (figure 2.29c) between the CaF_2 when compared to the SrF_2 and BaF_2—the ligand field about the Eu^{2+} ion is different than that of the Eu^{3+} ion and will influence the overall asymmetry of the lattice sites. SrF_2 shows a slight increase in HR with time, which implies a change in the local environment for the Eu^{3+} that can be attributed to the diffusion of the Eu^{3+} into the undoped volume. The HR of BaF_2 in this case decreases following the onset of heat treatment and remains constant. This suggests the environment of the Eu^{3+} ion is more stable, making more intense emissions from the higher manifolds more likely.

3 Shell

In the case of the three shell nanoparticles, the most pronounced differences between the host materials are exhibited. The emissions from the Eu^{2+} within the 3 shell CaF_2 (figure 2.28a) decrease with processing time while the HR (figure 2.29d) increases by nearly 4x, indicating a highly asymmetric environment. The $^5D_0 \rightarrow {}^7F_0$ (as well as the $^5D_0 \rightarrow {}^7F_2$) emission increases with processing time, confirming the conversion of $Eu^{2+} \rightarrow Eu^{3+}$ with the overall concentration of europium diffused into a larger volume. At smaller volumes, it can be assumed that the europium ions are in closer proximity to one another and causing larger distortions to the crystal lattice with incorporation into the smaller Ca^{2+} sites (r_{Ca2+} = 0.112 nm, r_{Eu2+}=0.125 nm) as well as more interaction with the ligand field of adjacent ions. As the europium diffuses into a larger volume by thermal stimulation, this interaction is reduced and the overall behavior of the Eu:CaF_2 nanoparticle reverts to that of its bulk counterpart as suggested by Pandey et al.[2.47].

The 3 shell SrF_2 (figure 2.28b) shows a reduction in $^5D_1$ and $^5D_2$ emissions and the $^5D_0 \rightarrow {}^7F_0$ emission increases with processing time. The reduction in higher manifold emissions may be a result of interactions of surface atoms interacting with a phosphorous oxide layer that forms when the dithiophosphate ligands are oxidized during heat treatment indicated by the low intensity, broad transition centered at ~440 nm (inset, figure 2.28b). The 3 shell SrF_2

hypersensitivity ratio (figure 2.29d), shows a slight increase with processing time, indicating there is some diffusion of the Eu^{3+} which results in a slightly more asymmetric environment.

The BaF_2 3 shell has pronounced, increasing emissions from the $^5D_1$, $^5D_2$ and $^5D_3$ manifolds with increasing processing time and the HR decreases upon heating, remains constant and low in value. This can be attributed to the reduction in concentration quenching as a result of the Eu^{3+} diffusion from the core region to the undoped shell volume as well as the low phonon energy of this host material.

Optically-Estimated Diffusion Coefficients

Using the emission spectra as evidence of diffusion, the diffusion coefficient for europium in each alkaline earth fluoride host can be estimated. The diffusion coefficient was calculated by applying a simple one-dimensional approximation[2.51]:

$$D = \frac{L^2}{4t}$$

L = Diffusion length in meters (average radius of the nanoparticle)

t = time at which steady state diffusion is assumed in seconds

It was assumed steady state diffusion is reached when the spectroscopic properties no longer change with processing time, here, 4500 s (75 minutes). Tabulated values are shown in Table 2.4 for each of the nanoparticle types by host. The average D for Eu:CaF_2 is ~1 x 10^{-20} m^2/s, for Eu:SrF_2 is ~7 x 10^{-21} m^2/s and for Eu:BaF_2 is ~1 x 10^{-19} m^2/s. While these values assume linear diffusion of the Eu^{3+} from the center of the core to the outermost edge of the AEF_2 shell, the values corroborate in order of magnitude with published values for similar materials[2.52,2.53].

TABLE 2.4

Calculated Diffusion Coefficients, in m^2/s, for Eu^{3+} in Alkaline Earth Fluoride Nanoparticles

Particle Type	Eu:CaF_2	Eu:SrF_2	Eu:BaF_2
Core	1.9 x 10^{-21}	2.9 x 10^{-21}	1.1 x 10^{-20}
1 Shell	3.2 x 10^{-21}	3.6 x 10^{-21}	3.6 x 10^{-20}
2 Shells	5.4 x 10^{-21}	4.1 x 10^{-21}	1.3 x 10^{-19}
3 Shells	3.4 x 10^{-20}	1.6 x 10^{-20}	3.1 x 10^{-19}

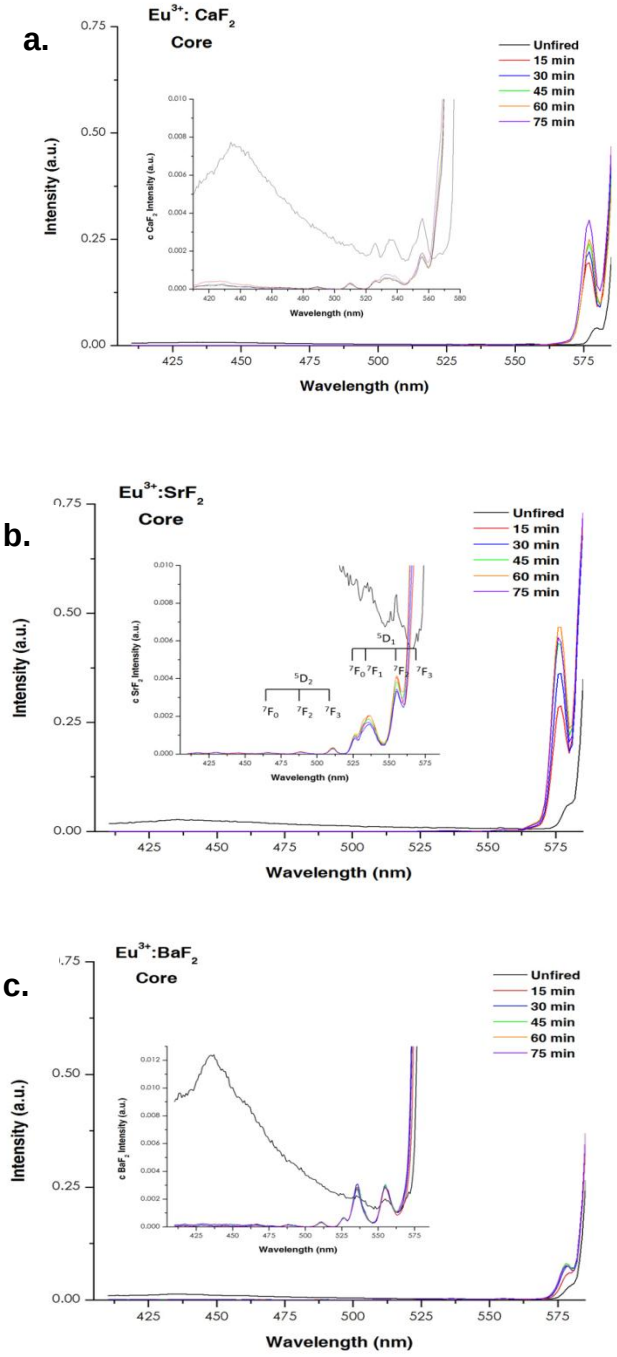

Figure 2.25. Core Photoluminescence Spectra for a) 20Eu:CaF_2 b) 20Eu:SrF_2 c) 20Eu:BaF_2

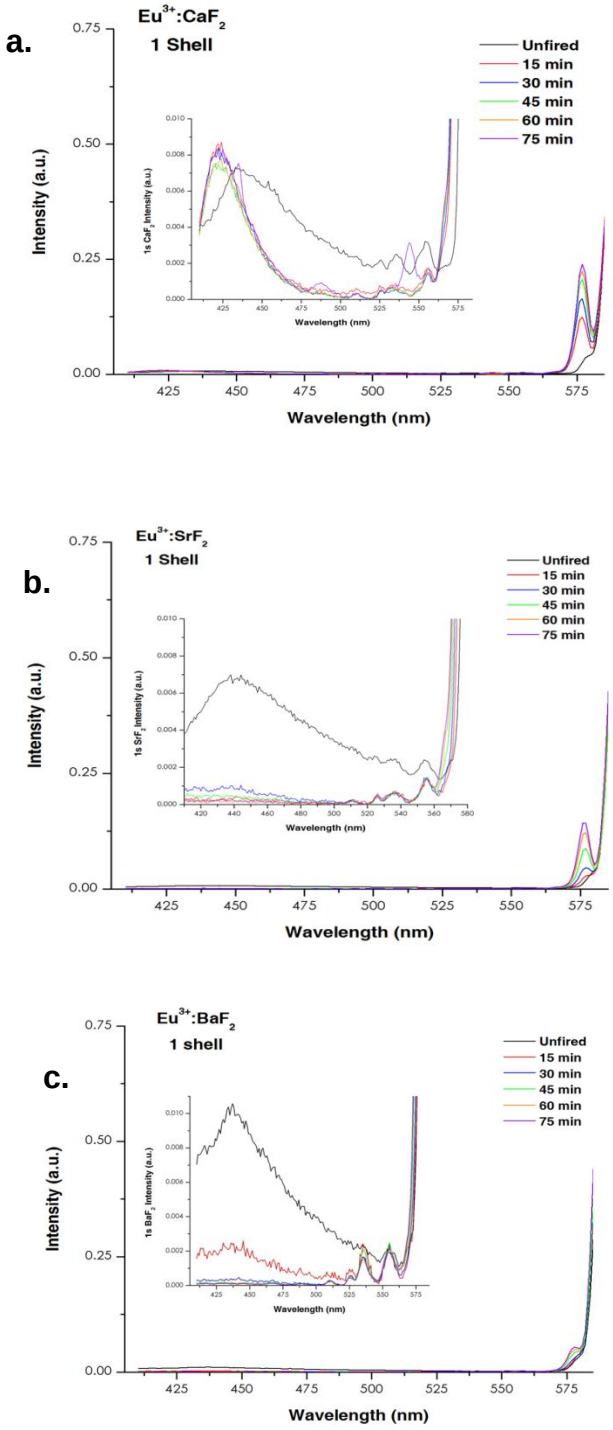

Figure 2.26. 1 Shell Photoluminescence Spectra for a) CaF_2(20Eu:CaF_2) b)SrF_2(20Eu:SrF_2) c) BaF_2(20Eu:BaF_2)

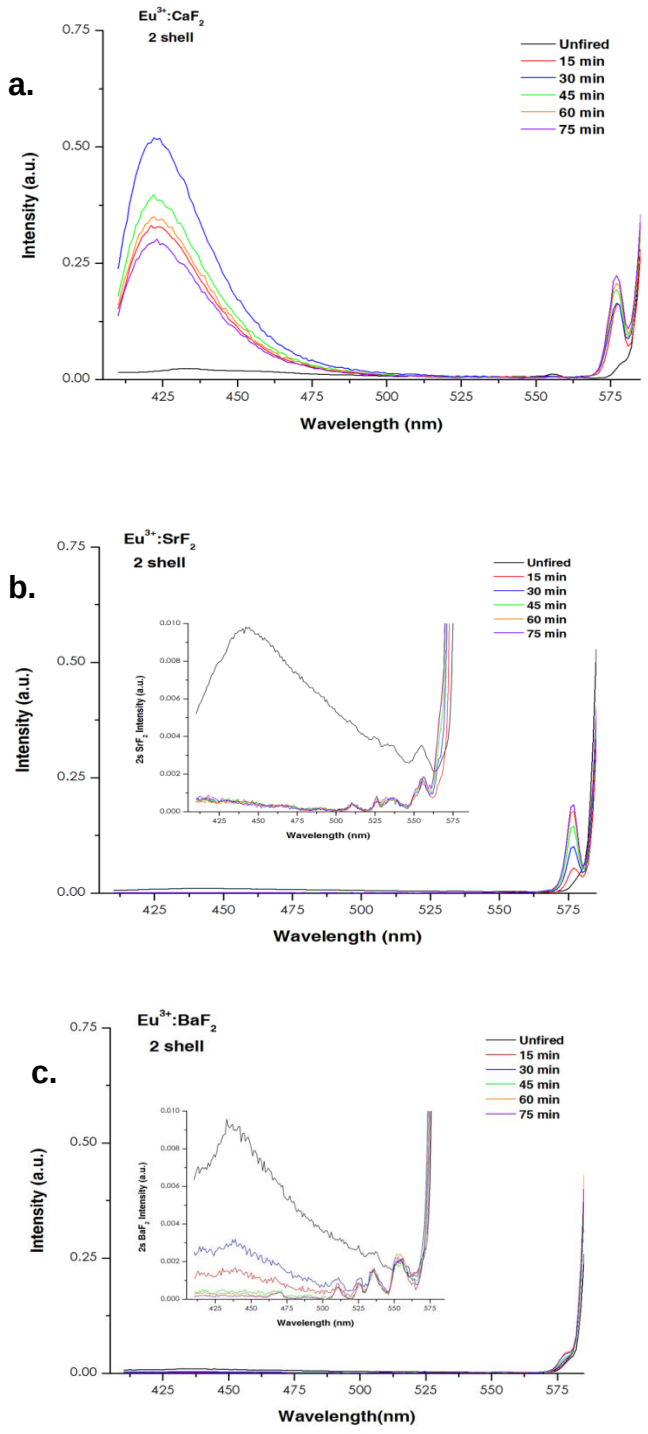

Figure 2.27. 2 Shell Photoluminescence Spectra for a) $CaF_2(CaF_2(20Eu:CaF_2))$ b) $SrF_2(SrF_2(20Eu:SrF_2))$ c) $BaF_2(BaF_2(\ 20Eu:BaF_2))$

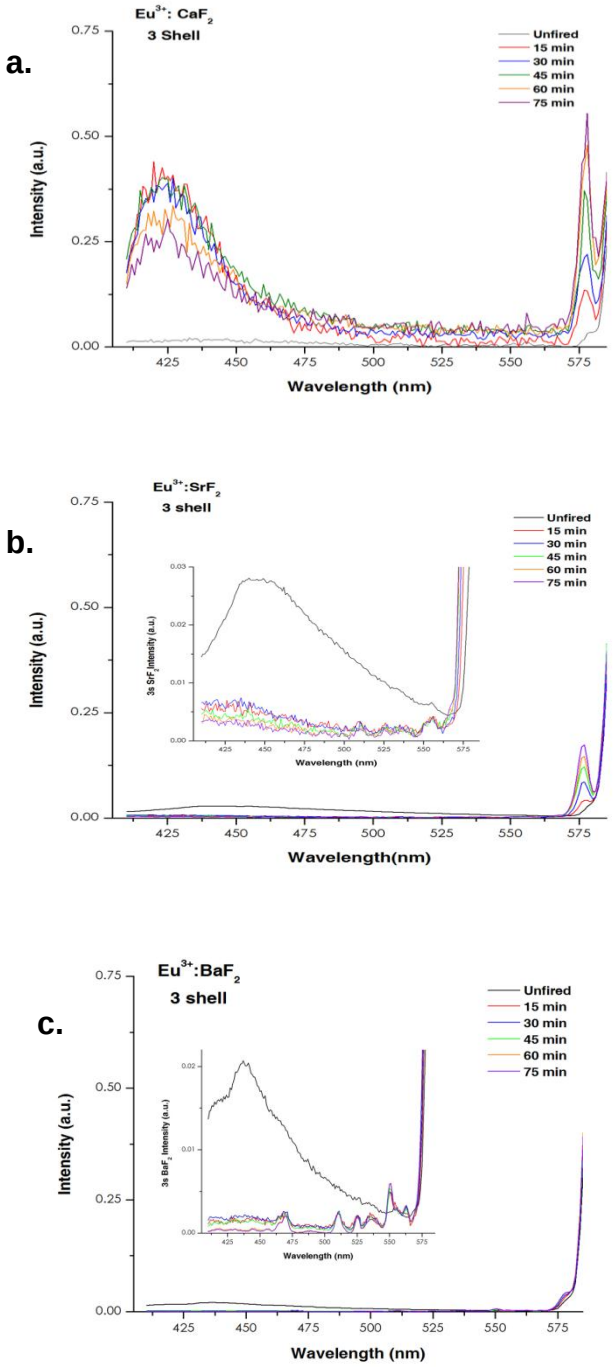

Figure 2.28. 3 Shell Photoluminescence Spectra for a) $CaF_2(CaF_2(CaF_2(20Eu:CaF_2)))$ b)$SrF_2(SrF_2(SrF_2(20Eu:SrF_2)))$ c)$BaF_2(BaF_2(BaF_2(20Eu:BaF_2)))$

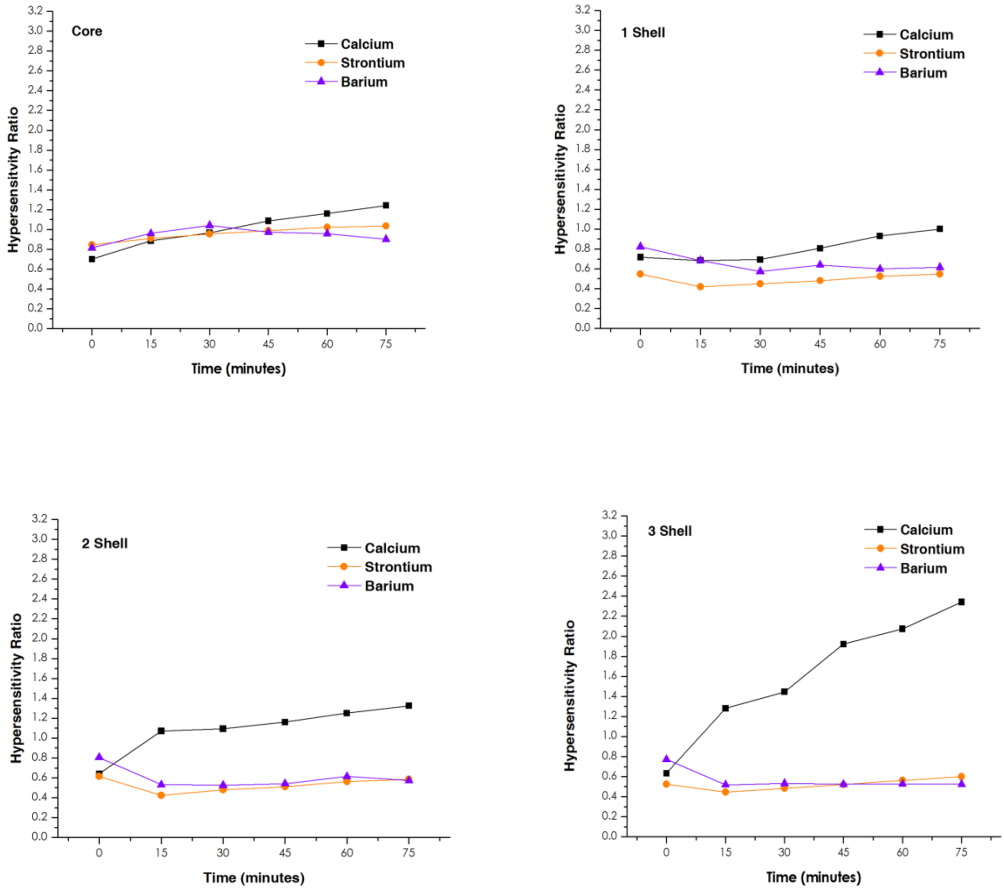

Figure 2.29. Local Eu^{3+} environment within AEF_2 nanoparticles comparison by particle type as represented in the hypersensitivity ratio as a function of time at temperature.

Summary

Various calcium, strontium and barium fluoride nanoparticles which are dispersible in organic solvents were successfully produced and characterized for their physical, chemical and optical behavior. Distinct spectroscopic differences between the different host materials were demonstrated, as well as for varying rare earth dopant levels. The hypersensitivity dependence exhibited with varying dopant level indicates an ability to control/influence emission of the rare earth dopant which has not been seen before. There is a prominent influence of processing on the spectroscopy of these nanoparticles as well. The variations in emission behavior and subsequently, the hypersensitivity ratio, of the heat treated nanoparticles demonstrate a difference in environment for the rare earth ion from host to host. By applying a simple one dimensional model for diffusion, an order of magnitude accuracy for predicting the diffusion coefficient of europium ions in alkaline earth fluorides was shown, and demonstrates that photoluminescence is a useful tool to predict diffusion behavior.

Overall, it has been demonstrated that by rare earth doping alkaline earth fluoride nanoparticles it is possible to engineer their spectroscopic behavior. The ability to ‘tune’ these materials to specific applications through the use of different host materials, processing conditions and doping levels make rare earth doped alkaline earth nanoparticles a viable option for use as dopant materials in active optical fiber.

References

2.1 Bjarklev, A., Optical Fiber Amplifiers: Design and System Applications, Artech House, Boston, 1993.

2.2 Peretti, R., Jurdyc, A.M., Jacquier, B., Blanc, W., Dussardier, B., "Spectroscopic signature of phosphate crystallization in erbium-doped optical fibre preforms," Optical Materials, 33 [2011] 835.

2.3 Mahmoud, F., Muller, H.R., Morl, K., Bartlet, H., "Scattering loss in Nd-doped silica based optical fibers," Optick, 113 [2002] 421.

2.4 Blanc, W., Mauroy, v., Nguyen, L, Shivakiran Bhaktha, B.N., Sebbah, P., Pal, B.P., Dussardier, B., "Fabrication of Rare Earth-Doped Transparent Glass Ceramic Optical Fibers by Modified Chemical Vapor Deposition," Journal of the American Ceramic Society, 94 [8] 2315.

2.5 Sudarsan, V., van Veggel, F.C.J.M., Herring, A., and Raudsepp, M., "Surface Eu^{3+} ions are different than 'bulk' Eu^{3+} ions in crystalline doped LaF_3 nanoparticles," Journal of Materials Chemistry, **15** [2005] 1332.

2.6 Stouwdam, J.W. and van Veggel, F.C.J.M., " Near-infrared Emission of Redispersible Er^{3+}, Nd^{3+}, and Ho^{3+} Doped LaF_3 Nanoparticles," NanoLetters, **2** [2002] 733.

2.7 Labeguerie, J., Gredin, P., Mortier, M., Patriarche, G. and de Kozak, A., "Synthesis of Fluoride Nanoparticles in Non-Aqueous Nanoreactors. Luminescence Study of Eu^{3+}:CaF_2," Zeitschrift fur anorganische und allgemeine Chemie, **632** [2006] 1538.

2.8 Kömpe, K., Borchert, H., Storz, J., Lobo, A., Adam, S., Moller, T. and Haase, M., "Green-emitting $CePO_4$:Tb/$LaPO_4$ core-shell Nanoparticles with 70% Photoluminescence Quantum Yield," Angewandte Chemie, 42 [2003] 5513.

2.9 Viswanatha, R. and Sarma, D.D., in Nanomaterials Chemistry; Rao, C.N.R., Muller, A., and Cheetham, A.K., Eds., Wiley-VCH, Weinheim, 2007.

2.10 Lo, A.Y.H, Sudarsan, V., Sivakumar, S., van Veggel, F. and Schurko, R.W., "Multinuclear Solid-State NMR Spectroscopy of Doped Lanthanum Fluoride Nanoparticles," Journal of the American Chemical Society, **129** [2007] 4687.

2.11 Stouwdam, J.W. and van Veggel, F.C.J.M., "Improvement in the Luminescence Properties and Processability of LaF_3/Ln and $LaPO_4$/Ln Nanoparticles by Surface Modification," Langmuir, **20** [2004] 11763.

2.12 DiMaio, J.R., Kokuoz, B., James, T.L. and Ballato, J., "Structural Determination of Light-Emitting Inorganic Nanoparticles with Complex Core/Shell Architectures," Advanced Materials, **19** [2007] 3266.

2.13 Jacobsohn, L.G., Kucera, C.J., James, T.L., Sprinkle, K.B., DiMaio, J.R., Kokuoz, B., Yazgan-Kokuoz, B., DeVol, T.A., Ballato, J., "Preparation and Characterization of Rare Earth Doped Fluoride Nanoparticles," Materials, 3 [2010] 2053.

2.14 Dejneka, M.J., "The luminescence and structure of novel transparent oxyfluoride glass-ceramics," Journal of Non-Crystalline Solids, **239** [1998] 149.

2.15 Frantz, J.D., and Mysen, B.O., "Raman spectra and structure of $BaO\text{-}SiO_2$, $SrO\text{-}SiO_2$, and $CaO\text{-}SiO_2$ melts to 1600C," Chemical Geology 121 [1995] 155.

2.16 Lian, H., Liu, J., Ye, Z., and Shi, C., "Synthesis and photoluminescence properties of erbium-doped BaF_2 nanoparticles," Chemical Physics Letters, **386** [2004] 291.

2.17 Sun, X. and Li, Y., "Size-controllable luminescent single crystal CaF_2 nanocubes," Chemical Communications, [2003] 1768.

2.18 Grass, R.N. and Stark, W.J., "Flame synthesis of calcium-, strontium, barium fluoride nanoparticles and sodium chloride," Chemical Communications, [2005] 1767.

2.19 Varshneya, A.K., Fundamentals of Inorganic Glasses, Academic Press, Inc., San Diego, 1994.

2.20 Kalampounias, A.G., "IR and Raman spectroscopic studies of sol-gel derived alkaline-earth silicate glasses," Bulletin of Material Science, 34 [2011] 299.

2.21 Buschow, K.H., Jurgen, H., Cahn, R.W., Flemings, M.C., Ilshner, B., Kramer, E.J., Mahajan, S., eds., Encyclopedia of Materials Science & Technology, Elsevier, 2001, Oxford, 2616.

2.22 Bueno, L.A., Gouveia-Neto, A.S., da Costa, E.B., Messaddeq, Y. and Ribeiro, S.J.L., "Structural and Spectroscopic study of oxyfluoride glasses and glass-ceramics using europium ion as a structural probe," Journal of Physics: Condensed Matter, 20 [2008] 145201.

2.23 Sudarsan, V., van Veggel, F.C.J.M., Herring, R.A. and Raudsepp, M., "Surface Eu^{3+} ions are different than "bulk" ions in crystalline doped LaF3 nanoparticles," Journal of Materials Chemistry, 15 [2005] 1332.

2.24 Cotton, S., Lanthanide and Actinide Chemistry, Wiley & Sons, West Sussex, 2006.

2.25 Blasse, G. and Grabmaier, B.C., Luminescent Materials, Springer-Verlag, Berlin Heidelburg, 1994.

2.26 Dejneka, M., Snitzer, E., Riman, R.E., "Blue, green and red fluorescence and energy transfer of Eu^{3+} in fluoride glasses," Journal of Luminescence, 65 [1995] 227.

2.27 Xie, F., Liang, H., Chen, B., Xu, J. and Fuquan, G., "Luminescence analysis of Eu complexes containing diphenanthryl β-diketone ligands doped silicone rubber," Journal of Material Science, 45 [2010] 405.

2.28 Hawkins, T.W., "The Optical and Spectroscopic Characterization of Rare Earth Doped Tellurite Glasses and Fibers," Masters Thesis, Clemson University, December 2005.

2.29 Fox, M., Optical Properties of Solids, " Oxford University Press, Oxford, 2001.

2.30 Tanabe, S., Hirao, K. and Soga, N., "Local structure of rare-earth ions in fluorophosphates glasses by phonon sideband and Mossbauer spectroscopy," Journal of Non-Crystalline Solids, 142 [1992] 148.

2.31 Ballato, J., Esmacher, R., Schwartz, R. and Dejneka, M., "Phonon sideband spectroscopy and 1550 nm luminescence from Eu^{3+} and Er^{3+} doped ferroelectric PLZT for active electro-optic applications," Journal of Luminescence, 86 [2000] 101.

2.32 Omar, M.A., Elementary Solid State Physics: Principles and Applications, Addison-Wesley, Menlo Park, CA, 1975.

2.33 Feldman, L.C., and Mayer, J.W., Fundamentals of Surface and Thin Film Analysis, North-Holland, New York, New York, 1986.

2.34 Lever, A.B.P., Inorganic Electronic Spectroscopy, Elsevier, Amsterdam, 1984.

2.35 "Raman Spectroscopy," www.chemsoc.org/entries/2004/birmingham-jones/raman.html

2.36 Payne, S.A., Caird, J.A., Chase, L.L., Smith, L.K., Nielsen, N.D., and Krupke, W.F., "Spectroscopy and gain measurements of Nd^{3+} in SrF_2 and other fluorite-structure hosts," Journal of the Optical Society of America B, 8 [1991], 726.

2.37 DiMaio, J., Kokuoz, B., James, T.L., Harkey, T., Monofsky, D., and Ballato, J., "Photoluminescent Characterization of Atomic Diffusion in Core-Shell Nanoparticles," Optics Express, 16 [2008] 11769.

2.38 Koch, C.C., Ovid'ko, I.A., Seal, S., and Veprek, S., Structural Nanocrystalline Materials Fundamentals and Applications, Cambridge, New York, 2007.

2.39 Faulques, E., Wery, J., Dulieu, B., Seybert, C., and Perry, D.L., "Synthesis, Fabrication, and Photoluminescence of CaF_2 Doped with Rare Earth Ions," Journal of Fluorescence, 8 [1998] 283.

2.40 Ponader, C.W., Youngman, R.E., and Smith, C.M., "Structural Studies of $(Ca,Sr)F_2$ Single Crystals with Raman and NMR Spectroscopies," Journal of the American Ceramic Society, 88 [2005] 2447.

2.41 Kadlec, F., Simon, P., and Raimboux, N., "Vibrational spectra of superionic crystals $(BaF_2)_{1-x}(LaF3)_x$," Journal of Physics and Chemistry of Solids, 60 [1999] 861.

2.42 Kaiser, W., Spitzer, W.G., Kaiser, R.H., Howarth, L.E., "Infrared Properties of CaF_2, SrF_2, and BaF_2," Physical Review, 127 [1962] 1950.

2.43 Bosomworth, D.R., "Far-Infrared Optical Properties of CaF_2, SrF_2, BaF_2 and CdF_2," Physical Review, 157 [1967] 157.

2.44 Richman, I., "Longitudinal Optical Phonons in CaF_2, SrF_2 and BaF_2," Journal of Chemical Physics, 41 [1964] 2836.

2.45 Jacobsohn, L.G., McPherson, C.L., Sprinkle, K.B., Yukihara, E.G, DeVol, T.A., Ballato, J., "Scintillation of rare earth doped fluoride nanoparticles," Applied Physics Letters, 99 [2011] 113111.

2.46 Justel, T. in Luminescence, Ronda, C. ed., Wiley-VCH, Weinheim, 2008.

2.47 Pandey, C., Dhopte, S.M., Muthal, P.L., Kondawar, V.K. and Moharil, S.V., "Eu^{3+} <-> Eu^{2+} redox reactions in bulk and nano CaF_2:Eu," Radiation Effects & Defects in Solids, 162 [2007] 651.

2.48 Hong, B., and Kawano, K., "Luminescence studies of rare earth ions-doped CaF_2 and MgF_2 films for wavelength conversion," Journal of Alloys and Compounds, 408-412 [2006] 838.

2.49 Luo, Q., Xvsheng, Q., Fan, X., Liu, S., Yang, H. and Zhang, X, "Reduction and luminescence of europium ions in glass ceramics containing SrF_2 nanocrystals," Journal of Non-Crystalline Solids, 354 [2008] 4691.

2.50 Hong, B. and Kawano, K., "Reduction of Eu^{2+}-activated nanoparticles by unique TCRA treatment," Journal of Alloys and Compounds, 451 [2008] 276.

2.51 Balluffi, R.W., Allen, S.M., Craig Carter, W., Kinetics of Materials, John Wiley and Sons, Hoboken, 2005.

2.52 Cherniak, D.J., Zhang, X.Y., Wayne, N.K., Watson, E.B., "Sr, Y and REE diffusion in fluorite," Chemical Geology, 181 [2001] 99.

2.53 Cherniak, D.J., "REE diffusion in calcite," Earth and Planetary Science Letters, 160 [1998] 273.

CHAPTER III

APPLICATIONS: USING RARE EARTH DOPED ALKALINE EARTH FLUORIDE NANOPARTICLES FOR THE SPECTRAL ENGINEERING OF OPTICAL FIBER

Providing a practical use of the alkaline earth fluoride nanoparticles studied in this work was a prime objective. Here, europium doped alkaline earth nanoparticles are incorporated into the core of an optical fiber preform in order to study their influence on the optical properties of an otherwise commodity glass like silica with the intent of providing the ability to tailor emissions in resultant optical fiber.

Introduction

Rare Earth Doping of Silica Glass

Demand for active devices which improve the optical signals within a long-haul optical fiber network (fiber amplifiers) and lasers based on single mode fibers for high power generation necessitated the development of methods to incorporate rare earth ions into the core of an optical fiber[4.1-4.5]. Over the years, two primary processes have been employed: gas/vapor phase doping[4.3] or solution doping[4.4], as an additional step in the fabrication of a modified chemical vapor deposition (MCVD) silica preform.

Glass Formation and Structure

In order to understand the intricacies of doping a silica glass, a basic understanding of how a glass forms and the local area structure which comprises the glass matrix is necessary. Glass is defined as 'an amorphous solid completely lacking in long range, periodic atomic structure and exhibiting a region of glass transformation behavior'[3.6]. This material is conventionally formed by the cooling of a substance from a molten state and can be constituted of any inorganic, organic or metallic elements/material which exhibits this glass transition behavior[3.7]. However, the lack of long range order in these materials does not imply the absence of short range order, which is considered to be on the order of a few angstroms. It is the short range order or local structure, which characterizes a particular glass[3.10].

There are three basic building blocks that constitute the basis for glass formation: network formers, intermediates and modifiers[3.6-3.8]. Network formers, also known as glass forming oxides, include silica (SiO_2), boric oxide (B_2O_3) and phosphorous pentoxide (P_2O_5)[3.6-3.9]. These substances readily form single component glasses and serve as the 'backbone' in multi-component glasses[3.6]. Other substances such as alumina (Al_2O_3), gallium oxide (Ga_2O_3) and germania (GeO_2), may also act as glass formers in certain instances[3.6]. The primary network former used in the fabrication of optical fiber is SiO_2, while GeO_2 is used as an additive to impact the optical properties of the fibers[3.1-3.2]. A schematic depiction of a glass comprised solely of SiO_2 is shown in figure 3.1.

Intermediates are components that are generally added to a glass batch to enhance and stabilize the glass system[3.8]. Elements used in this capacity include oxides of Ti, Al, Pb, Zn, and Zr[3.6-3.8]. Typical solution doped active fibers utilize Al to act as a modifier/intermediate to aid in rare earth solubility within the rigid structure of a SiO_2 glass matrix..

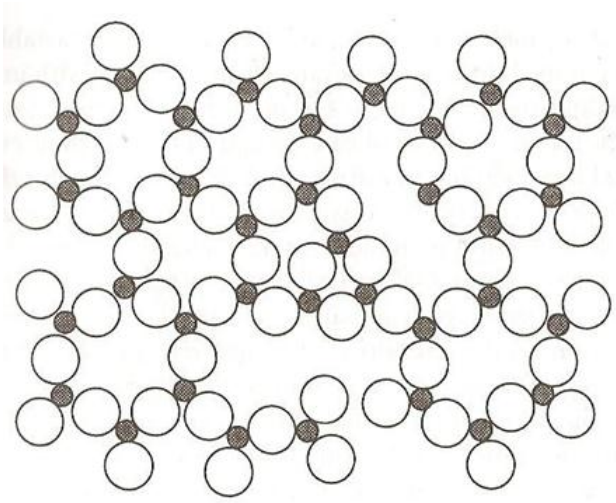

Figure 3.1. A two–dimensional representation of the local area structure within a SiO_2 glass[3.6]. Open circles are oxygen atoms, black circles are silicon atoms.

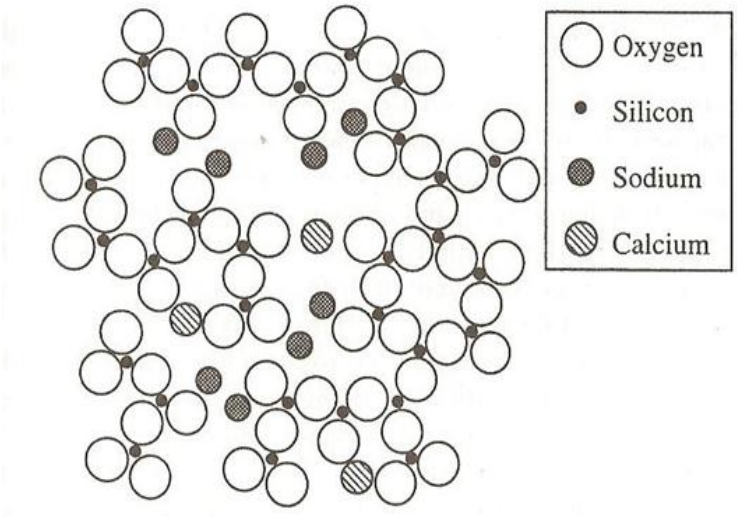

Figure 3.2. A two dimensional representation of the local area structure within a SiO_2 glass which has been modified with Na_2O and CaO[3.6].

Network modifiers are elements that are added to a glass composition to assist in the formation of a glass. Oxide modifiers include alkali oxides (Na_2O) and alkaline earth oxides (CaO). Modifiers are also known as fluxes, which act to reduce processing temperatures and can improve many of the properties of the resulting glass product such as durability and strength[3.6,3.8]. A schematic depiction of a SiO_2 glass which has been modified is shown in figure 3.2.

Traditional Methods of Rare Earth Incorporation

In the MCVD process, a thin porous fused silica layer is deposited on the inner surface of a substrate tube by the oxidation of a halide vapor of silicon tetrachloride, $SiCl_4$. Cladding material or soot is 'layed down" first, followed by the core soot which is typically comprised of silica (SiO_2) doped with germania (GeO_2) for control over the refractive index of the fiber. The soot is then densified at temperatures in excess of 2000ºC, and the tube is collapsed to produce a concentric, uniform, glass fiber preform with the desired refractive index profile[3.1,3.3,3.4,3.11]. The incorporation of rare earth dopants via vapor phase addition is completed during the core deposition step, where small quantities of vapor comprised of volatile rare earth compounds (halides, chelates) are carried downstream by the reactant flow within the substrate tube, oxidized in the hot zone and thereby incorporated into the core soot. This method requires modifications to the MCVD laydown/deposition process itself, to provide the dopant materials to the location of interest within the preform[3.3]. Additionally, this

method proves difficult to achieve high concentrations of rare earth dopant in the core, requires very precise temperature control to maintain dopant concentration and limits the potential for incorporation of more than one dopant ion[3.4]. Halide compounds of rare earth ions have low volatility, in general, making their incorporation at the high temperatures of MCVD processing more difficult[3.1].

In 1987, Townsend et al.[3.4], reported the method now known as solution doping, and is the most commonly used for rare earth incorporation. In this case, the fiber preform is fabricated using MCVD, where conventional cladding soot is deposited, after which the core soot layers are deposited at a reduced temperature to produce an unsintered porous soot. The soot-filled tube is then removed from the MCVD lathe and aqueous solutions of the desired dopant precursors are poured into the center of the tube, allowed to remain/soak for one hour, drained and allowed to dry. The doped soot tube is then returned to the lathe and the soot is subsequently sintered and collapsed per standard operating conditions.

Much work has been reported on the optimization of this technique to determine reproducible deposition and uniform doping along the length of the preform, the effect of solvent used, and desired doping concentrations[3.5,3.12]. Low rare earth solubility and rare earth clustering is a result of the difficulty of incorporating large quantities of lanthanide ions into the rigid SiO_2 network. The incorporation of network intermediates or modifiers, such as alumina (Al_2O_3) and

phosphate (P_2O_5), has been determined to be a crucial addition to the solution doping process to allow better control of rare earth concentration and profile within the core[3.1,3.13,3.14]. These modified glasses allow for higher concentrations of rare earth dopants without clustering effects as the modifier ions 'open up' the silicate structure which aids in solubility[3.13].

When solution doping at a ratio of modifier to rare earth of greater than one, the spectral emissions of rare earth ions within the active fibers are more typical of those seen from a rare earth doped bulk oxide glass. This indicates the rare earth ions and co-dopant/modifier ions are in close proximity of each other, providing a modified local environment about the rare earth ion. Phosphorous is considered more useful in this incorporation when compared to aluminum, however, phosphorous can cause an increase in the base-line loss of the optical fiber, making Al the preferred co-dopant. With the addition of Al, a broadening of emission spectra results and it prevents depletion of the rare earth in the core during preform fabrication at high temperatures. High Al concentration is preferred to improve fiber performance, however, at aluminum concentrations greater than one mole percent, a defect at the core clad interface may be generated that can lead to scattering of the signal within the fiber core[3.15].

Adaptation/Variation of Rare Earth Incorporation

Numerous studies have been reported[3.16-3.23] in which the incorporation by MCVD/solution doping of rare earth ions into the core of an optical fiber preform has been modified to better utilize the addition of glass modifier ions, in some cases to manipulate the defects seen at the core/clad interface, and a re-tooled method of vapor phase deposition, through the use of nanoparticle constituents.

Liekki Corporation of Lohja, Finland has developed a "Direct Nanoparticle Deposition" (DND) technology[3.16], where outside chemical vapor deposition (OVD) is used. Very similar to vapor phase deposition, the glass is doped in flame where the glass particles are formed using atomized liquid raw materials. Particles comprised of refractive index changing materials (alumina, germania) and doping materials (Yb, Er, Nd) are formed through evaporation/condensation with a small size distribution of 10-100 nm, are evenly distributed of the length of the fiber preform in the core region. Liekki reports this results in broad absorption and emission cross sections as a result of a highly doped core with improved emissions.

Blanc et al.,[3.17,3.18] and Dussadier[3.19], report a method where commercially available nanopowders of rare earth chlorides and calcium chloride are used in the soaking solution to incorporate Ca^{2+} and Er^{3+} ions into a MCVD fabricated preform by solution doping. Through the subsequent high temperature processing, germania and phosphorous are added to the core and erbium doped

particles are formed *in-situ* on the order of 100-250 nm. This technique is an extension of particles grown in bulk Cd-S-Se silicate glasses, where Cd nanoparticles of 2-6 nm are grown in commercially made borosilicate glasses during annealing at 650ºC[3.24]. Blanc reports an increase in the number of nanoparticles with increasing calcium concentration, a dependence of emission broadening with an increase in calcium concentration and signature emissions of Er^{3+} present. This method appears to manipulate the formation of the core/clad interface defect[4.10], to form nanoparticles in this region with desirable emission properties. The fibers made as a result of this process are reported to have high losses due to scattering and the average nanoparticle size is considered too large to allow acceptable transmission[4.12]. As these particles are made *in-situ,* and result in particles greater than 100 nm in diameter, this method is not a direct corollary to what was done in this study, but it is a method which is trying to achieve similar properties out of the resulting fiber.

Podrasky et al.[4.15], reports a similar method to Blanc, by using alumina and erbium oxide nanopowders in the solution doping step, with water as the aqueous media and phosphorous is present in the core region of the preform. These nanoparticles are produced during the high temperature sintering process of MCVD and improved intensity of erbium emissions result when compared to conventionally solution doped preforms containing erbium and aluminum. This is concluded to be a result of the reduction in quenching by virtue of better homogeneity of erbium ion concentration distribution within the preform.

Boivin, et al., of Draka Communications (France)[4.16], has developed a method in which erbium doped alumina nanoparticles are “synthesized in a soft chemical way”, on the order of 5-50 nm, put in an aqueous suspension and “incorporated using the classical liquid doping technique.” They claim this method results in fibers exhibiting standard erbium emission behavior with much lower aluminum content, and improved fiber performance from the homogenous distribution of erbium along the fiber length.

La Sauze et al., of Alcatel Research & Innovation (France)[4.17], detail the use of ‘erbium doped nanoparticles’ which are synthesized in a preliminary step and are ‘inserted’ within the glass matrix via classical soaking process. The resulting fiber shows similar bandwidth and power conversion efficiency when compared to alumino-silica fibers and high homogeneity.

Recent work by the Ballato group[4.17] utilized Tb^{3+}- and Eu^{3+}-doped lanthanum fluoride, LaF_3, nanoparticles dispersed in water/ethanol to traditionally solution dope a MCVD produced optical preform. The resulting glass produced designer emission spectra through tailored energy transfer. This demonstrated the feasibility of using nanoparticles produced in this lab as rare earth host materials to readily incorporate RE^{3+} ions into silica glass preforms.

All of the methods discussed here suggest the use of nanoparticles in various forms as dopant delivery, provides high homogeneity in the distribution of the rare earth ions as well as suggests the opportunity exists for further control

over the local environment of the rare earth ion, and potentially control over the specific emissions themselves. Here, the use of rare earth doped alkaline fluoride nanoparticles to solution dope demonstrates an impact on not only the 'bulk' homogeneity characteristics of the rare earth ion as previously reported, it will show an impact on the local surroundings/environment of the rare earth ion which results in a change in emission behavior, indicating the ability to tailor or engineer the spectral emissions of an optical fiber preform.

Experimental Procedures

Nanoparticle Synthesis

Five mole percent europium doped calcium, strontium and barium fluoride nanoparticles were produced as per the details in Chapter 2, Experimental Procedures, Basic Core Doped.

Preform Fabrication

The combination of modified chemical vapor deposition (MCVD) and solution doping was used to fabricate GeO_2-SiO_2 core/ SiO_2 clad optical fiber preforms. Four individually solution doped preforms were produced: 5Eu:CaF_2, 5Eu:SrF_2, 5Eu:BaF_2 and Eu/Al doped.

MCVD was carried out on the SG Controls lathe at COMSET Laboratories per standard operating conditions. Clad soot was deposited at temperatures above 1500ºC inside a standard silica tube from a reactant stream of silicon tetrachloride, $SiCl_4$. The porous, core soot layers were then deposited at 1600ºC from a reactant stream of $SiCl_4$ and germanium tetrachloride, $GeCl_4$ at an approximate ratio of 14:1 in excess oxygen. The unsintered, porous soot preform was removed from the lathe, inserted into a vertical holding table/vice and the individual solution* was drawn into the open centerline of the preform and allowed to soak for one hour, drained and dried overnight, in air. The precursor doped preform was then returned to the lathe where it was heated

progressively to insure burnoff of excess solvent in an oxygen, O_2, atmosphere. The soot was then sintered to reduce porosity at 1650ºC (Sr & Ba preforms), 1750ºC (Ca) or 1600ºC (Eu/Al). The soot was then consolidated into solid glass at 2000ºC and the centerline was collapsed.

*The nanoparticles were individually suspended in anhydrous tetrahydrafuran (THF) to achieve a doping level of nanoparticles in solution of 0.1M. Nanoparticles were batched by weight and added to 150 ml of THF, sonicated for 30 minutes to insure a uniform suspension and made approximately one hour before the solution doping step. This solution results in a preform which is doped to ~2500 parts per million of 5Eu:AEF_2 nanoparticles (estimated values based on Reference [3.4, 3.5]) The Eu/Al solution was made to a ratio of 0.1M/1M in a solution containing equal parts water and ethanol.

Photoluminescence

Emission and phonon sideband measurements were performed on polished, 10 mm cross-sections of the doped glass preforms using a Jobin Yvon Fluorolog Tau 3 fluorometer as detailed in Chapter 2, Experimental Procedures, Photoluminescence.

Raman Spectroscopy

Vibrational energies were determined for heat treated undoped alkaline earth fluoride nanoparticles via Raman spectroscopy. Raman measurements were completed on a Senterra 178 Raman Microscope (Bruker Optics) operating at a laser wavelength of 532 nm, laser power of 20 mW and integration time of 100 s , as detailed in Chapter 2, Experimental Procedures, Raman Spectroscopy.

Lifetime Measurements

Lifetime measurements of the core doped glass preforms were completed by Prof. M. Bass and co-workers at CREOL, the University of Central Florida. The system set-up is detailed in Reference 3.25. Measurements were completed at a pump wavelength of 464 nm and data was collected for the 613 nm emissions at room temperature, at three different time settings per sample. Background measurements were collected and subtracted from each corresponding data set, and the lifetime, τ, was calculated.

Results and Discussion

Spectral Behavior

The emission spectra (λ_{ex} = 393 nm) from the 5Eu:(AE)F_2 nanoparticles and the corresponding nanoparticle doped preforms are shown in Figure 3.3. All spectra were normalized to the intensity of the $^5D_0 \rightarrow {}^7F_1$ magnetic dipole transition since such transitions are insensitive to the local environment. The Eu^{3+} in the as-made nanoparticles emits characteristically at 590 nm ($^5D_0 \rightarrow {}^7F_1$) and 610 nm ($^5D_0$—$^7F_2$) as well as at about 650 nm ($^5D_0 \rightarrow {}^7F_3$) and 695 nm ($^5D_0 \rightarrow {}^7F_4$). As discussed in Chapter 2 , there is a marked difference in europium environment between that of the CaF_2 hosted nanoparticles and the SrF_2 and BaF_2 nanoparticles, as further demonstrated by the different values of hypersensitivity ratio (Table 3.1). The hypersensitivity ratio, HR, is the relative emission ratio of the electric dipole emission ($^5D_0 \rightarrow {}^7F_2$ for Eu^{3+}) to the magnetic dipole emission ($^5D_0 \rightarrow {}^7F_1$ for Eu^{3+}) and its value is a good measure of the nature and symmetry of the rare earth ion within a host material.

In the 5Eu:(AE)F_2 nanoparticle doped preforms, the emissions are predominately that of the $^5D_0$ manifold of Eu^{3+}, with single peaks at ~590 nm ($^5D_0 \rightarrow {}^7F_1$), 610 nm ($^5D_0$—$^7F_2$), 650 nm ($^5D_0 \rightarrow {}^7F_3$) and ~700nm ($^5D_0 \rightarrow {}^7F_4$), which directly correlates to the emissions of the as-made nanoparticles. In contrast, the conventionally Eu-doped preform emissions are also shown in figure 3.3b, which correspond to the $4f^6 5d^1 \rightarrow 4f^7$ transition of Eu^{2+} that emits at ~424 nm, as

previously reported[3.26]. This stark change in emission behavior (Eu^{3+} vs. Eu^{2+}) indicates a distinct change in local environment for the Eu ion which can be assumed to be directly related to the change in precursor dopant as well as distinguishes differences between the nanoparticle and glass preforms. In examining the hypersensitivity ratios of the nanoparticles to their corresponding preforms (Table 3.1, figure 3.5), this distinct difference in the environment about the europium ion is demonstrated. Changes in the structural and chemical surroundings of the europium ion are evidenced by the hypersensitivity ratio (figure 3.5). The extensive change in HR between the doped nanoparticle and the corresponding nanoparticle doped preform for each alkaline earth type demonstrates the change in structural environment of the Eu ion as it changes from the highly ordered, cubic structure to that of the random structure of the glass. The hypersensitivity ratio changes significantly in the glass preforms from that of the nanoparticles - the 610 nm emission becomes the dominant emission in the glass host matrix, indicating that the environment about the rare earth ion is much more symmetric in the fluoride crystal than that of the oxide glass. In comparing Eu:AEF_2 doped preforms, the change in local chemical environment for the europium ion becomes evident, as the SrF_2 and BaF_2 doped preforms appear to have similar hypersensitivity ratios, while the CaF_2 doped preform has a lower HR, indicating a slightly more ordered environment when compared to the other preforms. This difference may be correlated to the slightly opaque core of the CaF_2 preform, while the SrF_2 and BaF_2 preforms were transparent. This

physical difference in the glass suggests the nanoparticles were more ‘in-tact’ following the high temperature processing of the CaF_2 doped preform, indicating the Eu^{3+} ion environment did not change as significantly as the other cases. However, the difference in surroundings is consistent with its as-made nanoparticle counterparts. . This also suggests that SrF_2 and BaF_2 nanoparticles are more influenced by the surrounding SiO_2 matrix, due to the larger volume they occupy upon incorporation and subsequently diffuse into at elevated temperatures. The change in emission behavior between the conventional solution doped preform and the nanoparticle doped preforms suggest that the nanoparticles, though oxidized during the MCVD process, yield a spatial localization of the rare earth ion in the glass host, and the rare earth ion largely remains near the volume originally comprised by the nanoparticle. The Eu^{3+} emissions demonstrated by the preforms are reasonably similar to that of the heat treated, multi-shell nanoparticle emissions, further substantiating the rare earth ion is ‘insulated’ from the surrounding silica matrix by the immediate surrounding remaining from their original nanoparticle host. Figure 3.5 is a schematic representation of the believed local structural environment of the rare earth within the core region of the silica optical fiber preform.

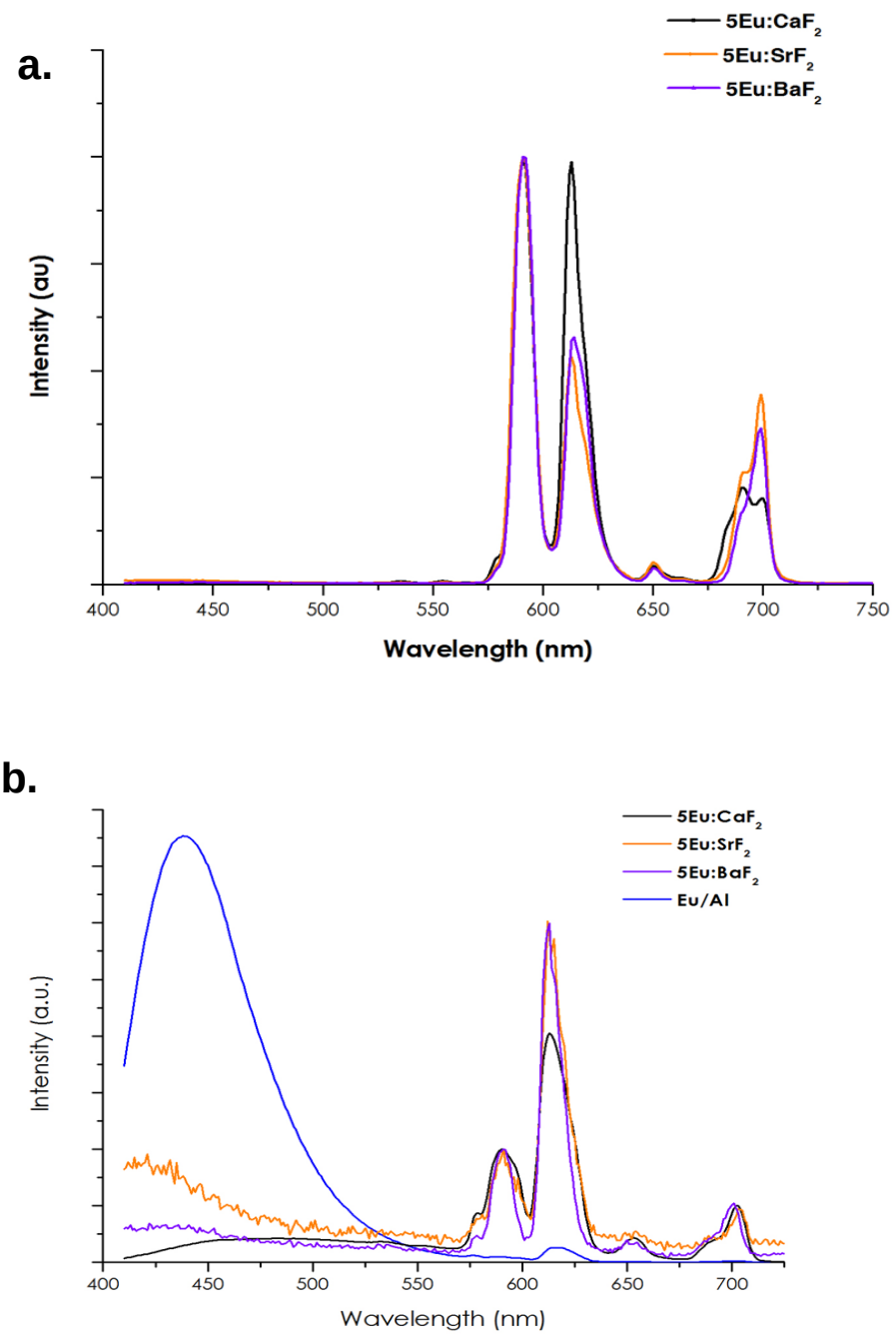

Figure 3.3. a) Emission spectra of precursor europium doped $(AE)F_2$ nanoparticles, b) Emission spectra of 5Eu:$(AE)F_2$ nanoparticle doped silica preforms

Table 4.1

Calculated Eu^{3+} Hypersensitivity Ratios

Material Type	$(^5D_0 \rightarrow {}^7F_2)/(^5D_0 \rightarrow {}^7F_1)$
5Eu:CaF_2 nanoparticles	1.045
5Eu:CaF_2 doped preform	2.18
5Eu:SrF_2 nanoparticles	0.623
5Eu:SrF_2 doped preform	3.04
5Eu:BaF_2 nanoparticles	0.717
5Eu:BaF_2 doped preform	3.06

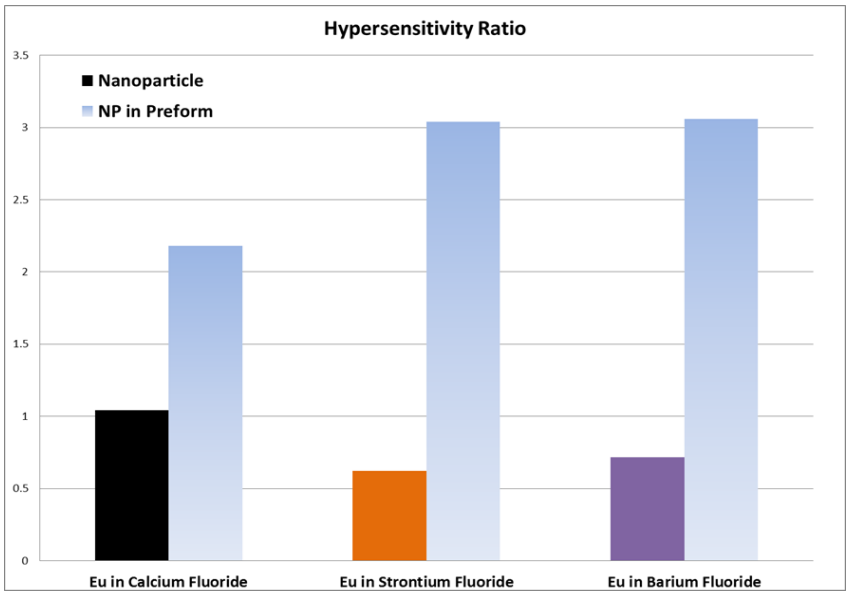

Figure 3.4. Comparison of hypersensitivity ratio, nanoparticle vs. nanoparticle doped preform.

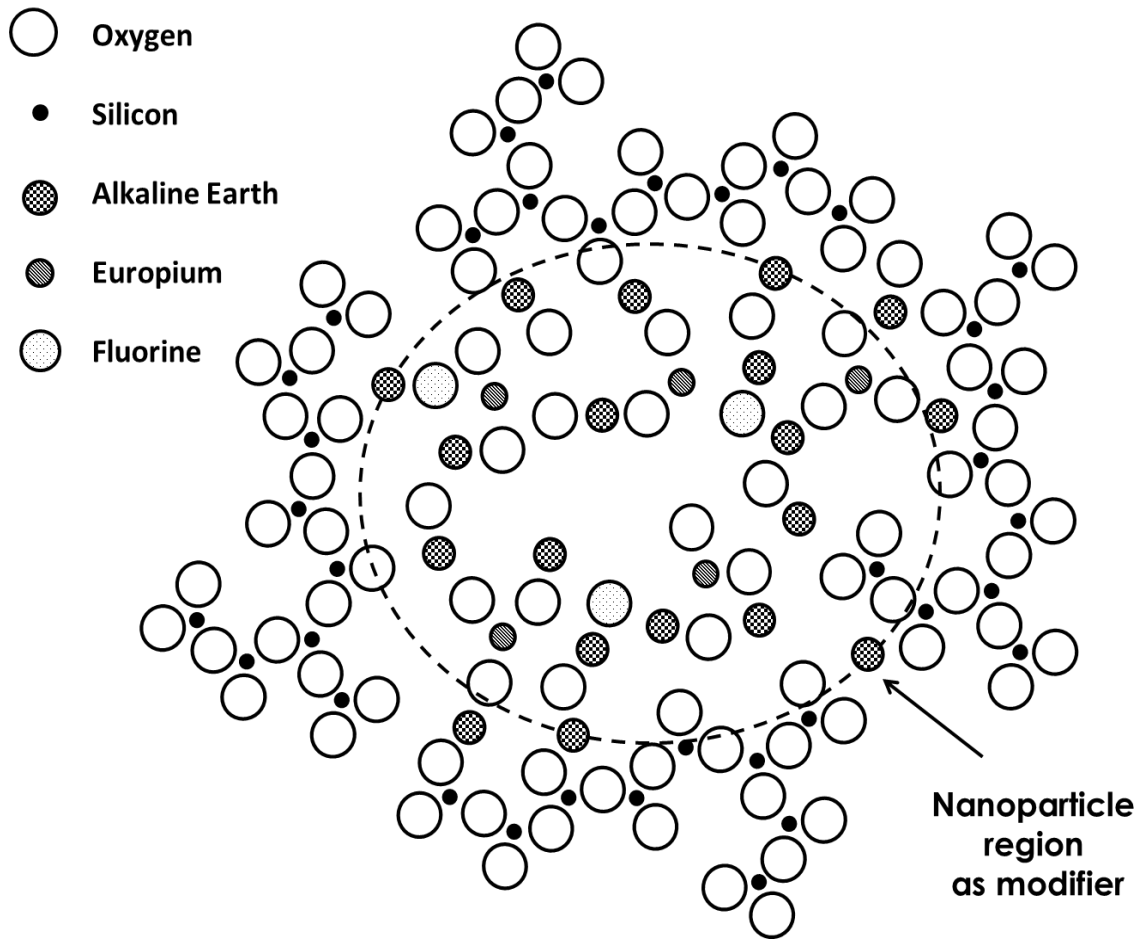

Figure 3.5. Schematic representation of Eu:(AE)F_2 nanoparticle incorporation into the core region of a silica optical fiber preform.

Vibrational Energy

The influence of the change in environment is further evidenced by the analysis of the phonon or vibrational energy of the different materials systems. Phonon sideband spectroscopy, PSB, measurements (details in Chapter 2) were completed on the nanoparticles and their preform counterparts, shown in Figure 3.6. Additionally, an attempt to simulate the behavior of the alkaline earth fluoride nanoparticles during MCVD processing and for comparison to the PSB , undoped $(AE)F_2$ nanoparticles were heat treated for one hour at 700ºC and 1100ºC, in air. These particles were then analyzed using Raman spectroscopy to determine the vibrational energies of the presumed oxidized alkaline earth host component of the nanoparticles (figure 3.7).

The PSB associated with the alkaline earth fluorides was previously determined, (detailed in Chapter 2) to be ~250 cm^{-1} for CaF_2, ~280 cm^{-1} for SrF_2 and ~320 cm^{-1} in the as-made nanoparticles (figure 3.6a). In comparison, the first sideband associated with PSB measurements for the corresponding nanoparticle doped preforms (figure 3.6b) yield vibrational energies for Ca-O = 965 cm^{-1}, Sr-O = 1001 cm^{-1}, Ba-O = 992 cm^{-1}. The vibrational energy of a Si-O bond in the glass is reported[3.27] to be very close to these values, at ~1050 cm^{-1}, however, a detailed study of Raman spectra of alkaline earth oxide-silicates at 1600ºC by Frantz and Mysen[3.28], report a second component of this value to be associated with the alkaline earth oxide present in the glass matrix, and

approximate the vibrational energy of Ca-O, Sr-O and Ba-O to be ~915 cm^{-1}. Here, the values for these alkaline earth species are shown to be less than the silica, indicating the influence of the alkaline earth ion on the environment of the Eu ion, despite the proximity of the Si-O. The Raman analysis of the heat treated nanoparticles (figure 3.7) determined the vibrational energies to be: Ca-O = 965 cm^{-1}, Sr-O = 951 cm^{-1} and Ba-O = 934 cm^{-1}, with these values similar to that reported by Frantz and Mysen[3.28] as well as the values determined by PSB. It is interesting to note, the Raman shift associated with the alkaline earth fluorides is still present in the heat treated nanoparticles (figure 3.7a and figures 2.7-2.9)., indicating the complete oxidation of the nanoparticles themselves does not take place at elevated temperatures. The comparison of the PSB of the conventionally doped preform to the nanoparticle doped preforms (figure 3.7b) indicates the chemical and vibrational environment differences of the local europium surroundings, evidenced by the lack of a sideband presence in the Eu/Al solution doped preform. Further, in comparing the different alkaline earth hosts, the environments can be viewed as completely different, supporting the postulation that the incorporation of rare earths via alkaline earth fluoride nanoparticle hosts provides a predictable localized environment for the rare earth ion, and in turn, a method to predetermine the emissions of an optical glass fiber.

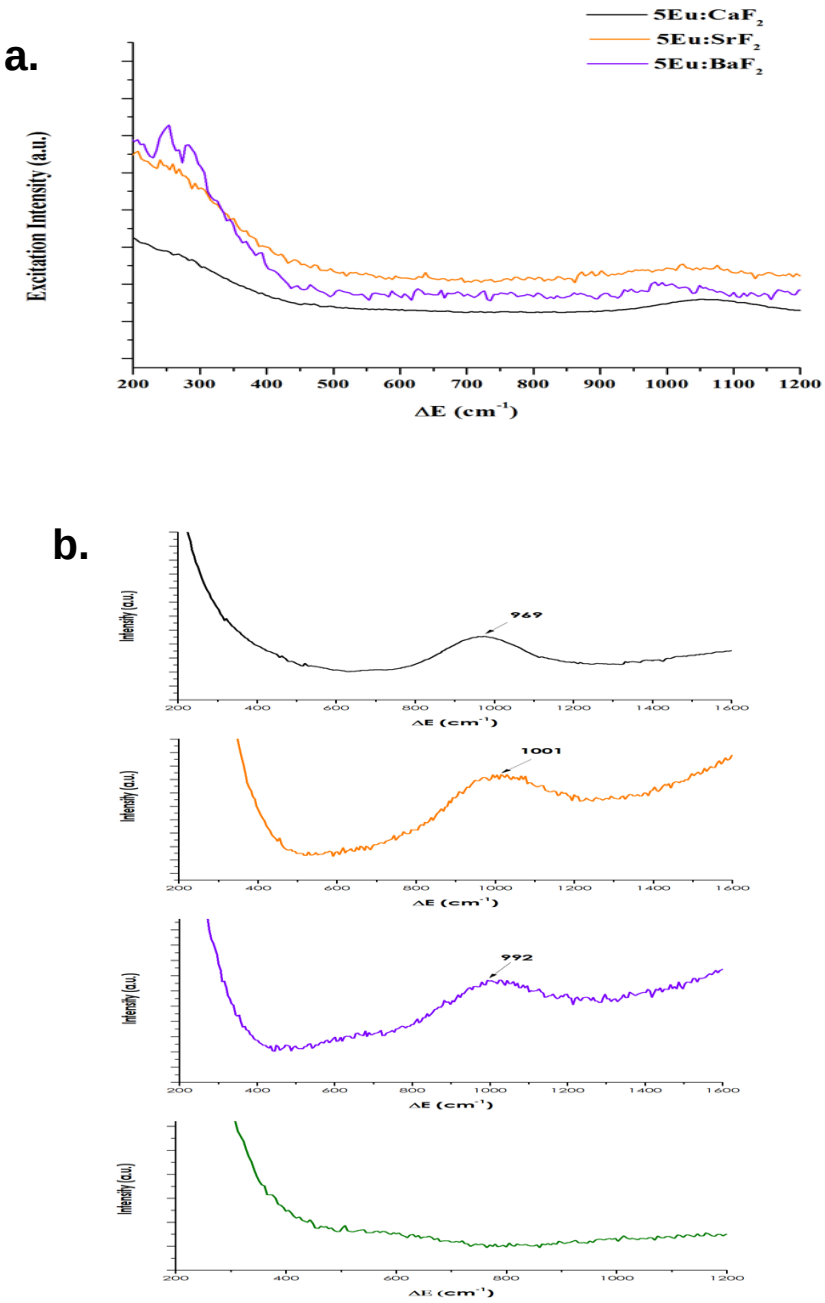

Figure 3.6. Phonon Sideband (ΔE) measurements (λ_{em}=613 nm) for a)Eu:(AE)F_2 precursor nanoparticles, b) Eu:(AE)F_2 nanoparticle doped preforms (CaF_2, SrF_2, BaF_2, Eu/Al)

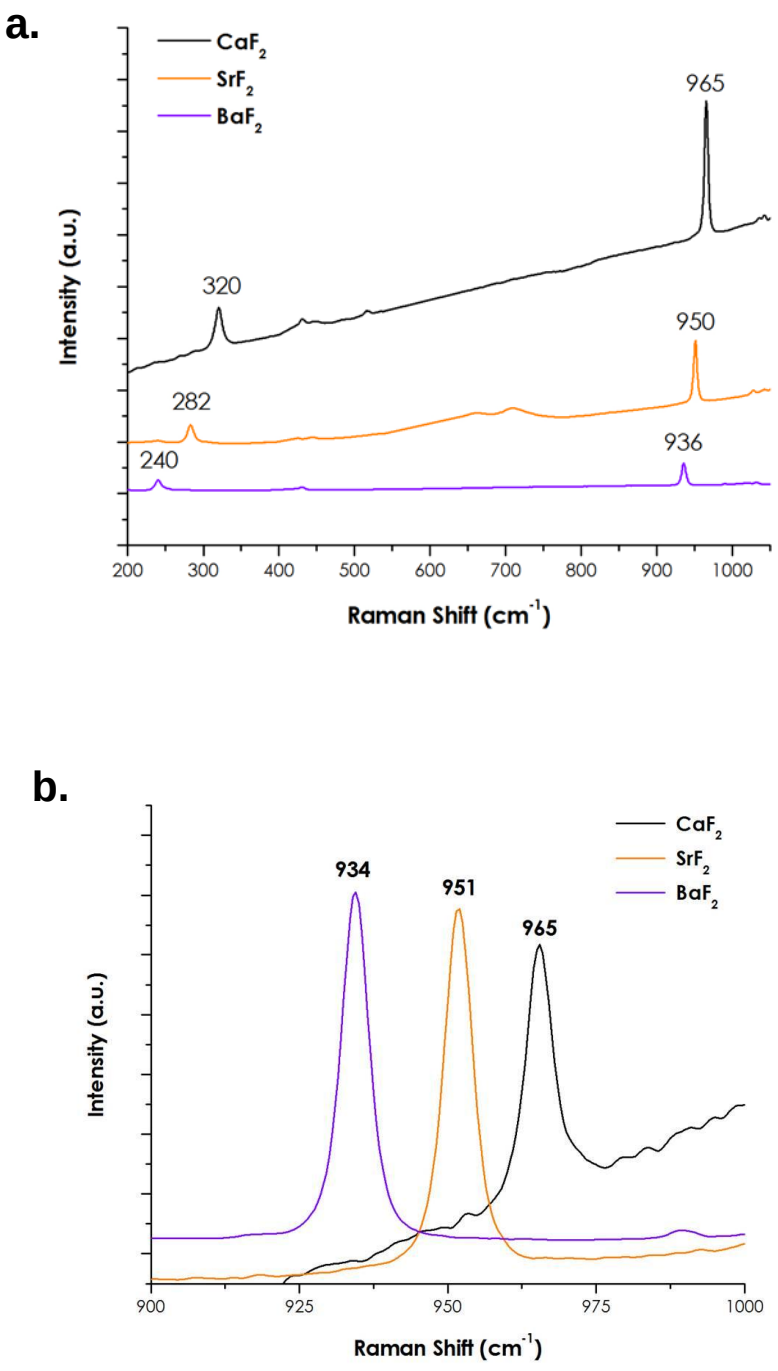

Figure 3.7. Raman spectra of undoped $(AE)F_2$ nanoparticles heat treated for one hour at a) 700ºC b) 1100ºC

Fluorescence Lifetime

The length of time between the absorption of a photon and the subsequent emission of another photon can be very short (< 1 nanosecond) or long (> 1 millisecond) and this time interval is referred to as the fluorescence lifetime. The interaction of the emitting ion with its local environment affects this decay. Investigating the rare earth ions interaction with the glass matrix by evaluating the lifetime offers information about the local microstructure in the vicinity of the doped ion and the glass matrix itself[3.28-3.30].

Resultant decay curves for the three 5Eu:(AE)F_2 doped preforms are shown in Figure 3.8. These values are found by monitoring emission as a function time while exciting the sample with a pulse or modulated excitation and data is then plotted with a semi-logarithmic scale with the slope of the resulting line corresponding to the fluorescence lifetime[3.31,3.32]. If the decay contains more than one exponential component, the curve will deviate from a linear slope.

The calculated lifetime values are summarized in Figure 3.9. The curves for Eu:BaF_2 doped preform present single slope or monoexponential decay, with an average lifetime of 2.69 ms. The Eu:CaF_2 doped preform presents two distinct decay components (calculated values are within 2% of each other); a slow decay of 1.96 ms and a fast decay of 3.71μs. The Eu:SrF_2 doped preform has a slow decay component of 2.19 ms, however, a hardly noticeable fast decay component varies from 7 μs to 13.7 μs. The higher vibrational energy of the

CaF_2 as compared to SrF_2 and BaF_2 is an indication of the shorter lifetime exhibited and the difference in the surroundings from one host material to the next. This may explain the weak, but distinct fast decay component of the CaF_2 preform and the single lifetime of the BaF_2 doped preform. In glasses with low vibrational energy, the europium ions have a more ionic local environment which supports relatively long fluorescent lifetime. Here, the lifetime values increase with decreasing vibrational energy of the host alkaline earth fluoride, further suggesting the environment about the europium ion is coincident with the original dopant nanoparticle matrix, with less influence from the silica glass matrix.

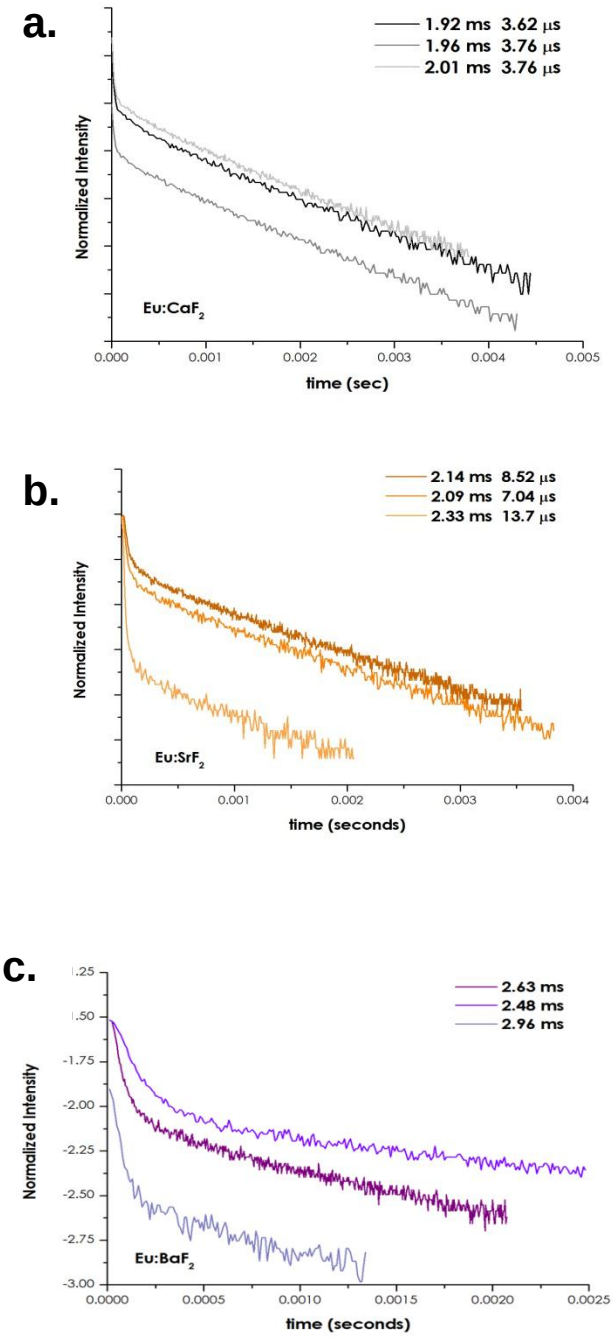

Figure 3.8. Fluorescence decay curves for a) 5Eu:CaF_2 doped preform, b) 5Eu:SrF_2 doped preform, c) 5Eu:BaF_2 doped preform (legend denotes corresponding slow and fast decay values)

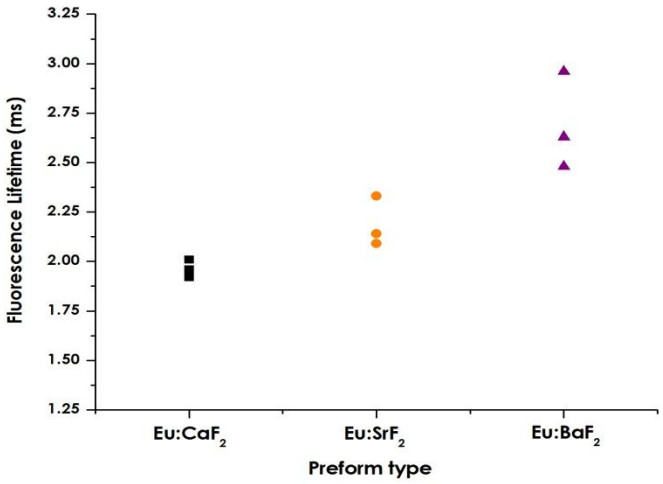

Figure 3.9. Fluorescence lifetime as a function of preform type.

Summary

Various rare earth doped alkaline earth fluoride nanoparticles were successfully used as dopant delivery materials in the fabrication of optical fiber preforms. As a result, the optical properties of the preforms were significantly influenced by their incorporation in the core region.

The spectral emissions of the nanoparticle solution doped preforms were characteristic of the rare earth ions, Eu^{3+}, demonstrating homogeneity and uniform distribution of the nanoparticles along the length of the preform, and in turn the europium is evenly distributed. The preform emissions correlated to the emission of their precursor dopant nanoparticles, suggesting the tailoring or engineering of the resultant optical fiber emissions is possible.

The distinct differences in the local chemical and structural environment about the europium ion, as evidenced by the emissions, hypersensitivity ratio and vibrational energies, demonstrate the impact the presence of the alkaline earth nanoparticles have as dopant materials. Additionally, fluorescence lifetimes of the nanoparticle doped preforms were shown increase with decreasing vibrational energy of the nanoparticle host material, indicating the local environment of the dopant nanoparticle is retained and influence the overall fluorescence behavior of the rare earth ion within the optical fiber preform.

A more detailed local structural model of the doped core glass region has been developed based on the resulting optical behavior which illustrates the

belief that the rare earth ion is ‘insulated’ from the surrounding silica matrix by the immediate surroundings remaining from the original nanoparticle host.

Overall, it has been shown that the use of rare earth doped alkaline fluoride nanoparticles as a dopant material by means of the conventional solution doping method for active optical fiber provides a method to tailor or engineer its spectral behavior. The ability to ‘tune’ the resultant spectral emissions through the choice of alkaline earth host, rare earth dopant and rare earth dopant concentration within the nanoparticle prior to solution doping has been demonstrated.

References

3.1 Bjarklev, A., Optical Fiber Amplifiers: Design and System Applications, Artech House, Boston, 1993.

3.2 Senior, J.M., Optical Fiber Communications Principles and Practice, Prentice Hall, Hertfordshire, 1992.

3.3 Poole, S.B., Payne, D.N., and Fermann, M.E., "Fabrication of Low-Loss Optical Fibres Containing Rare Earth Ions," *Electronics Letters*, 21 [1985] 737.

3.4 Townsend, J.E., Poole, S.B., and Payne, D.N., "Solution-Doping Technique for Fabrication of Rare Earth Doped Optical Fibres," *Electronics Letters*, 23 [1987] 329.

3.5 Khopin, V.F., Umnikov, A.A., Gur'yanov, A.N., Bubnov, M.M., Senatorov, A.K. and Dianov, E.M., "Doping of Optical Fiber Preforms via Porous Silica Layer Infiltration with Salt Solutions," *Inorganic Materials*, 41 [2005] 363.

3.6 Shelby, J.E., Introduction to Glass Science and Technology, The Royal Society of Chemistry, Cambridge, 1997.

3.7 Paul, A., Chemistry of Glasses, Chapman and Hall, New York, 1990.

3.8 Vashneya, A.K., Fundamentals of Inorganic Glasses, Academic Press, Inc., San Diego, California, 1994.

3.9 Volf, M.B., Chemical Approach to Glass, Elsevier, New York, 1974.

3.10 Kingery, W.D., Bowen, H.K., Uhlmann, D.R., Introduction to Ceramics, John Wiley and Sons, New York, 1976.

3.11 Langner, A., Shotz, G., Such, M., Kayser, T., Grimm, S., Kirchof, J., Krause, V., and Rehmann, G., "A new material for high power laser fibers," Proceedings of SPIE, 6873 [2008] 687311-1.

3.12 Dhar, A., Pal, A., Paul, M.C., Ray, P., Maiti, H.S., and Sen, R., "The mechanism of rare earth incorporation in solution doping process," Optics Express, 16 [2008] 12835.

3.13 Digonnet, M.J.F. ed., Rare-Earth-Doped Fiber Lasers and Amplifiers, Marcel Dekker, Inc., New York, New York, 2001.

3.14 Weber, M.J. in Ultrastructure Processing of Advanced Materials, Uhlmann, D.R. and Ulrich, D.R. eds., 1992.

3.15 Dhar, A., Das, S., Maiti, H.S. and Sen, R., “Fabrication of high aluminum containing rare-earth doped fiber without core-clad interface defects,” Optics Communications, 283 [210] 2344.

3.16 Tammela, S., Soderlund, M., Koponen, J., Philippov, V. and Stenius, P., “The Potential of Direct Nanoparticle Deposition for the Next Generation of Optical Fibers,” Proceedings of SPIE Photonics West, 6116-16 [2006].

3.17 Blanc, W., Dussardier, B., Monnom, G., Peretti, R., Jurdyc, A., Jacquier, B., Foret, M. and Roberts, A., “Erbium emission properties in nanostructured fibers,” *Applied Optics*, 48 [2009] G119.

3.18 Blanc, W., Dussardier, B., and Paul, M.C., “Er-doped oxide nanoparticles in silica-based optical fibers,” Physics and Chemistry of Glasses: European Journal of Glass Science and Technology Part A50, 1 [2009] 79.

3.19 Dussardier, B., Blanc, W., and Monnom, G., “Luminescent Ions in Silica-Based Optical Fibers,” Fiber and Integrated Optics, 27 [2008] 484.

3.20 Podrazky, O., Kasik, I., Pospisilova, M. and Matejec, V., “Use of nanoparticles for preparation of rare-earth doped silica fibers,” Physica Status Solidi C, 6 [2009] 2228.

3.21 Boivin, D., Fohn, T., Burov, E., Pasouret, A., Gonnet, C, Cavani, O., Collet, C. and Lempereur, S., “Quenching investigation on New Erbium Doped Fibers using MCVD Nanoparticle Doping Process,” Proceedings of SPIE, 7580 [2010] 75802B-1.

3.22 Le Sauze, A., Simonneau, C., Pastouret, A., Gicquel, D., Bigot, L., Choblet, S., Jurdyc, A.M., Jacquier, B., Bayart, D. and Gasca, L., “Nanoparticle Doping Process: towards a better control of erbium incorporation in MCVD fibers for optical amplifiers,” in Optical Amplifiers and Their Applications, OSA Technical Digest Series, (Optical Society of America, 2003), paper WC5.

3.23 Kucera, C., Kokuoz, B., Edmondson, D., Griese, D., Miller, M., James, A., Baker, W. and Ballato, J., “Designer emission spectra through tailored energy transfer in nanoparticle-doped silica preforms,” Optics Letters, 34 [2009] 2339.

3.24 Cereyon, A., Jurdyc, A., Martinez, V., Burov, E., Pastouret, A., and Champagnon, B., “Raman amplification in nanoparticles doped glasses,” Journal of Non-Crystalline Solids, 354 [2008] 3458.

3.25 Turri, G., Sudesh, V., Richardson, M., Bass, M., Toncelli, A. and Tonelli, M., "Temperature-dependent spectroscopic properties of Tm3+ in germinate, silica and phosphate glasses: A comparative study," Journal of Applied Physics, 103 [2008] 093104.

3.26 Oh, K., Morse, T.F., Reinhart, L. Kilian, A. and Risen, Jr., W.M., "Spectroscopic analysis of a Eu-doped aluminosilicate optical fiber preform," Journal of Non-Crystalline Solids, 149 [1992] 229.

3.27 Tanabe, S., "Optical properties and local structure of rare-earth-doped amplifier for broadband telecommunication," Journal of Alloys and Compounds, 408-412 [2006] 675.

3.28 Frantz, J.D., and Mysen, B.O., "Raman spectra and structure of $BaO-SiO_2$, $SrO-SiO_2$, and $CaO-SiO_2$ melts to 1600C," Chemical Geology 121 [1995] 155.

3.29 www.assaymetrics.com/fluorescence_lifetime.htm

3.30 www.olympusview.com/theory/glossary.html

3.31 Herrmann, A., Fibikar, S. and Ehrt, D., "Time-resolved fluorescence measurements on Eu^{3+} and Eu^{2+} doped glasses," Journal of Non-Crystalline Solids, 355 [2009] 2093.

3.32 Demas, J.N., Excited State Lifetime Measurements, Academic Press, New York, New York, 1983.

CHAPTER IV

CONCLUSIONS

This study aimed to advance the spectral engineering of active optical fiber by providing a novel method to control local chemistry about the site of the rare-earth dopant within the core of the optical fiber. Optically active nanoparticles based on alkaline earth fluorides were investigated and used as the primary core additives in optical fiber preforms to establish this alternative method.

Doped and undoped calcium, strontium and barium fluoride nanoparticles were successfully synthesized and characterized for their physical, chemical, and optical behavior. Distinct spectroscopic differences as a result of the different host materials and varying rare earth dopant levels were demonstrated. Through evaluation of specific spectroscopic traits (hypersensitivity ratios, photoluminescence) of the dopant rare earth ion, the resulting emissions of the rare earth dopant were determined to be influenced by alkaline earth host and dopant concentration. Variations in emission behavior and hypersensitivity ratio of heat treated nanoparticles demonstrated a difference in local environment for the rare earth ion from host to host, which provides another means of controlling the spectroscopic behavior of the alkaline earth fluoride nanoparticles. By using photoluminescence to predict diffusion behavior, the application of a simple one dimensional model for diffusion provided a method for predicting the diffusion

coefficient of europium ions in alkaline earth fluorides with order of magnitude accuracy.

By using the rare earth doped alkaline earth fluoride nanoparticles as the dopant materials in the core of optical fiber preforms, the resultant optical properties of the glass were significantly influenced by their presence in the core. The spectral emissions of the nanoparticle doped preforms demonstrated homogeneity and uniform distribution of the rare earth dopant. Additionally, the emissions of the preforms correlated directly to the emissions of the precursor dopant nanoparticles, rather than the emissions of a conventionally doped optical fiber preform. This difference in spectral behavior as well as the correlation of emissions to the original nanoparticles, provide additional proof that this method provides a means to tailor the optical behavior of the resulting optical fiber. The optical behavior resulting from these nanoparticle doped preforms provided information with regards to the chemical and structural environment of the rare earth ion within the silica glass matrix. As a result, a more detailed structural model of the doped core glass region was developed which illustrates the 'insulation' of the rare earth ions from the surrounding silica matrix by the immediate surroundings from the original rare earth ion's nanoparticle host.

It has been shown that rare earth doping of alkaline earth fluoride nanoparticles provides a material which can be 'tuned' to specific applications through the use of different host materials, processing conditions and doping

levels of the rare earth. Furthermore, these nanoparticles were successfully used as dopant delivery materials in the fabrication of active optical fiber. As a result, it was shown that the resulting optical fiber can be tailored to specific spectral emissions through the choice of alkaline earth host, dopant and dopant concentration. Such tailoring is critical to the continued value-added advancement in optical fiber technologies.

CHAPTER V

FUTURE WORK

In order to maintain the focus of the study presented here with regards to alkaline earth fluoride nanoparticles and their use in optical fiber, there were results and questions which arose through the analysis of the findings which were deemed beyond the scope of this study. Therefore, the following are recommended pursuits that would be beneficial to further the understanding of various aspects of the materials and phenomenona discovered over the course of experimentation.

Alkaline Earth Fluoride Nanoparticles

First, a further optimization of the synthesis process is suggested. The synthesis method chosen was not optimized for the specific kinetics of growth and nucleation for alkaline earth fluorides, and is reflected in the broad particle size distribution noted for the basic core and core/shell nanoparticle types. An investigation of this nature may also aid in explaining the difference in 'shelling' behavior between the host species.

Second, a study of the phenomenon which results in divalent europium ion emissions from calcium fluoride hosted core/shell nanoparticles when heat treated while the strontium and barium fluoride exhibit trivalent europium ion

emissions under the same conditions. Initial attempts to quantify the Eu^{2+} were inconclusive, however, a study which analyzes the effects of size of the host ion with respect to the europium ion emission is suggested. This should include a study of the crystal field effects of the interaction of the host ion and dopant ion and any charge compensation effects.

Finally, an investigation of other alkaline earth host materials and doping of the nanoparticles with optically active ions is of interest. Magnesium fluoride, MgF_2, is a tetragonal rather than cubic crystal system and the alkaline earth has a smaller ionic radius than that of Ca^{2+}, Sr^{2+}, and Ba^{2+}. If made in the core/shell capacity and heat treated, this may give insight into the size effects associated with the Eu^{3+}/Eu^{2+} phenomenon. Work was begun in this regard, however, the different crystal structure did not allow a direct comparison of the MgF_2 to the CaF_2, SrF_2 and BaF_2 and was not pursued further (Appendix D).

The doping of the nanoparticles with optically active transition metal ions is also of interest, specifically chromium. Solid state materials which lase in the near infrared region are of extreme interest and the incorporation of chromium in forsterite ($MgSiO_2$) and YAG ($Y_3Al_5O_{12}$) has been studied at length due to their emissions in the near IR. The technology presented here lends itself to the possibility of an 'easier' method of doping materials with chromium for use in other practical applications. Work was begun in this regard (Appendix D), however, transition metal chemistry and optical behavior is quite different from

that of rare earth ions, and pursuit of this study would be a dissertation in and of itself.

Glass and Optical Fiber

The current study used the traditional concentration of dopant in solution (0.1 M dopant solution) for simplicity in order to determine the feasibility of using the nanoparticles in this application. A study which investigates variations in nanoparticle concentration in order to optimize the rare earth doping levels in the resulting optical fiber preform, and the impact the changes in doping level has on the resulting optical behavior is recommended. This would provide further evidence of the extent of control that exists over spectral behavior when using this method.

The control over the spectral behavior of optical fiber demonstrated though the use of rare earth doped alkaline earth fluoride nanoparticles as the dopant delivery material suggests this technique will lend itself to other types of dopants within the nanoparticles. The incorporation of Cr^{4+} into the core of an optical fiber is of particular interest because this would result in a fiber amplifier which can be used from 1.3-1.6 μm. However, this requires the separate growth of a of rod single crystal Cr^{4+} doped YAG which is then placed inside a silica rod and drawn into fiber. If Cr3+/Cr^{4+} doped alkaline earth fluoride nanoparticles could be fabricated with the simple synthesis method detailed here, and used to solution dope a silica fiber preform, this would provide a more cost effective and

simple process for fabricating preforms of this type. Attempts using chromium doped calcium and magnesium fluoride nanoparticles were made (Appendix D), however, a full study was not completed.

APPENDICES

APPENDIX A

NANOPARTICLE BATCH CALCULATIONS

The following spreadsheets were used for calculating batching ratios when making various alkaline earth fluoride nanoparticles. Figure A.1 is the batch sheet used to make basic core and basic core doped nanoparticles, Figure A.2 is the batch sheet used in making the core/shell nanoparticles. Pertinent corresponding calculations are highlighted in color in each figure. Batch ratio refers to the multiplier used to increase batch size. The ***BASE*** value is multiplied by the batch ratio to yield the ***ACTUAL*** value in each case, and is the actual amount weighed for use in the synthesis.

CaF2 Nanoparticle Synthesis

Date	22-Jun-11
Experiment	**25% Eu doped CaF2**
Batch Ratio	5.00

Rare Earth	Complex	Doping
Eu(NO3)3*6H20	**446.05**	25
Ca(NO3)2*4H2O	236.15	
Total moles of host	2	

Rare Earth	MW
Eu(NO3)3*6H20	446.05
Tb(NO3)3*5H2O	435.02
Er(NO3)3*5H2O	443.35
Tm(NO3)3*5H2O	445.03
Yb(NO3)3*5H2O	449.13
Cr(NO3)3*9H2O	400.14

Core CaF2			
Solution 1	Base	Actual	
Ca(NO3)2*4H2O	0.3542	1.7711	g
Eu(NO3)3*6H20	0.2230	1.1151	g
Water	2.0000	10.0000	mL

Base Solution			
	Base	Actual	
Ammonium solution	0.6140	3.0700	g
NH4F	0.1260	0.6300	g
Water/ethanol	35	175.0	mL
Heat to 75 C			
Ca/RE dropwise	2	10.0	mL
Stir for 2 hours at 75 C			
Cool to room temperature			
Centrifuge and wash with Water and Ethanol			
Disperse in dichloromethane and precipitate with ethanol			
Dry in vaccum over P2O5 for two days			
Disperse in apolar solvent			

$$AE(NO_3)_2\,(g) = \frac{MW_{AE(NO3)2}}{1000}\left[(Total\ Moles\ of\ Host) - \left[\frac{(RE\ doping\ level\ in\ mole\ \%)(Total\ Moles\ of\ Host)}{100}\right]\right]$$

$$RE(NO_3)_3\,(g) = \frac{MW_{REdopant}}{1000}\left[\frac{(RE\ doping\ level\ in\ mole\ \%)(Total\ Moles\ of\ Host)}{100}\right]$$

AE = Alkaline Earth, RE = Rare Earth, MW = Molecular Weight in grams/mol

Figure A.1. Batch sheet for basic core and basic core rare earth doped alkaline earth fluoride nanoparticles

Core/Shell CaF2 Nanoparticle Synthesis

Date	14-Jul-11
Experiment	20Eu Core/Undoped CaF2
Batch Ratio	5.00
Mg(NO3)2*6H2O	256.41
Ca(NO3)2*4H2O	236.15
Sr(NO3)2	211.63
Ba(NO3)2	261.35
Total Moles Host	2

Rare Earth	MW
Eu(NO3)3*5H20	428.05
Tb(NO3)3*5H2O	435.02
Er(NO3)3*5H2O	443.35
Tm(NO3)3*5H2O	445.03
Yb(NO3)3*5H2O	449.13
Ce(NO3)3*6H2O	434.22
Cr(NO3)3*9H2O	400.14

Rare Earth Dopant	MW Dopant	Doping

3 Shell			
Solution 1			
Ca(NO3)2*4H2O	0.4723	2.3615	g
0	0.0000	0.0000	g
Water	2.0000	10.0000	mL
Solution 2			
NH4F	0.1260	0.6300	g
Water	2	10.0000	mL

Rare Earth Dopant	MW Dopant	Doping
		0

2 Shell			
Solution 1			
Ca(NO3)2*4H2O	0.4723	2.3615	g
0	0.0000	0.0000	g
Water	2.0000	10.0000	mL
Solution 2			
NH4F	0.1260	0.6300	g
Water	2	10.0000	mL

Rare Earth Dopant	MW Dopant	Doping
		0

1 Shell			
Solution 1			
Ca(NO3)2*4H2O	0.4723	2.3615	g
0	0.0000	0.0000	g
Water	2.0000	10.0000	mL
Solution 2			
NH4F	0.1260	0.6300	g
Water	2	10.0000	mL

Rare Earth Dopant	MW Dopant	Doping
Eu(NO3)3*5H20	428.05	20

Core			
Solution 1			
Ca(NO3)2*4H2O	0.3778	1.8892	g
Eu(NO3)3*5H20	0.1712	0.8561	g
Water	2.0000	10.0000	mL

Base Solution			
Ammonium solution	0.6140	3.0700	g
NH4F	0.1260	0.6300	g
Water/ethanol	35	175.0	mL
Heat to 75 C			
AK/RE dropwise	2	10.0	mL
Stir for 2 hours at 75 C			
Cool to room temperature			
Centrifuge and wash with Water and Ethanol			
erse in dichloromethane and precipitate with eth			
Dry in vaccum over P2O5 for two days			
Disperse in apolar solvent			

$$AE(NO_3)_2\,(g) = \frac{MW_{AE(NO3)2}}{1000}\left[(Total\ Moles\ of\ Host) - \left[\frac{(RE\ doping\ level\ in\ mole\ \%)(Total\ Moles\ of\ Host)}{100}\right]\right]$$

$$RE(NO_3)_3\,(g) = \frac{MW_{REdopant}}{1000}\left[\frac{(RE\ doping\ level\ in\ mole\ \%)(Total\ Moles\ of\ Host)}{100}\right]$$

AE = Alkaline Earth, RE = Rare Earth, MW = Molecular Weight in grams/mol

Figure A.2. Batch sheet for core/shell rare earth doped alkaline earth fluoride nanoparticles

APPENDIX B

ADDP SYNTHESIS AND CHARACTERIZATION

Synthesis of ADDP

The following procedure was used to produce the ligand, ammonium di-n-octadecyldithiophosphate (ADDP):

1. Add 19 grams of 1-Octadecanol (Acros Organics, 95%) and 4.4 grams of phosphorous pentasulfate (Acros Organics, 98+%) to a 500 ml glass, round bottom flask with a football stir bar.
2. Place the flask in a room temperature water bath and close the system under a nitrogen purge, and ramp the water bath to 75ºC while stirring at about 200 rpm.
3. Once the contents of the flask are completely melted, (about 5-10 minutes after the water bath reaches temperature), stir for 3 hours.
4. Remove flask from water bath and remove nitrogen purge.
5. Cool contents of flask, while stirring, for approximately 10 minutes.
6. Add 50 ml dichloromethane (Acros, Acroseal, anhydrous, 99.9%) to the flask, and stir at room temperature for 15 minutes.
7. Stop stirring, remove stir bar and allow solids in the flask to settle to bottom of flask.

8. Pour liquid mixture into filter paper, (Whatman Grade 5 filter paper), lined funnel set in a beaker and allow to filter until all the original contents are separated. Discard the solids and filter paper in the solid waste container.
9. Pour the resulting filtrate liquid in a 500 ml round bottom flask and attach the flask to the rotovap (Yamato RE200 Rotary Evaporator). Rotovap the liquid to remove dichloromethane and dry to a powder, approximately 45 minutes. There should be solid, white material in the flask at the end of this step.
10. Remove the flask and add 50 ml of hexanes (BDH, ACS) and agitate the flask by hand, in a circular motion, until the solids are completely dissolved into the hexanes. The solution will have a slightly opaque color, but should be transparent.
11. Bubble in NH_4, ammonia gas, (National Specialty Gases, Anhydrous) for approximately 30 seconds, adding in excess, rotating the flask while adding. The contents of the flask will be a bright white, thick slurry after this step.
12. Add excess hexanes to the flask (~ 50 ml at a time), and pour contents into a vacuum filter to separate the solid, wet ADDP. Continue adding hexanes until all of the white material from the flask is removed to the filter.
13. Place the solid, white material in a glass petri dish and dry over phosphorous pentoxide (EMD, ACS) for 2 days.

Characterization of ADDP

Photoluminescence

In order to verify the contribution, if any, of the ADDP to the spectra of the various as-made europium doped alkaline earth fluoride nanoparticles, photoluminescence was measured for a bulk sample of ADDP. The sample was excited at the same excitation wavelength (393 nm) as the various nanoparticles and the resultant emission spectra is shown in Figure B.1.

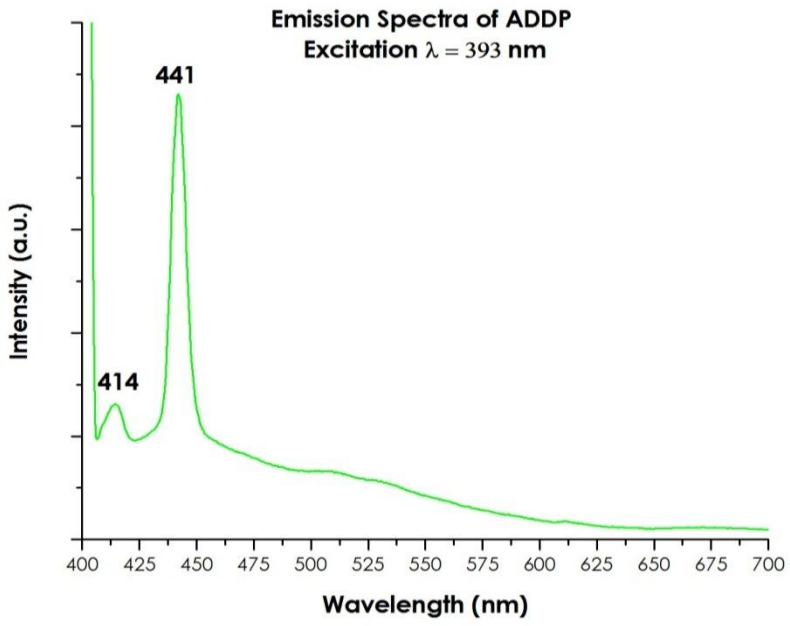

Figure B.1. Emission spectra of as-made ADDP, λ_{ex}=393 nm.

Raman Spectroscopy

In order to verify the contribution, if any, of the ADDP to the Raman measurements of the various undoped, as-made, alkaline earth fluoride nanoparticles, a Raman spectra was collected for a bulk sample of ADDP and is shown in figure B.2.

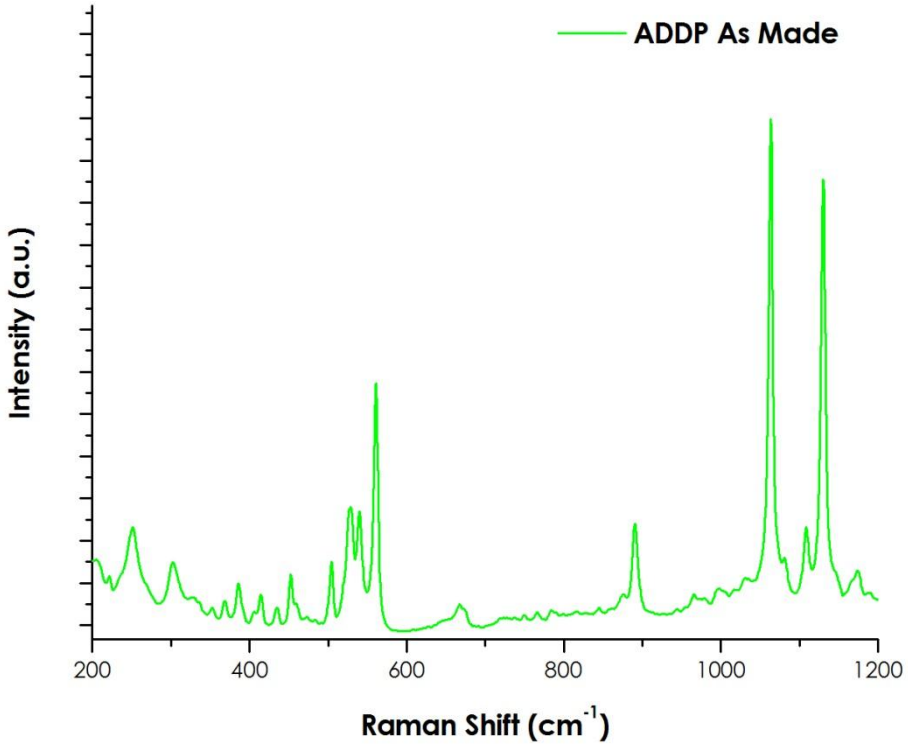

Figure B.2. Raman spectra for as-made ADDP.

Thermogravimetric Analysis

Thermogravimetric analysis was completed on as-made alkaline earth nanoparticles to determine the decomposition temperature of the attached ADDP and to estimate the amount of ligand believed attached to the different nanoparticle types. Figure B.3 summarizes the resulting thermogravimetric analysis on the individual alkaline earth fluoride nanoparticles and the ligand, ADDP, itself.

It was found that the nanoparticles are 'capped' with ~35-60% ligand, by weight, when calculated between the onset of decomposition temperature and 650ºC. The amount of ADDP increases with increasing particle size, and hence, the increase in available surface area for coordination with the ligand. Interestingly, there is also a steady increase in the onset of decomposition with increasing particle size, at temperatures higher than for the ADDP alone. This indicates that more of the ligand dithiophosphate headgroups are coordinated directly to the surface of the nanoparticle, rather than each other, thereby, requiring more thermal energy (higher temperature) to 'remove' the higher volume of ligand at the surface of the nanoparticle.

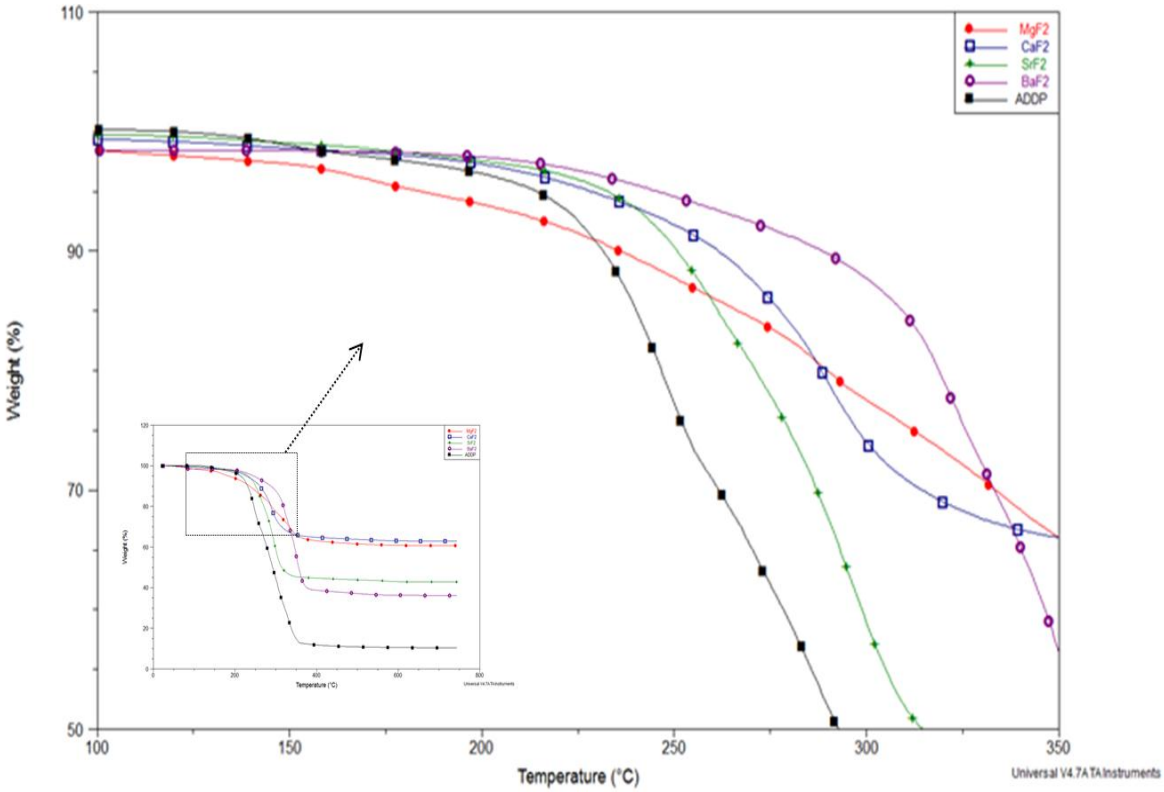

Material	Onset Decomposition Temperature T_D	% Weight Loss @ 650^{0}C	Final Decomposition Temperature T_{Df}
MgF_2	250	36	363
CaF_2	265	36	318
SrF_2	270	56	318
BaF_2	318	61	370
ADDP	232	89	337

Figure B.3. TGA analysis of undoped, alkaline earth fluoride nanoparticles made with ADDP. *Inset*: Full summary TGA scan, demonstrating decomposition with temperature.

APPENDIX C

Eu^{2+} CHARACTERIZATION

In order to address the divalent europium emissions seen solely in the heat treated 20Eu:CaF_2 nanoparticles, additional measurements were performed on these particles. X-Ray Photoelectric Spectroscopy (XPS) and Mossbauer Spectroscopy were attempted as means potentially to quantify and characterize the existence of Eu^{2+} ions within these core/shell nanoparticles.

The XPS study was completed by Erin Garber and reported in her senior thesis for the materials science and engineering department at Clemson University (included here) with the XPS measurements conducted by JoAn Hudson in the Clemson University Electron Microscopy Laboratory. Mossbauer spectroscopy was completed by Charles Johnson at the University of Tennessee Space Institute. Results and comments from Dr. Johnson are found in this appendix.

The results from both studies were inconclusive and further understanding of this anomalous behavior was not pursued (making it an area for future study), as it was not pertinent to the current study beyond noting the difference in europium emission behavior between europium doped alkaline earth fluoride hosts.

XPS Study by Erin Garber

Determination of Eu Species in Eu Doped CaF_2 Nanoparticles

A method previously developed for studying rare earth diffusion via optical means yielded two studies of core/shell nanoparticles. In europium doped LaF_3 nanoparticles, the diffusion coefficient was approximated to order of magnitude accuracy using the photoluminescence measurements of systematically heat treated particles as a marker/measurer of extent of diffusion[3]. When the study was replicated with alkaline earth elements (Ca, Sr, Ba) as a host material for the europium, an anomalous peak/emission was found in the Eu:CaF_2 3 shell particles[1]. Upon further investigation, the peak was attributed to the Eu^{2+} emission. However, this can be a somewhat uncommon state for Eu and a means of verifying and quantifying the presence of the Eu^{2+} species was sought. Here, X-Ray Photoelectric Spectroscopy, a surface x-ray technique is explored as a possible method for identifying and quantifying Eu species within heat treated Eu doped 3 shell CaF_2 nanoparticles.

In this study, 20 mole percent Eu doped core/shell CaF_2 nanoparticles will be fabricated and heat treated. This research will specifically investigate the use of X-Ray Photoelectric Spectroscopy (XPS) for determining Eu species in rare earth doped nanoparticles.

EXPERIMENTAL

In order to complete an XPS study on core/shell Eu:CaF_2 nanoparticles the following needed to be complete to verify anomalous photoluminescence behavior: production of Eu doped CaF_2 core/shell nanoparticles, TEM imaging, and simultaneous heat treatment and photoluminescence measurements of nanoparticles

Nanoparticles were produced using a previously developed solution doping extraction method[2]. Particles were doped with 20 mol% Eu in the core with Calcium Fluoride as the host and shell material. Particles were annealed in a tube furnace at 650C in 15 minute intervals for 75 minutes. Photoluminescence measurements were taken after each interval using a Jobin Yvon Fluorolog-322. TEM was completed on a Hitachi 7600 scope. XPS measurements were taken using an XPS-Kratos Axis 165. XPS was tested for its capability to determine and quantify chemical composition. XPS uses x-rays to excite electrons from their ground state to their excited state. The energy needed for excitation is called the electron binding energy and is given in electron volts (eV). An element's binding energy is not only unique to that element, but is different for electrons in each of its atomic sub shells. For instance, the binding energy for Eu_{3d} (electrons in n=3 l=3) will be different for those in Eu_{4d} (electrons in n=4 l=3). Analysis of the 4d region is preferred to the 3d because binding energies are both lower and easier observed. Less energy is needed to excite electrons in the outer shells of an

element, than the inner shells. Analysis of binding energies specific to an element's oxidation state is more complex. It involves research of XPS findings on compounds specific to the elements oxidation states and comparing the data. The publications researched in this study, compared EuO and Eu_2O_3 to evaluate binding energies for Eu^{2+} and Eu^{3+} in the 4d region[4,5]. Casa XPS Version 2.3.15 was used to calibrate and compare the XPS results.

RESULTS

Transmission Electron Microscopy (TEM)

Figure C.1 confirms that there is an average increase in particle size with each additional CaF_2 shell.

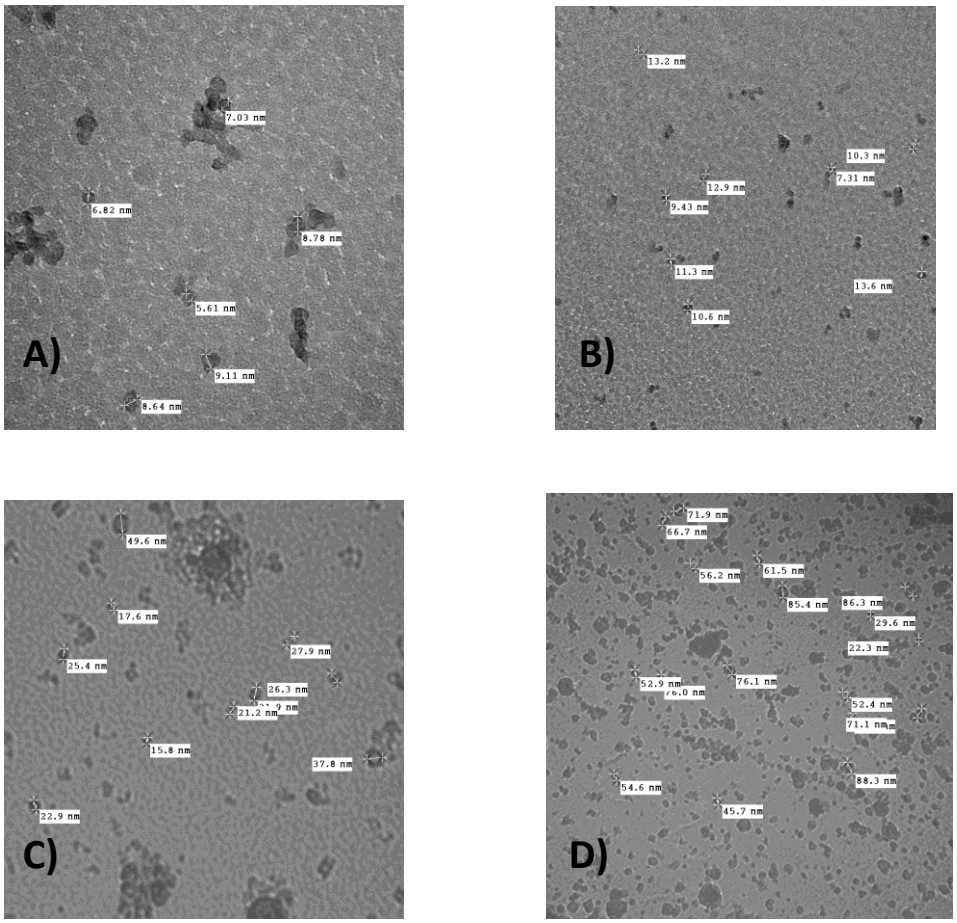

Figure C.1. Representative TEM images of A) Core, B) 1 Shell, C) 2 Shell and D) 3 Shell Eu:CaF_2 nanoparticles.

Photoluminescence

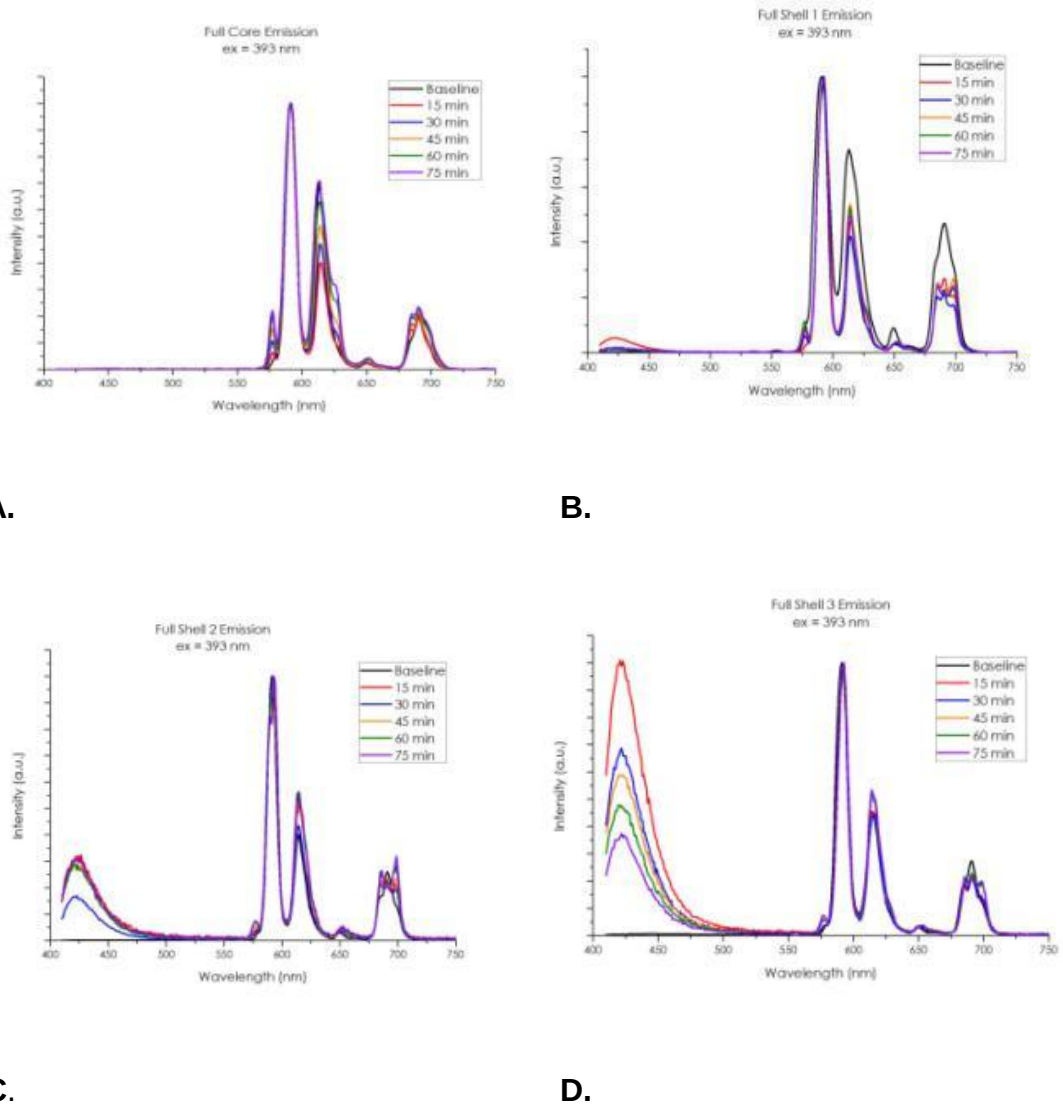

Figure C.2. Photoluminescence spectra of Eu:CaF_2 nanoparticles fired at 650C for the A) core, B) 1 shell, C) 2 shell, and D) 3 shell types.

Figure C.2 shows the results of the photoluminescence test. All measurements were taken at an excitation of 393 nm. In Figure C.2B, an emission peak at 425 nm characteristic of Eu^{2+} begins to show. The intensity of the 425 nm peak increases with each additional shell. This is consistent with the theory that Eu emission will increase as it diffuses from the core to the surface as shells are added[3]. Figure C.2D shows that the intensity of the Eu^{2+} peak increases to a point higher than that of the Eu^{3+} emission in the 3 shell particles. These photoluminescence results with respect to each type of particle are important to consider for analysis of the XPS study.

X-ray Photoelectric Spectroscopy (XPS)

All XPS data was analyzed using CasaXPS version 2.3.15 software, and calibrated using the contaminant carbon to 284.6 eV.

According to research found on XPS measurements for Eu species, binding energies for Eu^{3+} fall within a range of approximately 134-147 eV[4,5]. Binding energies that range 125-134 eV are characteristic of Eu^{2+}. CasaXPS confirms a definite peak at 135.5 eV for core particles in the Eu_{4d} region and possibly second peak around 141 eV (figure C.3). These results suggest that the rare earth in the CaF_2 particles can only be characterized by Eu^{3+}. However, the photoluminescence data of core particles did not show the characteristic Eu^{2+}

peak so it was necessary to consider XPS data for the 1 shell, 2 shell and 3 shell particles instead.

Unfortunately, the XPS scans for the shelled CaF_2 particles fail to show any Eu at all (Figures C.4-C.6). Photoluminescence has proven that Eu exists in all particles (core, 1shell, 2shell, 3shell) and therefore the problem lies with the technique used. XPS is a surface scanning technique which scans the surface of a sample to a depth of ~1 nm. It is extremely accurate in analyzing compounds of uniform elemental concentration. However, in the shelled Eu:CaF2, particles, Eu diffuses from the core to the surface of the nanoparticle. This creates a concentration gradient of the Eu in the particles. Although some of the Eu diffuses to the particle surface, the amount is too small to be detected by XPS. Therefore, XPS is insufficient to accurately determine the Eu species in these particles.

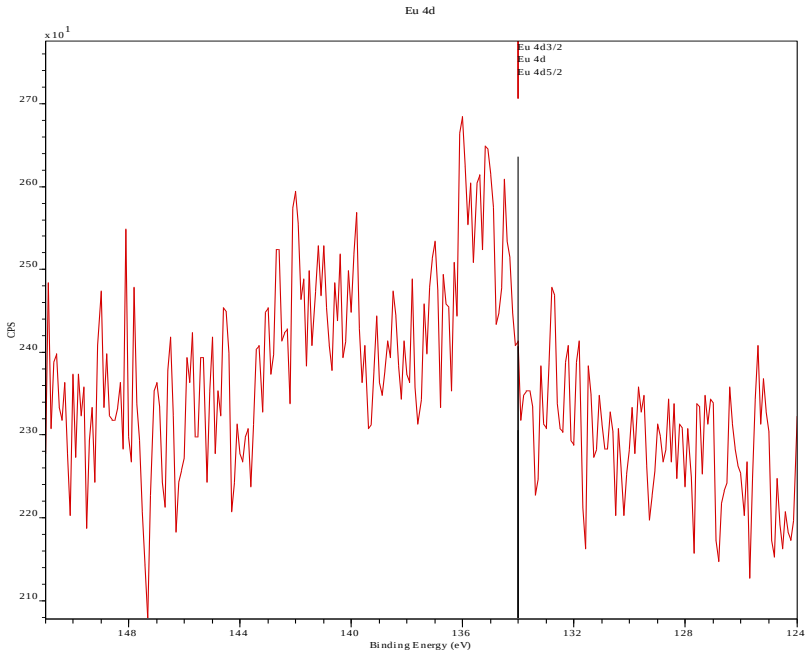

Figure C.3. XPS of Eu4d Region of 20Eu:CaF_2 Core Particles

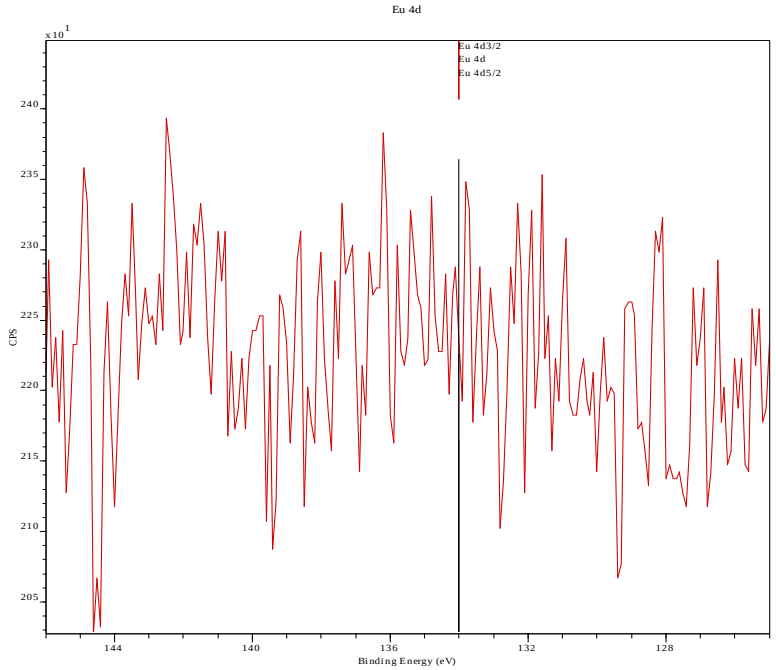

Figure C.4. XPS of Eu4d Region of 20Eu:CaF_2 1Shell Particles

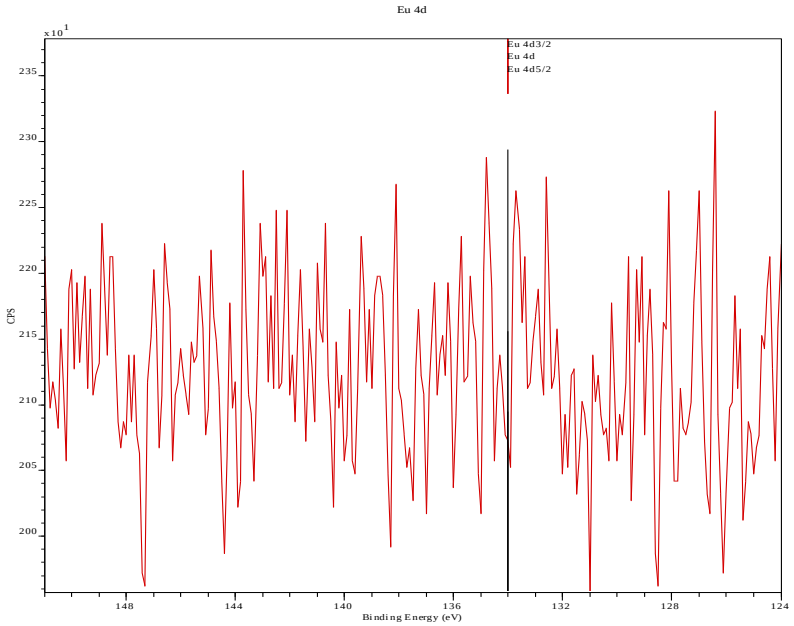

Figure C.5. XPS of Eu4d Region of 20Eu:CaF_2 2 Shell Particles

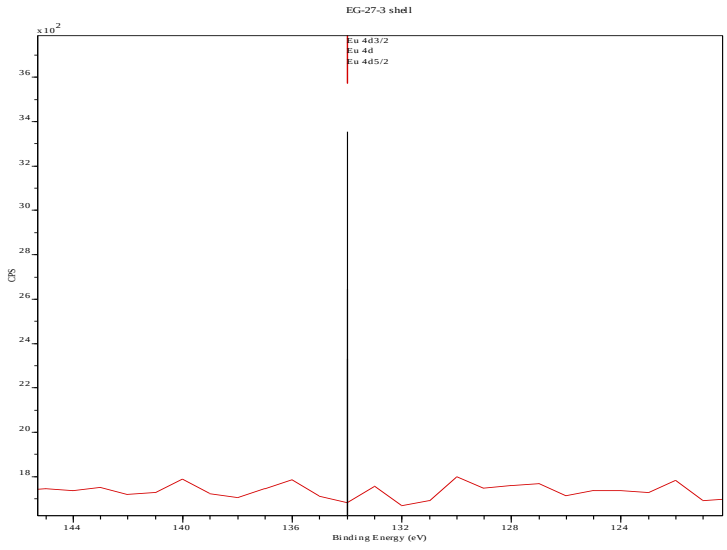

Figure C.6. XPS of Eu4d Region of 20Eu:CaF_2 3 Shell Particles

CONCLUSION

Analysis of the XPS data was done using of CasaXPS Version 2.3.15 to compare binding energies reported by to be characteristic of Eu^{2+} and Eu^{3+}. XPS data was found was unable to detect any Eu in the 1 shell, 2 shell and 3 shell particles which is inconsistent of results of the photoluminescence spectra. Due to a concentration gradient of Eu in shelled particles, the surface scan used to measure XPS is inefficient for characterizing the Eu in these CaF_2 particles.

FUTURE WORK

Other testing equipment will be investigated to accurately characterize the valence of Eu in the CaF_2 nanoparticles. Mössbauer spectroscopy will be considered first. By the use of gamma rays in this technique, it is one of the most sensitive in terms of energy solutions and has the capability of detecting changes in energy of just a few parts per 10^{11}. Further research will be done before attempting this spectroscopy technique. If the research supports the classification of valence state for these nanoparticles, plans will be made to run this test.

REFERENCES

C.1. James, Tiffany L. “Characterization of Rare Earth Doped Alkali Earth Nanoparticles.” *A Research Proposal for PhD Candidacy* (2008).

C.2. DiMaio, Jeffrey R., Baris Kokuoz, Tiffany L. James, and John Ballato. "Structural Determination of Light-Emitting Inorganic Nanoparticles with Complex Core/Shell Architectures." *Advanced Materials* 19 (2007): 3266-3270.

C.3. DiMaio, J., B. Kokuoz, T.L. James, T. Harkey, D. Monofsky, and J. Ballato. "Photoluminescent Characterization of Atomic Diffusion in Core/Shell Nanoparticles." *Optics Express* 16 (2008): 11769-11775.

C.4. Cario, Laurent , Pierre Palvadeau, Alain Lafond, Catherine Deudon, Yves Moe¨lo, Benoıˆt Corraze, and Alain Meerschaut. "Mixed-Valence State of Europium in the Misfit Layer Compound (EuS)1.173NbS2." *Chemical Materials* 15 (2003): 943-950.

C.5. Wu, Honge, Xuyong Yang, Hongbin Lv, and Kaizhong Yin. "Preparation and optical properties of Eu3+/Eu2+ in phosphors based on exchanging Eu3+-zeolite 13X." *Journal of Alloys and Compounds* 480 (2009): 867-869.

C.6. Casa XPS Version 2.3.15 Software

Mossbauer Spectroscopy

Three shell 20Eu:CaF_2 nanoparticles which had been fired for 75 minutes at 650C were measured to determine the presence of Eu^{2+} ions in the sample via Mossbauer spectroscopy. The resulting scan is shown in figure C.7.

Results indicate there is no distinction between the Eu^{3+} ions and Eu^{2+} ions and it was suggested that the Eu^{2+} concentration was too low to detect with this technique. The Eu^{3+} line is shifted to the right, indicating the ion is in an oxygen environment rather than a fluoride environment.

The photoluminescence measurements (Chapter 2) of these particles clearly exhibit emissions due to Eu^{2+}, however, attempts to substantiate the Eu^{2+} ions quantitatively with alternate spectroscopy methods were inconclusive.

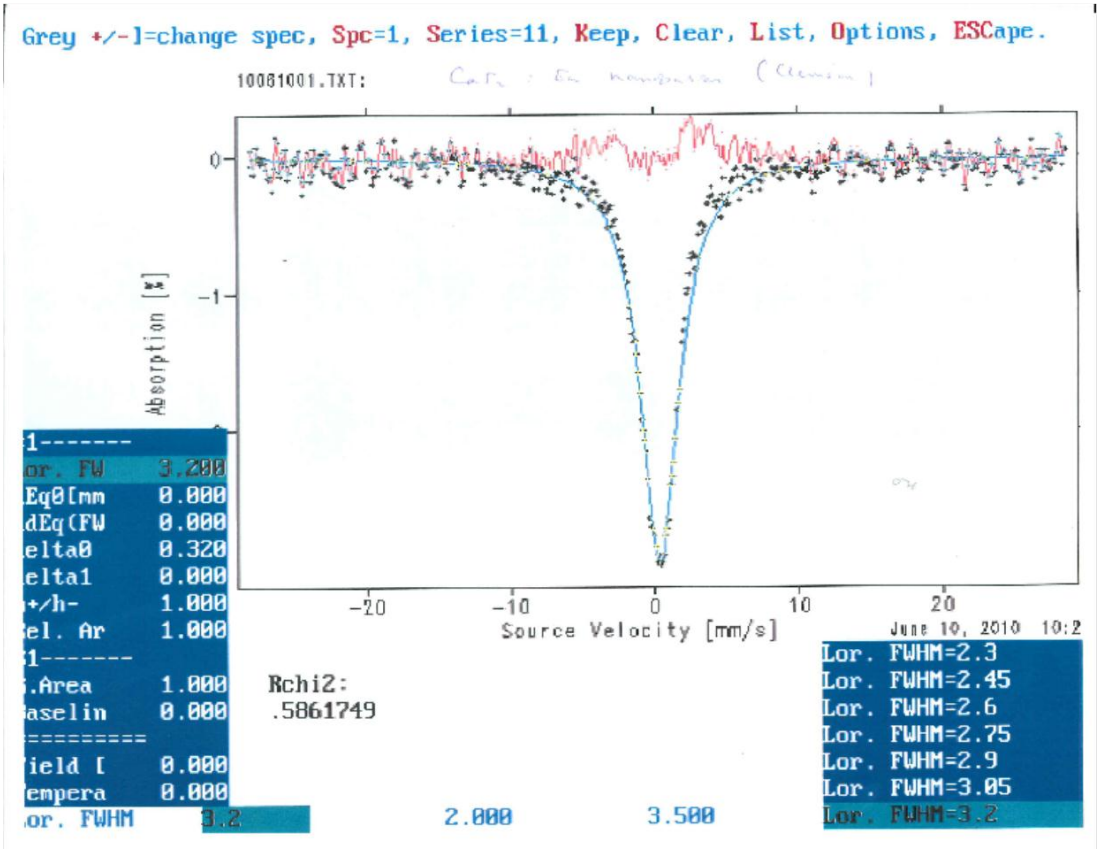

Figure C.7. Mossbauer spectra of 3 Shell 20Eu:CaF_2 nanoparticles fired for 75 minutes at 650ºC.

APPENDIX D

OTHER OPTICALLY ACTIVE

ALKALINE EARTH FLUORIDE NANOPARTICLES

Other alkaline earth host materials and doping of the nanoparticles with other optically active ions is of interest. Initial experimentation involving the alkaline earth magnesium as a host material and doping silica preforms with CaF_2 and MgF_2 nanoparticles doped with the transition metal chromium is detailed below. Magnesium fluoride, MgF_2, is a tetragonal rather than cubic crystal system and the alkaline earth has a smaller ionic radius than that of Ca^{2+}, Sr^{2+}, and Ba^{2+}. The difference in crystal structure did not allow for direct comparison to the other alkaline earth hosts, therefore, the MgF_2 nanoparticle survey was limited and included here.

Magnesium Fluoride, MgF_2

Magnesium fluoride nanoparticles were doped with various concentrations of europium as per the procedure detailed in Chapter 2, Nanoparticle Synthesis, Basic Core Doped and Europium Core Doped AEF_2 with Undoped AEF_2 Shells . Figure D.1 shows the XRD pattern of the magnesium fluoride nanoparticles. The pattern exhibits prominent peaks in accordance with JCPDS standards (70-0212)

of the tetragonal crystal, which verifies the successful synthesis of the MgF_2 nanoparticles.

Magnesium fluoride nanoparticles were doped separately with 5, 15 and 25 mole percent europium and their photoluminescence was measured at an excitation wavelength of 393nm. The resulting spectra (normalized to the 590nm transition) are shown in figures D.2-D4, as well as comparison spectra for all of the alkaline earth nanoparticles. The signature emissions of Eu^{3+} are clearly demonstrated with peaks at 590 and 610 nm. A prominent peak at ~437nm corresponds to the ligand, ADDP, used in synthesizing the nanoparticles (Appendix B).

Twenty mole percent europium doped MgF_2 nanoparticles were individually produced with a three additional layers or shells of undoped MgF_2 added in stages. Samples were then heat treated at 650ºC in fifteen minute intervals, for a total of 75 minutes. Following each time interval, photoluminescence was measured, with the resulting emission spectra for each nanoparticle type shown in figures D.5-D.8. The signature Eu^{3+} emissions are seen for each nanoparticle type, regardless of processing conditions, similar to the SrF_2 and BaF_2 host materials studied. However, it appears the presence of the ligand has more of an effect on the emission behavior than the other alkaline earth hosts studied, for all nanoparticle types and conditions (Chapter 2, Thermal Effects on Optical Behavior of Eu:AEF_2 Nanoparticles)

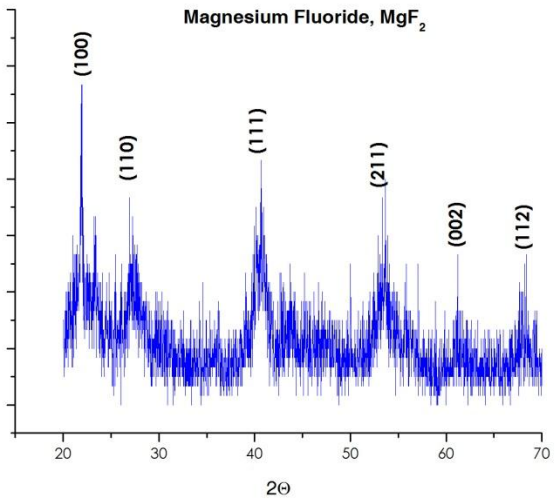

Figure D.1. X-Ray diffraction pattern for magnesium fluoride nanoparticles, matched to JCPDS card 70-0212.

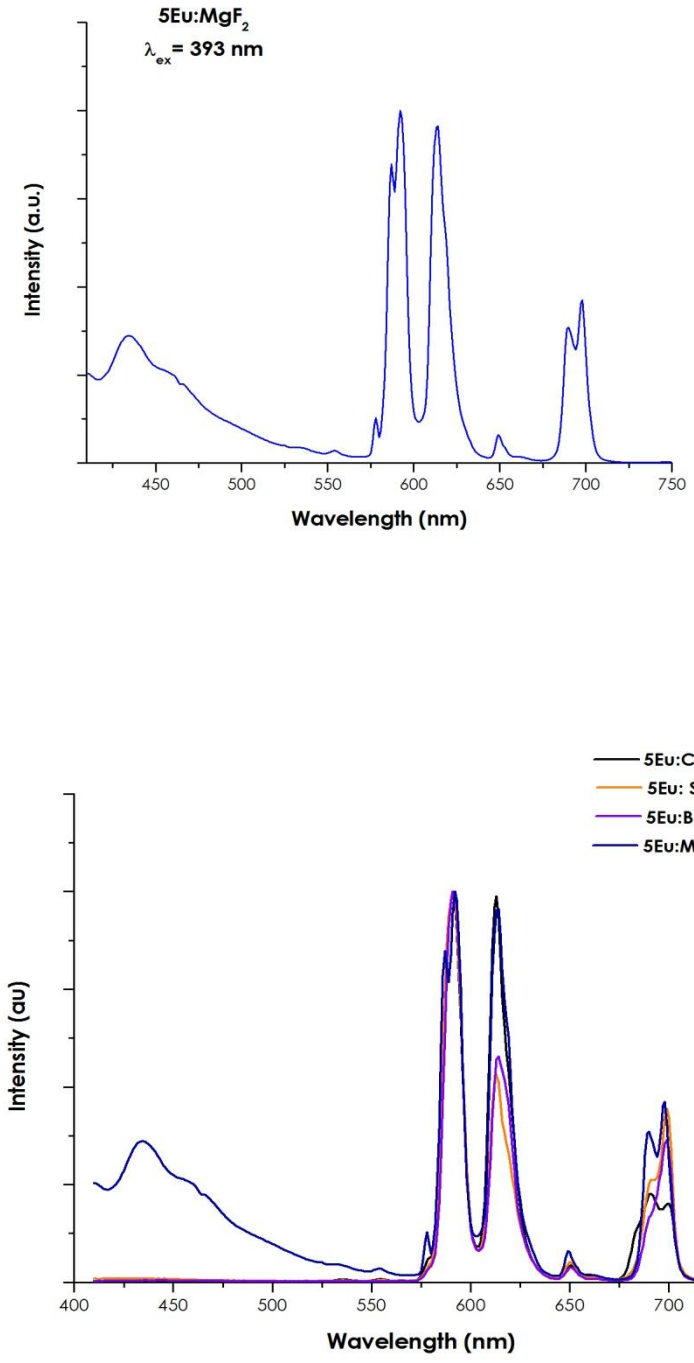

Figure D.2. Emission spectra of a) 5Eu:MgF_2 nanoparticles b) all 5Eu:AEF_2 nanoparticles.

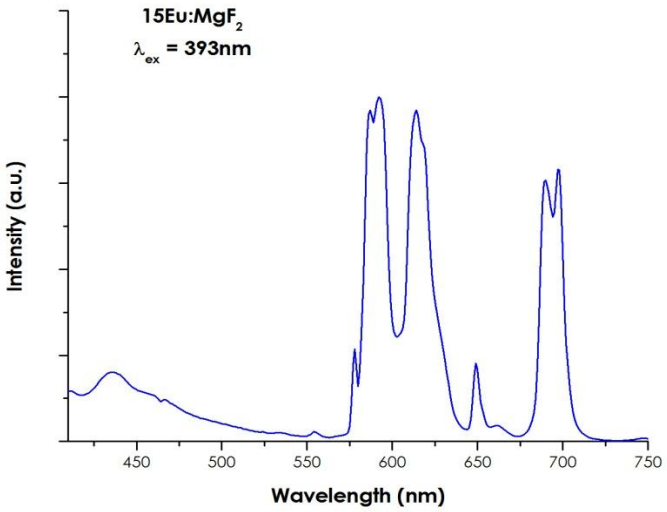

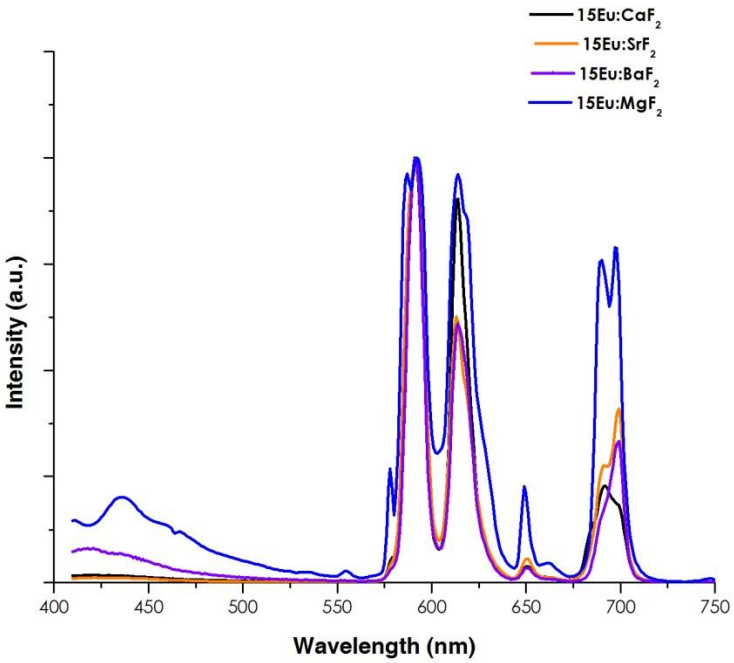

Figure D.3. Emission spectra of a) 15Eu:MgF_2 nanoparticles b) all 15Eu:AEF_2 nanoparticles..

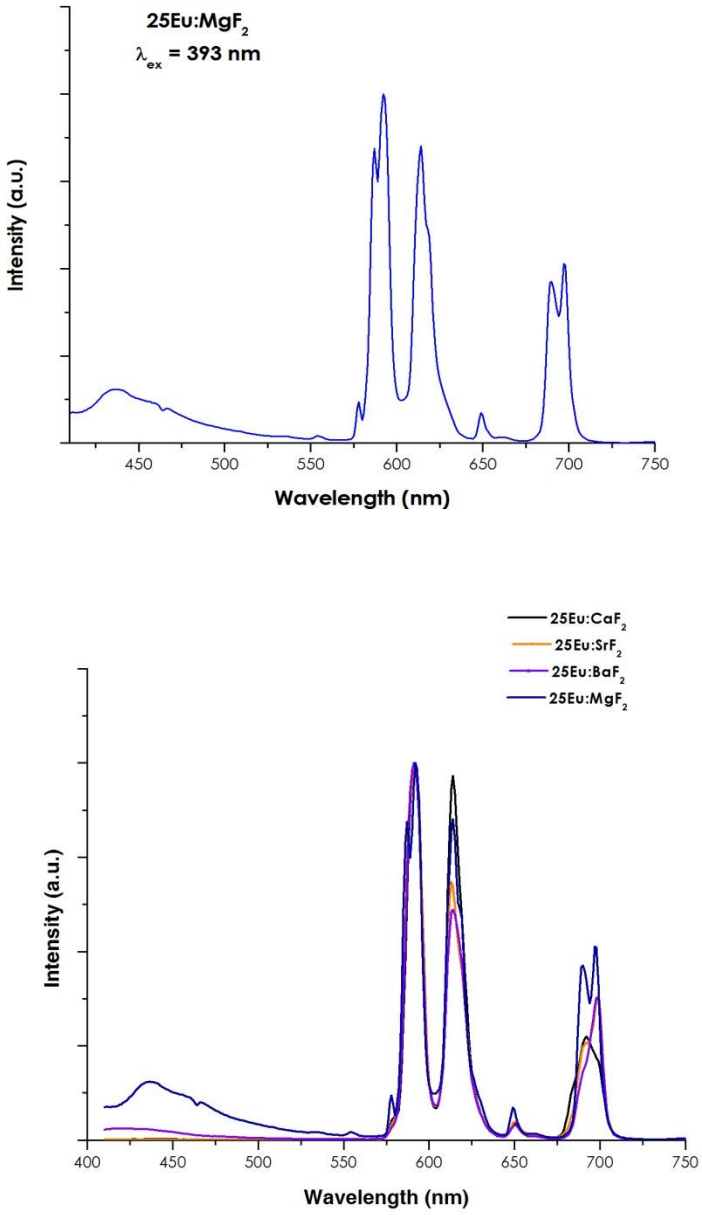

Figure D.4. Emission spectra of a) 25Eu:MgF_2 nanoparticles, b) all 25Eu:AEF_2 nanoparticles.

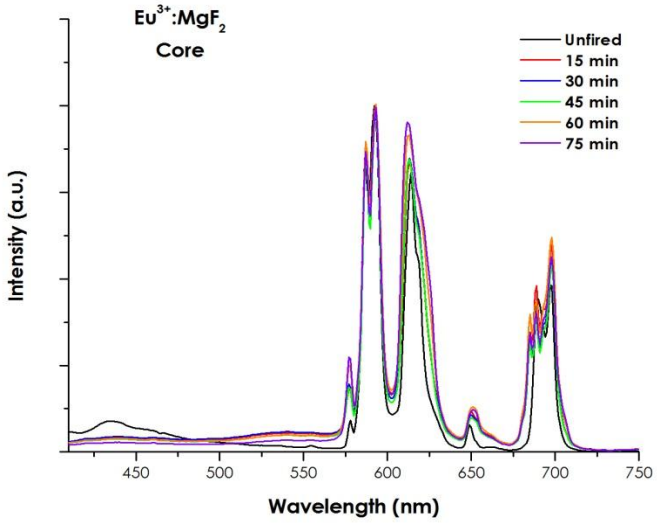

Figure D.5. Emission spectra as a function of time at 650ºC for core 20Eu:MgF_2 nanoparticles.

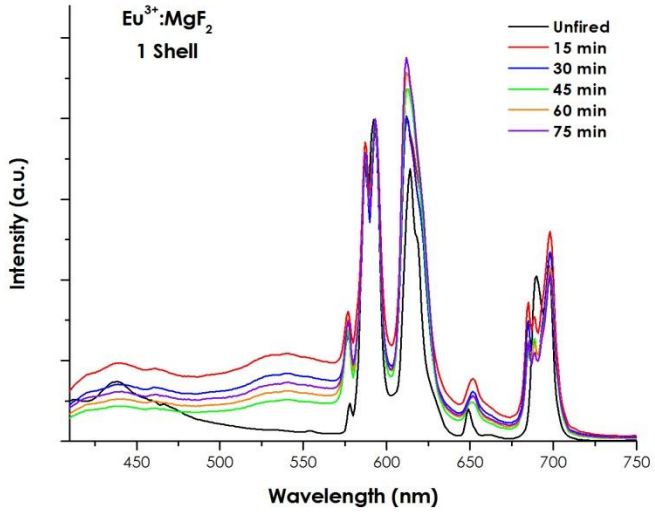

Figure D.6. Emission spectra as a function of time at 650ºC for 1 shell MgF_2/Core 20Eu:MgF_2 nanoparticles.

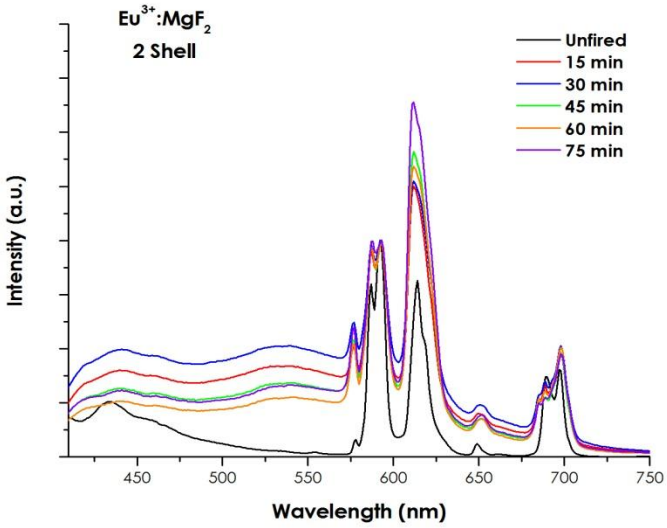

Figure D.7. Emission spectra as a function of time at 650ºC for 2 MgF_2 shells/Core 20Eu:MgF_2 nanoparticles.

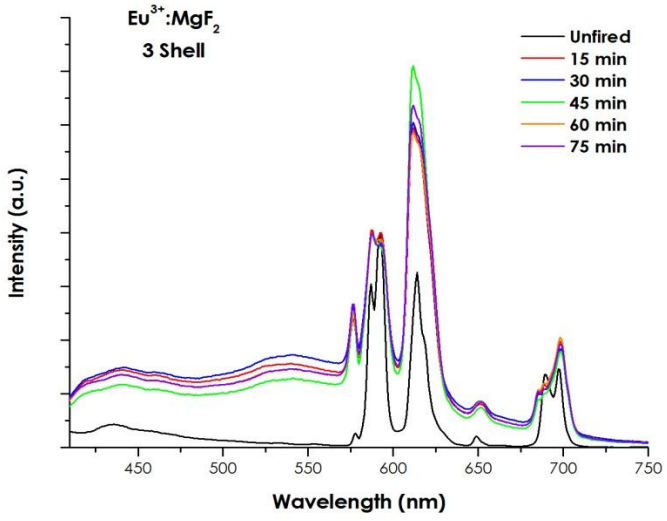

Figure D.8. Emission spectra as a function of time at 650ºC for 3 MgF_2 shells / Core 20Eu:MgF_2 nanoparticles.

Chromium doped Alkaline Earth Fluoride Nanoparticles

Solid state materials which lase in the near infrared region are of extreme interest and the incorporation of tetravalent chromium (Cr^{4+}) in forsterite ($MgSiO_2$) and YAG ($Y_3Al_5O_{12}$) has been studied at length due to their emissions in the near IR. Given the spectral behavior demonstrated by the nanoparticle doped preforms in this study, The doping of the nanoparticles with other optically active ions was also of interest, specifically the transition metal chromium, for incorporation into fiber preforms.

Transition metal spectroscopy is a result of optical transitions from 3d electrons rather than the 4f electrons of the lanthanide series, making their chemical and optical behavior very different, therefore, initial experimentation was begun to try and determine the feasibility of making this type of nanoparticle and using it as a dopant delivery material, but a full study was not completed. Chromium doped calcium fluoride and magnesium fluoride particles were synthesized using the procedure outlined in Chapter 2, Nanoparticle Synthesis, Basic Core Doped,

Synthesis of 15 mole percent chromium doped calcium fluoride nanoparticles, was successfully completed with the resulting nanoparticles similar to the various other rare earth doped calcium fluoride nanoparticles. Alternatively, the synthesis of 15 mole percent chromium doped magnesium fluoride nanoparticles was unsuccessful. At this doping level, there was a distinct

separation of the magnesium fluoride and chromium approximately 5-10 minutes after the final dropwise addition of the chromium solution while stirring. Two solids (one white, one purple) were noted within the stirring solution, as though the chromium had completely separated from the magnesium fluoride particles. Upon this finding, the nanoparticles were remade with varying concentrations of chromium until a successful synthesis was completed with 7.5 mole percent chromium doped magnesium fluoride nanoparticles. The maximum doping level of calcium fluoride has not been determined, nor has a reason for this separation been determined.

Various combinations of the 15Cr:CaF_2 and 7.5Cr:MgF_2 nanoparticles, with and without aluminum, (15Cr:CaF_2, 15Cr:CaF_2/Al, 7.5Cr:MgF_2/15Cr:CaF_2, 7.5Cr:MgF_2/15Cr:CaF_2/Al) were placed in solution to core dope optical fiber preforms per the procedure detailed in Chapter 3, Preform Fabrication. Polished cross-sections of the resulting core doped glass were measured by Professor Uwe Hommerich at Hampton University, in an attempt to determine the transmission behavior of the glass preform.

The resulting transmission measurements (example in Figure D.9) were deemed inconclusive as there is no clear band structure indicating Cr^{4+} absorption measuring through the core. It was suggested that the lack of color in the doped region indicates a very low doping concentration or no Cr incorporation at all. Samples doped with Cr^{3+} and Cr^{4+} tend to have a green or

blue tint to them, indicating the presence of these ions. These results suggest the chromium concentration is too low to sufficiently absorb and , going forward it is suggested that attempts to increase the overall doping level of the chromium within the preform be completed. The solutions used to solution dope the fiber preform were made based on the conventional method of solution doping (0.1M nanoparticles in solution), for which the resulting glass preform is estimated to contain 2500 ppm of the nanoparticle along the length of the core of the preform. For conventional solution doping, typical codopant solutions of rare earth salts and aluminum are made at a ratio of 0.1M to 1M. This suggests an increase in the molar ratio of chromium doped nanoparticle in solution can be increased and should be optimized to increase the total amount of chromium contained in the core, rather than the nanoparticle content, in order to determine if this method is viable for producing Cr4+ doped silica fiber.

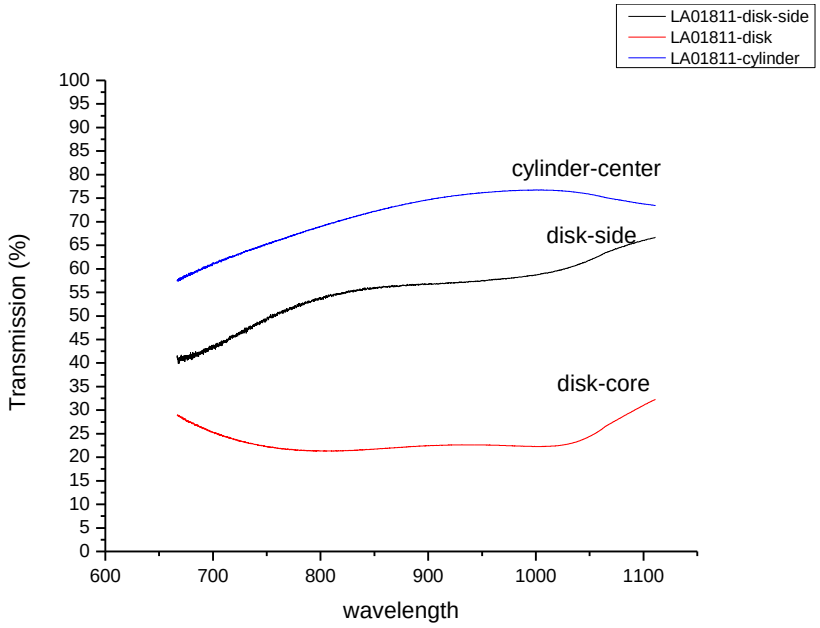

Figure D.9. Transmission measurement of a 15Cr:CaF_2/Al doped optical fiber preform.